

AFWAL-TR-85-4151

Volume VI

ADA 171221

MECHANICAL PROPERTIES VS MORPHOLOGY OF ORDERED POLYMERS
Volume VI



E.L. Thomas, R.J. Farris and S.L. Hsu

Polymer Science & Engineering Department
The University of Massachusetts
Amherst, MA 01003

June 1986

Final Report for Period September 1983 - August 1984

Approved for public release; distribution unlimited.

MATERIALS LABORATORY
AIR FORCE WRIGHT AERONAUTICAL LABORATORIES
AIR FORCE SYSTEMS COMMAND
WRIGHT-PATTERSON AIR FORCE BASE, OHIO 45433-6533

Best Available Copy

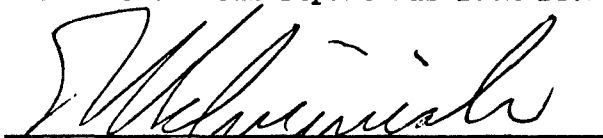
2004 0219 258

NOTICE

When Government drawings, specifications, or other data are used for any purpose other than in connection with a definitely related Government procurement operation, the United States Government thereby incurs no responsibility nor any obligation whatsoever; and the fact that the government may have formulated, furnished, or in any way supplied the said drawings, specifications, or other data, is not to be regarded by implication or otherwise as in any manner licensing the holder or any other person or corporation, or conveying any rights or permission to manufacture use, or sell any patented invention that may in any way be related thereto.

This report has been reviewed by the Office of Public Affairs (ASD/PA) and is releasable to the National Technical Information Service (NTIS). At NTIS, it will be available to the general public, including foreign nations.

This technical report has been reviewed and is approved for publication.



THADDEUS E. HELMINIAK
Work Unit Scientist



RICHARD L. VAN DEUSEN
Chief, Polymer Branch

FOR THE COMMANDER



MERRILL L. MINGES, Chief
Nonmetallic Materials Division

"If your address has changed, if you wish to be removed from our mailing list, or if the addressee is no longer employed by your organization please notify _____, W-PAFB, OH 45433 to help us maintain a current mailing list".

Copies of this report should not be returned unless return is required by security considerations, contractual obligations, or notice on a specific document.

UNCLASSIFIED

SECURITY CLASSIFICATION OF THIS PAGE

REPORT DOCUMENTATION PAGE

1a. REPORT SECURITY CLASSIFICATION AFWAL-TR-85-4151, Volume VI			1b. RESTRICTIVE MARKINGS		
2a. SECURITY CLASSIFICATION AUTHORITY Unclassified			3. DISTRIBUTION/AVAILABILITY OF REPORT Approved for public release; distribution unlimited		
2b. DECLASSIFICATION/DOWNGRADING SCHEDULE N/A			5. MONITORING ORGANIZATION REPORT NUMBER(S) AFWAL-TR-85-4151 Volume VI		
4. PERFORMING ORGANIZATION REPORT NUMBER(S)			7a. NAME OF MONITORING ORGANIZATION AFWAL/MLBP		
6a. NAME OF PERFORMING ORGANIZATION Polymer Science and Engineering Department		6b. OFFICE SYMBOL (If applicable)	7b. ADDRESS (City, State and ZIP Code) Wright-Patterson AFB, OH 45433-6533		
6c. ADDRESS (City, State and ZIP Code) University of Massachusetts Amherst, Massachusetts 01002		9. PROCUREMENT INSTRUMENT IDENTIFICATION NUMBER F33615-82-K-5068			
8a. NAME OF FUNDING/SPONSORING ORGANIZATION (AFWAL/ Materials Laboratory MLBP)		8b. OFFICE SYMBOL (If applicable)	10. SOURCE OF FUNDING NOS.		
8c. ADDRESS (City, State and ZIP Code) Air Force Wright Aeronautical Laboratories (AFSC) Wright-Patterson Air Force Base, Ohio 45433		PROGRAM ELEMENT NO. 62102F	PROJECT NO. 2419	TASK NO. 04	WORK UNIT NO. 07
11. TITLE (Include Security Classification) Mechanical Properties vs Morphology of Ordered Polymers					
12. PERSONAL AUTHOR(S) E.L. Thomas, R.J. Farris and S.L. Hsu					
13a. TYPE OF REPORT Final		13b. TIME COVERED FROM 9/83 TO 8/84		14. DATE OF REPORT (Yr., Mo., Day) June 1986	
15. PAGE COUNT 115					
16. SUPPLEMENTARY NOTATION					
17. COSATI CODES			18. SUBJECT TERMS (Continue on reverse if necessary and identify by block number)		
FIELD	GROUP	SUB. GR.	Rigid Rod Polymer PBT		
11	04		Fibers Mechanical Properties		
07	04		Films Morphology		
19. ABSTRACT (Continue on reverse if necessary and identify by block number)					
<p>This project seeks to determine for rigid rod polymer fibers and films of poly(p-phenylene benzobisthiazole) the relationships between mechanical properties and sample microstructures and to use this knowledge to obtain the maximum in strength and modulus for these materials.</p> <p>Structural studies involved primarily optical microscopy, electron microscopy (both scanning and transmission) and wide angle x-ray scattering. Spectroscopic studies employed Fourier transform infrared spectroscopy. Mechanical behavior was measured in uniaxial tension over a range of strain rates and temperatures. A special force-temperature apparatus permitted assessment of the thermal expansion coefficient of PBT.</p>					
20. DISTRIBUTION/AVAILABILITY OF ABSTRACT UNCLASSIFIED/UNLIMITED <input type="checkbox"/> SAME AS RPT. <input checked="" type="checkbox"/> DTIC USERS <input type="checkbox"/>			21. ABSTRACT SECURITY CLASSIFICATION Unclassified		
22a. NAME OF RESPONSIBLE INDIVIDUAL Dr. T. E. Helminiak			22b. TELEPHONE NUMBER (Include Area Code) 513-255-9155		22c. OFFICE SYMBOL AFWAL/MLBP

The microstructural studies concentrated on the structure developed during the fast coagulation stage of the spinning process, as well as the structure obtained by slow coagulation of a quiescent isotropic polymer solution. The structure formed in the coagulation stage of the spinning process of PBT fiber was examined by TEM of epoxy impregnated fibers. An oriented network of microfibrils with typical fibril diameters of about 80-100A was observed. We suggest that these microfibrils are the fundamental structural elements of the fiber. Thus knowledge of the mechanism by which this initial structure is formed may allow for better control of final fiber properties.

Growth of crystal solvates in the PBT/MSA system was observed for the first time through the slow diffusion of water into the quiescent isotropic solution. The crystalline PBT left as a residue upon removal of the acid solvent was also investigated. Lamellae were observed whose thickness corresponds closely with the molecular length of the PBT used.

Phase behavior was investigated and a pseudo-binary schematic phase diagram for the PBT/MSA.H₂O system was developed. The relation of structure formation during fast and slow coagulation to the phase diagram of a rigid polymer solution and to the kinetic mechanism of the phase transition was discussed in terms of nucleation and growth.

Spectroscopic measurements employed the attenuated total reflectance technique in conjunction with transmission infrared spectroscopy to quantitatively determine the residual water and acid content in PBT films. It was shown that post-processing annealing, even with very moderate temperatures, can remove the water effectively. The acid was found mainly in the interior of the film. Post-processing annealing at high temperature can remove acid as well. But films exposed to such high temperature treatment do show new spectroscopic features suggesting that the polymer structures have been altered. Using the absorbance values measured by infrared irradiation, the birefringence of PBT has been determined to be 0.88 ± 0.04 in the infrared region, a value much smaller than previously suggested, but close to that of poly(p-phenylene terephthalate).

The mechanical properties of PBT films feature an interesting temperature and strain rate dependence. The elastic modulus and yield behavior have been studied over a wide temperature range from 30°C to 650°C. The onset of a structural reorganization is observed at about 300°C. Enhancement of modulus was also observed due to deformation of the films under elevated temperatures, where better molecular orientation and lateral ordering are achieved.

The force versus temperature behavior (at constant length) of PBT and Kevlar fibers was also investigated. Thermal expansion coefficients were $-1.1 \times 10^{-6}/^{\circ}\text{C}$ and $-3.2 \times 10^{-6}/^{\circ}\text{C}$, respectively, for heat treated PBT and Kevlar® 49. Material changes which occur during heat treatment processing are detected in the force-temperature profile. A correspondence between thermal and mechanical energy input has been found to induce these material changes.

FOREWORD

This report covers the final year's work performed by the University of Massachusetts, Amherst, Massachusetts, 01003, on "Mechanical Properties versus Morphology of Ordered Polymers." The work was conducted under contract F33615-82-K-5068 for the Materials Laboratory. The performance period was from 1 September, 1983, to 31 August, 1984. This report was submitted in November, 1985.

The work was performed in the Polymer Science and Engineering Department with Professor Edwin L. Thomas acting as Principal Investigator. Professors R.J. Farris and S.L. Hsu were co-principal investigators. The assistance of Messrs. H.H. Frost, Y. Cohen and Drs. S.R. Allen, C. Chang, L. Feldman and L.A. Pottick is gratefully acknowledged. The project engineer was Dr. T.E. Helminiak, AFWAL/MLBP, Materials Laboratory, Wright Patterson Air Force Base, Ohio.

TABLE OF CONTENTS

	PAGE
SECTION I: OVERVIEW	1
SECTION II: STRUCTURE FORMATION DURING SPINNING OF PBT FIBER	5
A. Introduction.	5
B. Experimental Section.	5
C. Results and Discussion.	6
D. Conclusions	12
References.	13
SECTION III: MICROSTRUCTURE AND PHASE BEHAVIOR OF POLY- PARA-PHENYLENE BENZOBISTHIAZOLE)/METHANE SULFONIC ACID CRYSTAL SOLVATES	18
A. Introduction.	18
B. Background.	19
C. Experimental.	22
1. Materials	22
2. Sample Preparation.	23
3. Electron Microscopy	24
4. Optical Microscopy.	25
5. X-Ray	25
6. DSC	25

D.	Results and Discussion.	26
1.	Results	26
2.	Discussion.	31
3.	Conclusions	34
E.	Future Work	35
	References.	37
SECTION IV.	SPECTROSCOPIC ANALYSIS OF POLY(p-PHENYLENE BENZOBISTHIAZOLE) FILMS.	55
A.	Introduction.	55
B.	Experimental.	57
C.	Results and Discussion.	58
D.	Conclusions	68
	References	69
SECTION V.	TEMPERATURE AND STRAIN RATE DEPENDENCE OF THE DEFORMATION BEHAVIOR OF POLY(PARAPHENYLENE BENZOBISTHIAZOLE).	77
A.	Summary	77
B.	Introduction.	77
C.	Experimental Details.	79
1.	Material.	79
2.	Tensile Tests	79
3.	Oven Construction	79
4.	Force-Temperature Experiment	80

D.	Results and Discussion.	80
1.	Stress-Strain Behavior.	80
2.	Heating-Cooling Experiment.	84
3.	X-ray Data.	85
4.	Work-hardening Effect	86
E.	Activation Volume	86
1.	Extension-Contraction	88
F.	Conclusion.	89
	References.	91
SECTION VI.	FORCE-TEMPERATURE BEHAVIOR OF RIGID ROD POLYMERIC FIBERS	101
A.	Introduction.	101
B.	Experimental.	102
C.	Results and Discussion.	104
D.	Summary	108
	References.	109

LIST OF ILLUSTRATIONS

FIGURE		PAGE
II.C.1	a) A longitudinal section of coagulated PBT fiber infiltrated with epoxy resin. E-epoxy matrix; F-fiber	15
	b) A high magnification image of the outlined area	15
2	A schematic phase diagram of a rigid polymer solution: solid line - phase boundary; dashed line - incongruent phase boundary; dotted line - spinodal curve; XS - crystal solvate; P - crystalline polymer	16
3	Comparison of spinodal decomposition and nucleation and growth in a solution of oriented rods undergoing a phase transition with effectively one-dimensional mobility. c - polymer concentration, c_0 - composition of initial solution.	17
III.B.1	Superposition of liquid-liquid and solid-liquid phase diagrams. Top diagram is for a crystal having smaller melting transition temperature and heat of fusion; bottom diagram is for larger values.	40
2	Schematic phase diagram for rigid-rod polymer with the inclusion of a crystal solvent. (1) isotropic solution, (2) isotropic solution plus anisotropic solution, (3)	

	anisotropic solution, (4) isotropic solution plus crystal solvate, (6) crystal solvate plus crystalline polymer, (7) crystalline polymer plus anisotropic solution. .	40
III.C.1	a. Drop of PBT/MSA solution is put on a clean glass slide, b. cover slip is placed over drop, c. water diffusing into the solution induces growth of crystal solvate, d. crystal solvate is fully grown	41
2	a. Cover slip, crystal solvates, and glass slide, after heating at about 150°C, b. cover slip is split off, c. crystal solvate floated off onto deionized water, d. crystal solvate ready to be picked up with electron microscope grids	41
III.D.1	Differential scanning calorimeter trace of PBT/MSA.H ₂ O crystal solvates	42
2	a. Statton flat film x-ray diffraction of PBT/MSA.H ₂ O, b. schematic of x-ray pattern	42
3	Typical Maltese cross extinction pattern of PBT/MSA.H ₂ O crystal solvate spherulites viewed under crossed polars in an optical microscope	43
4	Scanning electron microscope photograph of PBT/MSA.H ₂ O spherulites having been washed in copious amounts of acetone and dried.	43

5	Optical micrographs showing melting of crystal solvates. a. at 27°C, b. at 92°C, c. at 94°C, d. and e. at 117°C. Note isotropic (1), anisotropic (2) and biphasic (3) liquid domains at 117°C equilibrium.	44
6	a. Superposition of liquid-liquid and solid-liquid phase diagrams with the chimney region inaccessible at equi- librium, b. with chimney region partially accessible at equilibrium.	45
7	Crystal solvates growing from metastable nematic liquid into equilibrium state of crystal solvate plus isotropic liquid	46
8	A crystal solvate spherulite growing from a nematic solu- tion	46
9	PBT lamellae remaining after solvent removal and drying. Electron diffraction (inset) reveals the chain orientation is perpendicular to the lamellae	47
10	Bright field/dark field pair (a and b respectively) showing lamellae and fracture paths of lamellar region of PBT	48
11	Schematic of proposed lamellar structure of PBT. a. cor- responds to lamellar width, b. corresponds to long period	49
12	Equatorial 2θ scan of PBT fiber.	49

13	Electron diffraction data revealing texturing in PBT. a. e1 - e4 all present in typical fiber symmetric intensities, b. e1 and e2 only, c. e2 only, d. e2 and e3 only with e2 being more intense, e. e2 and e3 only with e3 being more intense.	50
14	Bright field electron micrographs of lamellar PBT. a. sheaf like structures readily apparent and b. higher magnification of a. Note fine 100 angstrom cross-hatching perpendicular to lamellae	51
15	Bright field image of "grassy mat" formed by coagulation of isotropic solution.	52
16	a. electron diffraction of the a b plane of a twinned crystal. C axis is perpendicular to the page, b. schematic of diffraction pattern	52
III.E.1	Examples of crystal solvate diffraction. Pattern a has the e2 PBT arc superimposed upon it.	53
2	Crystal solvate growth from a. isotropic, b. anisotropic and c. biphasic solutions. Left: analyzer removed; Right: polarizer and analyzer crossed	54
IV.B.1	The infrared spectra obtained for the poly(p-phenylene benzobisthiazole) film S ₁ ; a) obtained using unpolarized irradiation; b) spectrum obtained using irradiation	

	polarized parallel to the extrusion (chain) direction;	
	c) spectrum obtained using irradiation polarized perpen- dicularly to the chain axis.	72
2	a) Infrared spectrum of pure polyphosphoric acid, b) difference spectrum between an as-prepared film and an annealed film. For the sake of clarity, the y axis of this spectrum has been expanded.	73
3	Schematic drawing of a S ₁ film cross-section	74
4	Infrared spectrum obtained for the poly(p-phenylene benzobisthiazole) film S ₁ using the attenuated total reflectance technique. Germanium crystal was used with an incident angle of 45°.	75
5	Infrared spectrum obtained for the poly(p-phenylene benzobisthiazole) film annealed at 415°C under tension.	75
6	ATR spectra of PBT film on KRS-5 as a function of angle of incidence θ = a) 42.1°, b) 42.9°, c) 43.7°, and d) 45°. This is done by using TM wave and the extrusion axis oriented perpendicular to the incident plane	76
V.C.1	Schematic of the test arrangement; A-sample; B-clamps of the testing machine; C-thermocouple; D-heating wire; E-thermoresistant glass; F-insulation.	93
V.D.1	Stress-strain curves at various temperatures for PBT film at a strain rate $0.08 \times 10^{-3} \text{ sec}^{-1}$	93

2	Effect of test temperature on the relative changes of the mean values of: 1) ultimate strength (●●●); 2) Young's modulus (ooo); 3) yield stress (ΔΔΔ); 4) elongation of PBT film (ooo)	94
3	Photograph of PBT film samples after fracture at evaluated temperatures: A) 60°C; B) 144°C, C) 185°C; D) 370°C; E) 440°C; F) 490°C; G) 550°C; H) 613°C; I) 650°C.	95
4	Variation of the modulus as a function of temperature in heating-cooling experiment. Notation explained in the text	96
5	Modulus vs. test temperature for various polymers: PBT, methylcellulose and poly(methylmethacrylate)	96
6	The WAXS flat film patterns of 1) the as-extruded sample and 2) tensioned at 300°C and 650°C samples.	97
7	The dependence of modulus increase measured at different temperatures on the number of cycles - top A: for a load amplitude 795 MPa; bottom B: for a load amplitude 320 MPa.	98
V.E.1	Deformation curves obtained at 30°C (solid lines) and 160°C (dashed lines) and various strain rates: $\epsilon_2 = 0.04 \times 10^{-3} \text{ sec}^{-1}$; $\epsilon_3 = 0.42 \times 10^{-3} \text{ sec}^{-1}$; $\epsilon_3 = 4.17 \times 10^{-3} \text{ sec}^{-1}$	99
2	The yield stress of PBT as a function of temperature and strain rate.	99
3	The dependence of the activation volume on the temperature.	

4	Force-temperature dependence for PBT film: without external constraint and with an applied stress of 16 MPa, 160 MPa and 290 MPa	100
5	The shrinkage force as a function of applied tension prior to annealing.	100
VI.B.1	Schematic of force-temperature apparatus.	111
VI.C.1	Force versus temperature profile for steel yarn (solid line = heating; dashed line = cooling).	112
2	a) Stress versus temperature profile for PBT heat treated yarn at 650°C for 8 seconds (solid line = heating; dashed line = cooling). b) Stress versus temperature profile for Kevlar® 49 yarn (solid line = heating; dashed line = cooling):	112
3	Stress versus temperature profile of Kevlar® 49 yarn 25 hours after the first heating cycle (solid line = undesiccated; dashed line = desiccated)	113
4	a) Stress versus temperature profile of as-spun PBT yarn (solid line = heating; dashed line = cooling). b) Stress versus temperature profile of Kevlar® 49 yarn (solid line = heating; dashed line = cooling).	113
5	Wide angle X-ray diffraction patterns of a) Kevlar® 29, b) FTC-Kevlar® 29 and c) Kevlar® 49	114

6	Wide angle X-ray diffraction patterns of PBT a) as-spun, b) FTC-PBT	114
7	Plot of T_T , temperature of onset of stress drop, versus applied stress for \circ = PBT (as-spun), \bullet = Kevlar [®] 29.	115

LIST OF TABLES

TABLE		PAGE
II.B.1	The Fiber Spinning Process	14
III.D.1	Melting Behavior of PBT/MSA.H ₂ O Crystal Solvates . .	39
2	Comparative Diffraction of PBT Fiber and Crystal Solvate.	39
IV.B.1	Properties of Sample Films	71
VI.C.1	WAXS Diffractiometric Data of As-Spun PBI (2855-50-2)	110
2	Mechanical Properties.	110

SECTION I: OVERVIEW

The goal of this project is to determine for rigid rod polymer fibers and films the relationships between mechanical properties and sample microstructures and to use this knowledge to obtain the maximum in strength and modulus for these materials. The fibers and films of poly(p-phenylene benzobisthiazole) (PBT) which have been investigated were produced at Celanese Research Corporation (Dr. E. C. Chenevey) from liquid crystalline solutions using a dry-jet wet-spin process for fibers and films. The PBT used in the study of crystal solvates was prepared by J. Wolfe of SRI.

Structural studies involved primarily optical microscopy, electron microscopy (both scanning and transmission) and wide angle x-ray scattering. Spectroscopic studies employed Fourier transform infrared spectroscopy to determine residual acid and water content in films as well as the parallel and perpendicular indices of refraction. Mechanical behavior was measured in uniaxial tension over a range of strain rates and temperatures. A special force-temperature apparatus permitted assessment of the thermal expansion coefficient of PBT.

The microstructural studies concentrated on the structure developed during the fast coagulation stage of the spinning process, as well as the structure obtained by slow coagulation of a quiescent isotropic polymer solution. The structure formed in the coagulation stage of the spinning process of poly(p-phenylene benzobisthiazole) fiber was examined by transmission electron

microscopy of epoxy impregnated fibers. An oriented network of microfibrils with typical fibril diameters of about 80-100A was observed. We suggest that these microfibrils are the fundamental structural elements of the fiber. Thus knowledge of the mechanism by which this initial structure is formed may allow for better control of final fiber properties.

Growth of crystal solvates in the PBT/MSA system was observed for the first time through the slow diffusion of water into the quiescent isotropic solution. Identification of the solid as at least one (and possibly two or three) solvate(s) was by diffraction and thermodynamic measurements. Upon observation under an optical microscope, negative spherulites from this system were observed. The tangential orientation of the rigid PBT chains in the spherulites indicated by the optical microscope were confirmed using an electron microscope for both direct visualization and diffraction studies of residual dried PBT.

The crystalline PBT left as a residue upon removal of the acid solvent was also investigated. Lamellae were observed whose thickness corresponds closely with the molecular length of the PBT used. The path dependent morphology of these samples was discussed and texturing of the PBT was described. For the first time a c axis projection electron diffraction pattern is obtained and reported. This represents the first significant departure from the unit cell obtained by Roche, et al., and points to the probability of polymorphism for PBT.

Phase behavior after the Ciferri and Krigbaum approach was investigated and a pseudo-binary schematic phase diagram for the PBT/MSA.H₂O system was presented. The relation of structure formation during fast and slow coagulation to

the phase diagram of a rigid polymer solution and to the kinetic mechanism of the phase transition was discussed in terms of nucleation and growth.

Spectroscopic measurements employed the attenuated total reflectance technique in conjunction with transmission infrared spectroscopy to quantitatively determine the residual water and acid content in poly(p-phenylene benzobisthiazole) films. It was shown that post-processing annealing, even with very moderate temperatures, can remove the water effectively. The acid was found mainly in the interior of the film. Post-processing annealing at high temperature can remove acid as well. But films exposed to such high temperature treatment do show new spectroscopic features suggesting that the polymer structures have been altered. Using the absorbance values measured by infrared irradiation, the birefringence of poly(p-phenylene benzobisthiazole) has been determined to be 0.88 ± 0.04 in the infrared region, a value much smaller than previously suggested, but close to that of poly(p-phenylene terephthalate).

The mechanical properties of PBT films feature an interesting temperature and strain rate dependence. The elastic modulus and yield behavior have been studied over a wide temperature range from 30°C to 650°C. The onset of a structural reorganization is observed at about 300°C. The dependence of yield stress on strain rate at different temperatures was examined in terms of the Eyring theory of an activated rate process. It was found that the stress activation volume varies with temperature. The overall elastic-plastic behavior as a function of temperature and strain rate was interpreted in terms of a previously suggested model that incorporates residual stresses in a rigid rod-like polymer.

Enhancement of modulus was also observed due to deformation of the films under elevated temperatures, where better molecular orientation and lateral ordering are achieved.

The force versus temperature behavior (at constant length) of poly-(p-phenylene benzobisthiazole) fibers (PBT) and Kevlar fibers was also investigated. Thermal expansion coefficients were $-1.1 \times 10^{-6}/^{\circ}\text{C}$ and $-3.2 \times 10^{-6}/^{\circ}\text{C}$, respectively, for heat treated PBT (PBT-HT) and Kevlar® 49. Kevlar® 49, PBT-HT, and steel fibers exhibit a linear thermal elastic behavior whereas Kevlar® 29 and as-spun PBT do not. Material changes which occur during heat treatment processing are detected in the force-temperature profile. A correspondence between thermal and mechanical energy input has been found to induce these material changes.

The following documents based on the above research have been published.

1. Y. Cohen and E.L. Thomas, Polym. Engr. and Sci. 25, 1093 (1985)
"Structure Formation During Spinning of Poly(p-phenylene benzobisthiazole) Fiber."
2. H.H. Frost, Master's Thesis, University of Massachusetts, September, 1984,
"Microstructure and Phase Behavior of Poly(Para-Phenylene Benzobisthiazole)/Methane Sulfonic Acid Crystal Solvates."
3. C. Chang and S.L. Hsu, J. Polym. Sci., Polym. Phys. Ed. 23, 2307 (1986)
"Spectroscopic Analysis of Poly(p-phenylene benzobisthiazole) Films."
4. L. Feldman, R.J. Farris and E.L. Thomas, J. Mat. Sci., to be published,
"Temperature and Strain Rate Dependence of the Deformation Behavior of Poly(p-phenylene benzobisthiazole)."
5. L.A. Pottick, S.R. Allen and R.J. Farris, J. Appl. Polym. Sci. 29, 3915 (1984).
"Force-Temperature Behavior of Rigid Rod Polymeric Fibers."

SECTION II: STRUCTURE FORMATION DURING SPINNING OF PBT FIBER

A. Introduction

High performance fibers obtained from lyotropic solutions of rigid polymers by the dry-jet wet spinning process have been a subject of much interest due to their excellent mechanical properties. The fiber spinning process involves several operations in which a polymer solution undergoes a succession of structural changes, leading to the final solid fiber, as outlined in Table II.A.1. In the coagulation stage a liquid to solid phase transition is induced, either by diffusion of a non-solvent or by a decrease in temperature. It is reasonable to assume that the structure formed by this phase transition is the basis for the structure of the final fiber. Thus, a better understanding of the possible equilibrium phases, the kinetic pathways between them, and their relation to the structure formed during coagulation may allow better control of the structure of the final fiber and its properties.

Poly p-phenylenebenzobisthiazole (PBT) is a rigid polymer from which high modulus, high strength fibers are spun (1,2). The object of this study is to describe the structure formed in the coagulation stage of PBT fiber spinning, prior to the drying process; an attempt is made to relate the formation of this structure to the phase diagram of a rigid-polymer solution and to possible mechanisms of phase separation.

B. Experimental Section

PBT (inherent viscosity of 18 in methane sulfonic acid, molecular weight about 25,000) was synthesized by J. Wolfe (3). A 5.6% w/w solution in

polyphosphoric acid (PPA) was spun through a 180 micron die, extended 2:1 in an air gap, coagulated in water at room temperature and kept subsequently immersed in water.

To preserve as much as possible the structure of the coagulated fiber during sample preparation for electron microscopy, a procedure for impregnating the wet fiber with Spurr epoxy resin (4) was used, as follows:

1. Gradual exchange of water to ethanol
2. Infiltration with Spurr resin
3. The impregnated fiber was mounted and cured in polyethylene capsules.

Longitudinal sections were cut using a Reichert ultramicrotome with a diamond knife. The cutting direction was done both parallel and perpendicular to the fiber direction.

The sections were viewed in a JEOL 100CX electron microscope, operated at 100 KeV.

C. Results and Discussion

A longitudinal section of a coagulated PBT fiber infiltrated with epoxy resin is shown in figure II.C.1. At low magnification (figure II.C.1a), the fibrillous appearing PBT is seen to be embedded in the epoxy resin. During longitudinal sectioning parallel to the fiber direction, the knife detached some fragments of the fiber from the section (arrows in figure II.C.1a). This allows imaging of the underlying fine structure with minimum interference from projection-overlap of the three dimensional structure onto the two-dimensional image. A higher magnification image of the thin part in the outlined area, with correct relative orientation, is given in figure II.C.1b. Dark longitudinal striations appear at low

contrast, each about 80-100/ in width, forming a highly oriented interconnected network in which junction points and branches can be observed. Electron diffraction patterns taken with a two micron selected area aperture from the inner portion of the sectioned fiber exhibit the characteristic PBT fiber diffraction pattern, as indexed by wide angle X-ray scattering from a wet fiber, as well as the diffuse ring characteristic of the amorphous epoxy resin. This gives evidence that the epoxy resin has infiltrated to within the PBT fiber. We interpret the structure shown in figure 1b as an interconnected network of highly oriented PBT microfibrils within a continuous epoxy matrix. The PBT microfibrils appear darker due to two contrast mechanisms. The density difference between PBT (1.5 gr/cm^3) and epoxy resin (about 1.0 gr/cm^3) results in stronger scattering of electrons by the microfibrils. In addition, due to the crystalline nature of the microfibrils, part of the intensity diffracted by them is blocked by the objective aperture used in obtaining the image.

On the basis of the electron-microscopic observation we conclude that the structure formed during the coagulation stage of PBT fiber spinning is an interconnected network of highly oriented microfibrils. We feel that the microfibrils are the fundamental structural elements of the final fiber. Their interconnectivity may be important for high tensile strength, and the width of the microfibrils may be related to the compressive strength of the fiber (5). Thus, an understanding of the phase transition leading to the interconnected microfibrillar morphology is desirable.

Several aspects of the phase diagram of a rigid polymer/solvent system may be relevant to the phase transition during coagulation. As the phase diagram of

the PBT/PPA system has not been determined fully, these aspects will be inferred to indirectly using a hypothetical phase diagram as shown in Figure II.C.2:

- a) Equilibrium between isotropic and nematic solutions was predicted by Flory (6) and verified in several experimental systems. Thus, a narrow biphasic region at negative polymer-solvent interaction parameter (χ) changes abruptly at a slightly positive value of χ to a wide region separating dilute isotropic and concentrated nematic phases. Tsai (7) observed such a narrow biphasic region in solutions of PBT in PPA, which shifted slightly to higher polymer concentrations at elevated temperature.
- b) A spinodal curve, marking the limit of metastability towards small concentration fluctuations, is plotted in the wide biphasic region. Wee and Miller (8) have shown, using Flory's theory, that the spinodal lies close to the binodal curve, thus allowing easy access into the unstable region by a decrease in temperature or increase in χ .
- c) Superimposed on the liquid-liquid phase equilibrium are liquid-solid transitions, as suggested by Ciferri and Krigbaum (9), due to the high melting point of the rigid polymer crystal. In addition to crystalline polymer, one or several crystal solvates form by cocrystallization of polymer and solvent molecules, as recently reviewed by Iovleva and Papkov (10). Formation of crystal solvates in the PBT/PPA system, under the influence of moisture, has been observed by Frost (11). The formation of one crystal solvate (XS) is included in Figure II.C.2.

The state of the solution as it enters the coagulation bath can be assumed to be a single nematic domain, with the molecular director in the direction of flow, irrespective of whether the original solution was isotropic or composed of randomly oriented nematic domains. This is a result of the shear stresses in the spinnerette and extensional flow in the air gap. At the end of the coagulation stage the thermodynamic state is that of crystalline polymer, in the form of a microfibrillar network permeated by the coagulant. The aspects of the phase diagram most relevant to the coagulation process are:

a) Liquid-solid equilibria between the nematic phase and one or more crystal solvates or crystalline polymer,

b) Liquid-liquid phase separation in the wide biphasic region. This region may be metastable relative to the liquid-solid transitions, yet it may be accessible for kinetic reasons.

Coagulation is a non-equilibrium process. Treatment of this process in terms of a binary phase diagram requires two assumptions:

a) The ternary polymer/solvent/nonsolvent system can be viewed as a pseudo-binary solution, with an apparent χ parameter which depends on the amount of nonsolvent present.

b) Local equilibrium is maintained.

Russo and Miller (12) considered the effect of a nonsolvent on the phase diagram of a rigid polymer solution, and showed that the assumption of a pseudo-binary solution is valid in the narrow biphasic region, although significant deviations occur at the wide biphasic region. They demonstrate that a small quantity of nonsolvent can dramatically increase the apparent χ parameter of the solution and induce phase separation. We assume that the structure formed during coagulation is highly dependent on the mechanism of the phase transition which occurs at the initial stage of nonsolvent diffusion. At such stage the assumption of local equilibrium may be valid. At later stages of coagulation, the solvent is essentially replaced by nonsolvent, but the main morphological features of the fiber may not be changed.

Several attempts have been made to relate a specific morphology to a mechanism of phase separation. Morgan et al., (13) studied the structure of poly p-

phenylene-terephthalamide (PPTA) fibers formed by dry-jet wet spinning. They suggest that the main phase transition determining the structure is crystallization of PPTA from its solution as a result of a decrease in temperature, prior to the diffusion of the coagulant. A row nucleation mechanism is proposed by which extended chains crystallize parallel to each other to form lamellae perpendicular to the fiber direction with a high concentration of chain ends in the interlamellar region. Iovleva et al., (14) observed the morphology obtained by addition of nonsolvent to a rigid polymer solution. They associate solidification under the effect of a weak coagulant, which leads to a lamellar morphology, with a nucleation and growth crystallization mechanism by which crystal-solvates are formed initially, and their lamellar morphology is preserved during further coagulation and subsequent drying. A fibrillar morphology, obtained by the effect of a strong coagulant, is associated with direct crystallization of the polymer. Miller et al., (15) studied in detail gelation of poly γ -benzyl-L-glutamate solutions from both isotropic and anisotropic phases, and demonstrated that the structure of the gel is a fibrillar network (16). Formation of the network is associated with passage to an unstable state in the wide biphasic region. Phase separation by spinodal decomposition is postulated to occur, resulting in a bicontinuous system of dilute isotropic and concentrated anisotropic phases. Crystallization of the polymer from the concentrated ordered phase, now well below its melting point, results in an interconnected fibrillar morphology.

In considering the mechanism of structure formation during coagulation of PBT, the fibrillous nature of the observed morphology excludes mechanisms which lead to lamellar structures, such as row nucleation. The initial state of the

solution, a monodomain nematic phase, is different than those studied by Miller et al., (15,16) which are either isotropic or randomly oriented liquid crystalline domains. The applicability of their model of network formation to coagulation during fiber spinning is not clear. We have considered the mechanisms of spinodal decomposition and nucleation and growth in a solution of oriented rigid polymers, and their relation to the structure of the phase separated state. Due to the inherent rigidity and relatively high molecular weight of the PBT molecules, polymer and solvent mobility is expected to be anisotropic, being much larger in the orientation direction than perpendicular to it. For simplification, the mobility is assumed to be one dimensional in the orientation direction. A schematic representation of the Cahn-Hilliard model of spinodal decomposition (17), as applied to oriented rods with one-dimensional mobility, is compared to one-dimensional nucleation and growth in Figure II.C.3. In the case of spinodal decomposition, a concentration fluctuation of a specific wavelength will have a maximum rate of growth (17). As the mobility is assumed to be one dimensional, only concentration fluctuations in the direction of molecular orientation are considered. Growth of such a fluctuation leads to regions of high concentration of rods, perpendicular to the orientation direction, with depletion zones between them. The length of the polymer rich regions perpendicular to the orientation direction, may be controlled by the correlation length of concentration fluctuations in that direction. Crystallization from such a phase separated system may result in a lamellar morphology. A one-dimensional nucleation and growth mechanism may be associated with formation of fibrils. Fibril width may be controlled by the density of nuclei, and deviations in the molecular orientation may account for their interconnectivity.

D. Conclusions

1. The structure formed during the coagulation stage of the dry-jet wet spinning process of PBT fibers is shown to be an interconnected network of oriented microfibrils, the width of which is 80-100/. These microfibrils may be the fundamental structural elements of the final fiber.

2. A schematic comparison of the mechanisms of spinodal decomposition and nucleation and growth, as applied to an oriented solution of rods with essentially one-dimensional mobility suggests that the former mechanism may lead to a lamellar morphology, whereas the latter may result in oriented fibrils, which is compatible with the structure observed in coagulated PBT.

References

- (1) S.R. Allen, A.G. Filippov, R.J. Farris, E.L. Thomas, C.P. Wong, G.C. Berry and E.C. Chenevey, *Macromolecules* 14, 1135 (1981)
- (2) S.R. Allen, A.G. Filippov, R.J. Farris and E.L. Thomas in "The Strength and Stiffness of Polymers", A.E. Zachariades and R.S. Porter, eds., Marcel Dekker, New York (1983)
- (3) J.F. Wolfe, B.M. Loo, and F.E. Arnold, *Macromolecules* 14, 915 (1981)
- (4) A.R. Spurr, *J. Ultrastruct. Res.* 26, 31 (1969)
- (5) S.J. DeTeresa, R.S. Porter and R.J. Farris, in press
- (6) P.J. Flory, *Proc. Royal Soc. London*, A234, 73 (1956)
- (7) H.H. Tsai, Ph.D. Thesis, Carnegie-Mellon University, Pittsburgh (1983)
- (8) E.L. Wee and W.G. Miller, in "Liquid Crystals and Ordered Fluids", Vol. 3, J.F. Johnson and R.S. Porter, eds., Plenum Press, New York (1978)
- (9) A. Ciferri and W.R. Krigbaum, *Mol. Cryst. Liq. Cryst.*, 69, 273, (1981)
- (10) M.M. Iovleva, S.P. Papkov, *Polymer Science U.S.S.R.*, 24, 236 (1982)
- (11) H. Frost, M.Sc. Thesis, University of Massachusetts, Amherst (1984)
- (12) R.S. Russo and W.G. Miller, *Macromolecules*, 17, 1324 (1984)
- (13) R.J. Morgan, C.O. Pruneda and W.J. Steele, *J. Polym. Science, Polym. Phys. Ed.*, 21, 1757, (1983)
- (14) M.M. Iovleva, S.I. Banduryan, *Polym. Sci. U.S.S.R.*, 22, 2758 (1980)
- (15) W.G. Miller, L. Kou, K. Tohyama, V. Voltaggio, *J. Polym. Sci., Polym. Symp.* 65, 91 (1978)
- (16) K. Tohyama, and W.G. Miller, *Nature*, 289, 813, (1981)
- (17) J. W. Cahn, *J. Chem. Phys.* 42, 93 (1965)

TABLE II.A.1

THE FIBER SPINNING PROCESS

<u>Operation</u>		<u>State of Matter</u>
1) Preparation of dope		Isotropic or unoriented nematic solution
2) Extrusion through die	}	Solution of oriented rods
3) Extension in air gap		
4) Coagulation		Liquid-Solid phase transition
5) Post treatments (drying, heat treatment)		Oriented solid Fiber

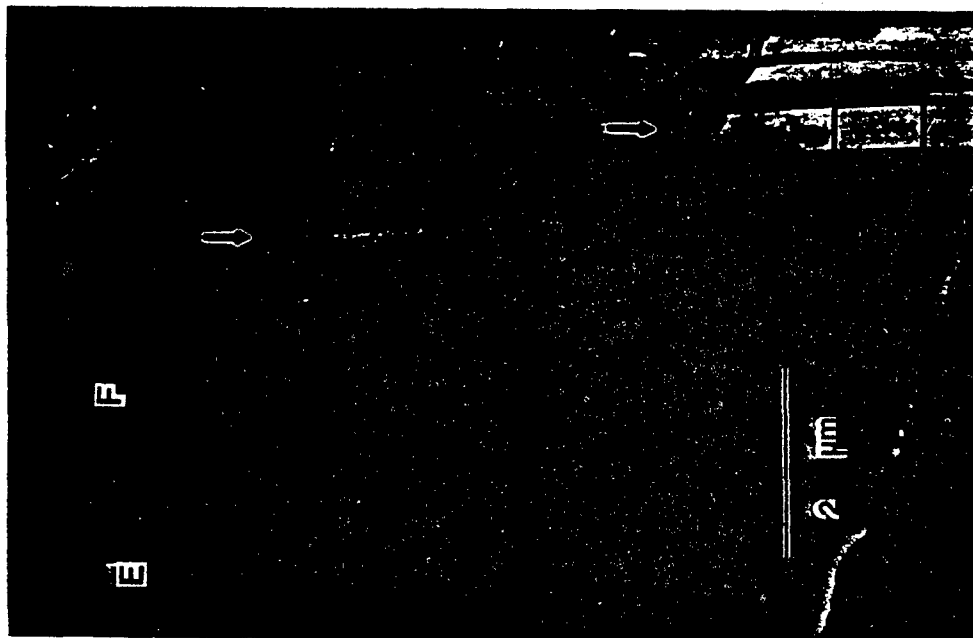


Figure II.C.1.a
A longitudinal section of coagulated PBT
fiber infiltrated with epoxy resin.
E-epoxy matrix; F-fiber.



Figure II.C.1.b.
A high magnification image of the
outlined area.

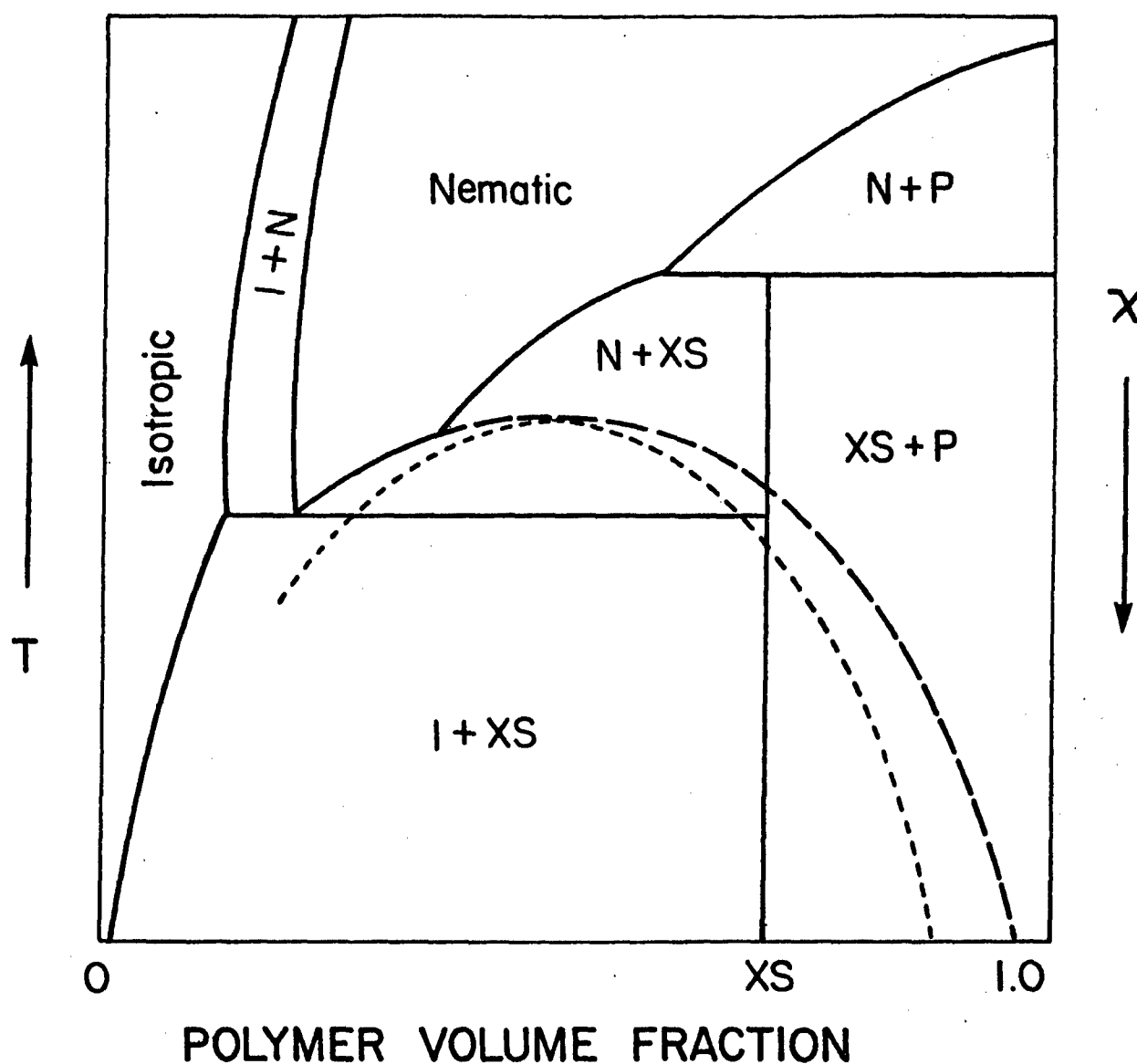
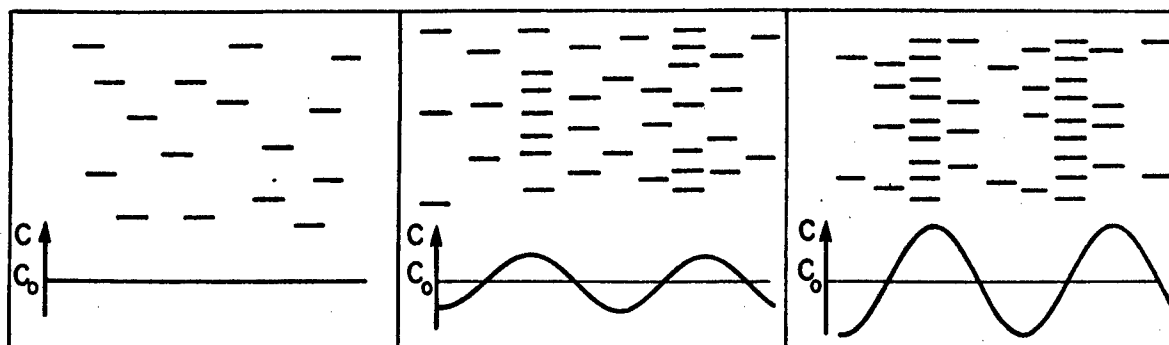


Figure II.C.2

A schematic phase diagram of a rigid polymer solution: solid line - phase boundary; dashed line - incongruent phase boundary; dotted line - spinodal curve; XS - crystal solvate; P - crystalline polymer.

SPINODAL DECOMPOSITION



NUCLEATION AND GROWTH

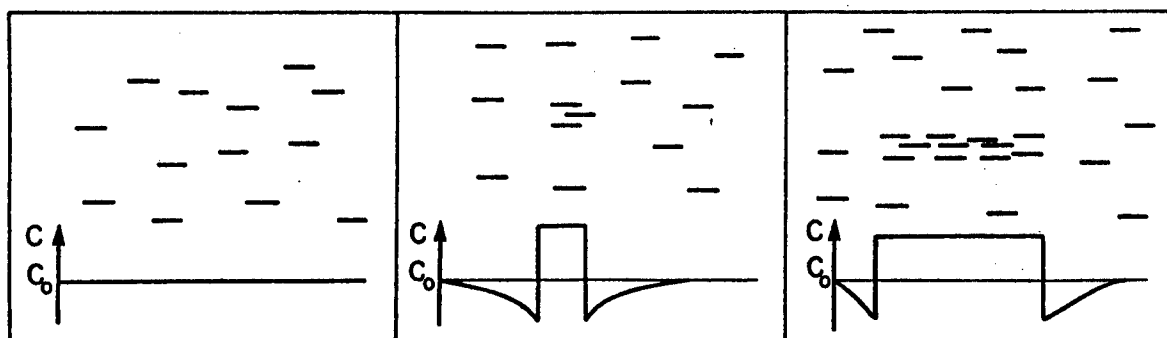


Figure II.C.3

Comparison of spinodal decomposition and nucleation and growth in a solution of oriented rods undergoing a phase transition with effectively one-dimensional mobility. c - polymer concentration, c_0 - composition of initial solution.

SECTION III. MICROSTRUCTURE AND PHASE BEHAVIOR OF POLY(PARA-PHENYLENE BENZOBISTHIAZOLE)/METHANE SULFONIC ACID CRYSTAL SOLVATES

A. Introduction

The study of rigid rod macromolecules has received increasing attention in recent years due primarily to the fabrication of ultra-high modulus, ultra-high strength fibers and films from these materials. These polymers frequently exhibit unusually good thermo-oxidative stability and resistance to most common solvents.

Poly(p-phenylene benzobisthiazole) is a fully aromatic rigid rod polymer. Its properties have improved to a point of superiority among ultra-high strength ultra-high modulus fibers. Tension heat treatment as a last stage of processing has proven to be a most significant step in the attainment of the highest possible properties to date. Investigations of PBT have generally focused on two areas, either properties in solution or properties of the solid-state fiber or film. Only recently has the as-coagulated wet fiber been examined, and to date no thorough study linking the solid state and solutions through phase behavior has been performed. The solvent used in this study was methane sulfonic acid (MSA). The formation of the crystal solvate was induced by the diffusion of the atmospheric water into the system.

The purpose of this investigation is to characterize the structure and microstructure of quiescently crystallized crystal solvates, to examine the crystalline polymer remaining upon removal of solvent from the solvate, and to relate these structures to the phase behavior of the PBT/MSA.H₂O system. Due to the excellent mechanical properties of PBT, crystal solvates should be of interest from a technological viewpoint to the extent that they affect the properties and processing of the final polymer product.

B. Background

Polymer crystal solvates belong to the class of crystalline compounds whose lattice contains both solvent and solute in particular molar ratios. The most well known compounds of this type are the low molecular weight hydrates. That polymers form crystal solvates is not well known, although neither is it surprising. Bimolecular crystalline compounds arise from interactions such as hydrogen bonding or attractions between acidic and basic groups. That these interactions between a polymer and its solvent would give rise to a bimolecular crystalline formation is not unusual behavior. One of the reasons that little attention has been paid to these formations is that the majority of polymer processing takes place through the bulk melt phase, not through solution. For cellulose/sodium hydroxide systems several crystal solvates of different stoichiometry have been observed, although they were simply described as swelling compounds (1). With the advent of the aromatic polyamides, solution processing of another important class of polymers has become a significant industrial process. Not surprisingly, in recent years the number of instances where polymer crystal solvates have appeared in the literature has greatly increased, in conjunction with the increased interest in solution processed polyamides. Iovleva and co-workers performed an extensive review of the literature in 1982 (2).

Evidence for the existence of polymer crystal solvates has been primarily by scattering and thermodynamic measurements. X-ray diffraction of polymer crystal solvates reveals unit cells which are expanded from those of the pure polymer.

The thermodynamic measurements generally involve observation of a melting transition. Melting phenomena are experimentally observed in several ways. Polarizing optical microscopy shows the melting of birefringence crystal solvates into isotropic or anisotropic solutions. Differential scanning calorimetry also gives melting transition data, although it is often experimentally difficult to obtain due to the corrosive nature of the solvents. Finally, turbidity measurements have been used to determine the melting point of the PPTA/H₂SO₄ crystal solvates (3).

Poly(p-phenylene benzobisthiazole) is a fully aromatic rigid rod polymer. Its persistence length in chlorosulfonic acid has been determined to be 640 angstroms (4). The PBT fibers investigated possess a high degree of axial orientation. Near perfect molecular alignment in the fiber direction has been shown by wide angle x-ray and electron diffraction studies. However true, three-dimensional order has not yet been achieved in any PBT fiber examined. Early diffraction studies done on as-spun PBT fibers were explained by a hexagonal packing of axially staggered periodic cylinders. Upon heat treatment, the molecular order in the PBT fiber is enhanced and a two-dimensional net allowing the molecules translational freedom along the chain axis explains the diffraction data. It has yet to be shown whether or not true large-scale three-dimensional order is possible for PBT. Minter has shown the crystallite size in tension heat-treated PBT fibers to be 100 angstroms by 150 angstroms (lateral and longitudinal dimensions, respectively). Previous investigation of PBT coagulated from solution in the absence of shear has been limited. However for poly(p-phenylene benzobisoxazole) (PBO), another fully aromatic rigid rod

polymer, Minter observed a fibrillar "grassy mat" in films prepared in this way (5). He did not, however, investigate them any further to determine molecular orientation within the fibrils.

Takahashi has done the most extensive work on PPTA crystal solvates using both sulfuric acid and hexamethyl phosphorous triamide (HMPTA) as solvents. He found that at concentrations higher than 11% at room temperature, the PPTA/ H_2SO_4 system formed a solid anisotropic phase. Optically negative spherulites were observed. Upon removal of solvent and observation under an electron microscope he observed 600 angstrom lamellae. The chain axis of the polymer was found to be perpendicular to the long axis of the lamellae (6). Takahashi does not confirm the crystal solvate nature of his solid anisotropic state; however, Platonov (7) and Iovleva (8) have independently confirmed the crystal solvate nature of the PPTA/ H_2SO_4 anisotropic solid by x-ray diffraction.

The phase behavior giving rise to polymer crystal solvates is an outgrowth of theoretical phase behavior of rigid rod solutions. Onsager (9) and Isihara (10) independently predicted the possibility of liquid-liquid phase separation of solutions of anisotropic molecules. Their treatment was improved upon and simplified by Flory. He used a lattice model to predict the phase behavior (11). His results have since been experimentally verified by others.

Ciferri and Krigbaum extended this phase behavior to include the crystallization of the polymer. By overlaying curves for crystallization from an isotropic solution and crystallization from an anisotropic solution, into the Flory phase diagram, they obtained the phase diagram shown in Figure III.B.1

(12). Others have since included crystal solvates which give a schematic phase diagram as shown in Figure III.B.2 (2). A partial phase diagram including crystal solvates has been obtained by Gardner et al., (13) for the PPTA/H₂SO₄ system.

Miller has shown that treating a solvent and non-solvent as a single component is an appropriate assumption in the biphasic chimney region (14). However, it is not clear whether this assumption is viable in other regions. The reason for making this assumption is to aid in the kinetics of crystal growth. If one is in the isotropic solution region of the phase diagram at room temperature, a phase boundary can be crossed either by increasing the polymer concentration or by decreasing the temperature. Either course of action severely impedes chain mobility. Alternatively one can label the ordinate as $-x$ and cross the phase boundary by increasing the parameter by slight absorption of non-solvent, in this case water. Miller has shown that even a slight addition of non-solvent has a drastic effect on the location of the phase boundary (14). Because of the ease of working with a binary phase diagram, and because of the improved kinetics when working at low concentrations at room temperature and above, this assumption and approach were made.

C. Experimental

1. Materials

The PBT used was prepared by J. Wolfe of SRI via a step growth polymerization of 2,5 diamino-1,4 benzenedithiol; hydrochloride and phthalic acid conducted in poly(phosphoric acid). The polymer possessed an intrinsic viscosity of 2.0 in MSA. Crosby et al., calculated the molecular weight (M_n) of this

polymer to be about 10,000 (4). Since the monomer repeat molecular weight is 266, this corresponds to a molecular length of about 470 angstroms.

The solvent used was methane sulfonic acid from Aldrich Chemical Company.

2. Sample Preparation

The methane sulfonic acid as received contains about 1.5% water. This was purified using a vacuum distillation apparatus. Increments of PBT powder were added into the acid at room temperature, the polymer being used as received. Each incremental amount of PBT was dissolved before the next was added. For the purposes of this study, samples of two to three milliliters of isotropic solution were prepared, generally to a concentration of two to five percent polymer. These solutions were the starting point for all samples studied.

A cleaning solution for the glassware was made. Seventy grams of sodium dichromate were dissolved in 300 milliliters of water. Six hundred milliliters of sulfuric acid was then added. Glass slides and cover slips were placed into a beaker of this solution for about one hour at 60 degrees Celsius. Upon removal they were rinsed in copious amounts of water, the final rinsings being done with deionized water.

A drop of solution was then placed on the clean dry slide and a clean dry cover slip was placed over the drop. Water diffusing in from the atmosphere induced the growth of the crystal solvate spherulites (e.g. Figure III.C.1). After two to three days, sufficient water had diffused in to complete the phase separation into crystal solvate and dilute isotropic solution. The crystal solvate was then scraped from the slide into a DSC pan, or alternatively was placed onto a hot stage of an optical microscope.

For X-ray work the PBT/MSA solution was put into an X-ray capillary and the top was left open to air. As water diffused in the crystal solvate, spherulites were induced to growth in the capillary. After several days the crystal solvate was grown and the capillary was sealed and X-ray diffraction was performed.

For electron microscopy the crystal solvates were melted (in the 90 to 100 degrees C range) and the now isotropic solution held at about 150 degrees C. As solvent was driven off, the solution went biphasic and new crystal solvate spherulites were observed to nucleate and grow. Once the crystal solvate was grown (a crystal solvate of different stoichiometry than that which melted at 90 degrees C) the cover slip and glass slide were split apart and the crystal solvate floated off onto water (e.g. Figure III.C.2). This material was allowed to stand for several minutes and then picked up with gold microscope grids in order to avoid reaction of residual acid with copper grids. The sample was dried at room temperature and observed in the electron microscope. It was characteristic of these polymer spherulites that they had such high birefringence that a sample thin enough to be used for electron microscopy was easily observable in the polarized optical microscope.

3. Electron Microscopy

A JEOL 100CX electron microscope operated at 100KV was used. Both bright field and dark field microscopy were performed in the conventional transmission mode. The diffraction data was generally collected using selected area diffraction. Preliminary studies of crystal solvate crystals were performed using micro-diffraction in the STEM mode. The radiation lifetime of PBT, following an

exponential decay to $1/e$ of original intensity of crystalline reflections, was determined by Minter to be 1.6 coulombs per square centimeter or about two orders of magnitude greater than that of polyethylene. This stability allowed considerable latitude in selection of microscope imaging conditions.

An ETEC scanning electron microscope was used at 40KV for the SEM studies of samples sputter coated with gold.

4. Optical Microscopy

A Zeiss polarizing microscope was used in conjunction with a Mettler FP-2 hot stage and a Leitz polarizing microscope was used with a Leitz hot stage. Heating was generally done at a rate of 5 degrees C per minute. A quartz quarter waveplate was used to determine the sign of birefringence of the spherulites, direct comparison being made to optically negative poly(ethylene oxide) (PEO) spherulites.

5. X-Ray

Wide angle X-ray diffraction was performed with a flat-film Statton camera using CuK X-rays. Samples were flame sealed. Settings were 30KV and 40mA for exposure times of 4 to 10 hours. Sample to film distance was 53.14mm.

6. DSC

A Perkin-Elmer DSC-2 was used for the calorimetry experiments, with indium and tin used for calibration purposes. The heating rate used was 10 degrees C per minute and a range of 10mcal. Reuseable gold plated stainless steel sample pans for volatile corrosives were used to prevent the MSA from corroding either the pan or the calorimeter.

D. Results and Discussion

1. Results

The identification of the solid formed upon diffusion of water into the polymer/acid solution as crystal solvate involved two forms of evidence: melting transition(s) and expanded unit cell.

Figure III.D.1 shows the DSC trace for the PBT/MSA.H₂O crystal solvate. In the corresponding temperature region the pure polymer has no thermal transitions. On the optical microscope we observed three melting transitions - the first at 90 to 100 degrees C, the second at 135 to 200 degrees C and the third varied from 200 to 300 degrees C. Table III.D.1 shows the relationship between the melting temperature observed optically and by DSC. The first two melting transitions correlate well. The discrepancy in the third melting temperature can be explained by the difference in the system for DSC and optical microscopy. For DSC the system is closed. The sample pans are sealed, allowing no escape of fuses. For optical microscopy, the sample was open to the atmosphere at the edge of the cover slip. White vapors were observed to escape at temperatures approaching 180 degrees C and above. Since the system consists of solvent and polymer, increasing the concentration of polymer by removal of solvent would tend to increase the equilibrium melting transition of the system. The time dependence of the melting transition at elevated temperature is supported by the fact that at very fast heating rates (ca. 30 degrees C per minute) the melting range is observed to be 200 degrees C to 220 degrees C. At very slow heating rates (ca. 2 degrees C per minute) the melting temperature was in the region of

295 to 305 degrees C. The slower the heating rate, the longer the time available for solvent to be driven off. This same effect is consistent with the slightly expanded range of the first melting transition.

The diffraction data in Table III.D.2 shows the expanded unit cell characteristic of crystal solvates. Figure III.D.2 is the flat film Statton photograph of the crystal solvent.

The spherulitic nature of these crystal solvates is clearly shown in the optical micrographs in Figure III.D.3. The typical Maltese cross-extinction pattern is shown under crossed polars. Washing and drying the spherulites followed by observation under a scanning electron microscope clearly confirms the spherulitic nature of the solid (e.g. Figure III.D.4).

Study of the PBT/MSA.H₂O crystal solvates confirmed several aspects of the schematic phase diagram given previously in Figure III.B.2. Melting behavior of the crystal solvates was followed by optical microscopy. Figure III.D.5 shows a sequence of photographs taken with increasing temperature. Each isolated area can be treated as a micro system. This has the disadvantage of not knowing the precise composition of each region but, assuming heat transport is greater than mass transport, it allows the effect of temperature on a pseudo-equilibrium state to be followed simultaneously in several different regions. The first area to melt, as expected, is the area in communication with the droplet of solvent, and it is observed to melt into an isotropic solution. This corresponds to melting along path 'a' in Figure III.D.6. (Figure III.D.6 represents a partial phase diagram showing the low polymer concentration region.) Then the surrounding area which is not in communication with the isotropic drop melts

into an anisotropic solution. This corresponds to heating along path 'b' in Figure III.D.6b. Finally at steady state temperature of 117 degrees C three different types of micro systems are observed: isotropic, anisotropic and biphasic. This shows that the chimney region of the phase diagram is indeed above the crystallization boundary and not below it (e.g. Figure III.D.6a). This helps to explain the following observations: if the crystal solvates are melted into an isotropic solution (path 'c' of Figure III.D.6b) and then cooled, the chimney region into the anisotropic region is crossed, for example, path 'c' of Figure III.D.6b. With cooling to room temperature the anisotropic solution is metastable with respect to crystal solvates, and phase separation along the tie line shown to crystal solvate plus isotropic solution ensues (e.g. Figure III.D.7). The growth of the spherulite follows the typical stages of maturity and a brush type hedrite structure is shown in Figure III.D.8.

Elucidation of the microstructure of the crystal solvate spherulites was complicated by the corrosive nature of the methane sulfonic acid. Utilization of a quartz quarter wave plate in a polarized optical microscope, and comparison with PEO optically negative spherulites, shows that the PBT crystal solvate spherulites were optically negative. This means that the tangential index of refraction is greater than the radial, indicating tangential orientation of the rod-like PBT molecules. Direct electron microscopy of the crystal solvates was not possible due to the highly corrosive nature of the solvent and the high vacuum of the electron microscope. Instead the MSA was first leached out by floating the spherulites off the glass slide onto water. After the acid was

removed, the sample was picked up with grids and viewed in the electron microscope. The tangential orientation of the chains was confirmed by electron diffraction of an area of radiating lamellae as shown in Figure III.D.9.

The crystalline nature of the lamella of the residual PBT is shown in the bright field pair shown in Figure III.D.10. The lamellar thickness measured from the micrographs is about 450 angstroms, with the long period being about 700 angstroms. This scale corresponds reasonably with the average molecular length determined by Crosby et al., for PBT of I.V. 2.0. The question of what is in the interlamellar region in a polymer that is essentially 100% crystalline is an interesting one. Gardner proposes a model for PPTA fibers which has a high concentration of chain ends in the periodic bands first observed by Dobb et al., (15,16). In our system the close correspondence of molecular length to the lamellar thickness suggests a similar model. A schematic of this type of morphology is shown in Figure III.D.11. Aggregation of chain ends in the interlamellar region would be favored for low I.V. PBT. According to the synthetic route proposed by Wolfe, et al., (17) we see that poly(phosphoric acid) would be covalently bonded to the ends of the molecules. Closer examination of these micrographs reveals that the film fracture generally takes place perpendicular to the lamellae, or alternatively, between them. Since the chains run perpendicular to the lamellae, fracture between lamellae is further evidence of a high concentration of chain ends in the interlamellar regions.

The texturing in these lamellae is observable through electron diffraction. For a PBT fiber a typical equatorial intensity profile would appear as in Figure

III.D.12. The peaks e1 - e4 are as indicated. The presence of all of these reflections in electron or X-ray diffraction with their relative intensities is generally evidence of fiber symmetry.

In these spherulites of PBT, however, a variety of diffraction patterns consisting of e1 - e4, e1 and e2, just e2, and e2 and e3, with their relative intensities, have all been observed. Upon tilting the sample, the pattern is shown to change with e1 appearing and disappearing with various degrees of tilt (e.g. Figure III.D.13). This indicates there is no fiber symmetry, but rather locally preferred a axis and b axis orientations. Further evidence for texturing is found in the micrographs of Figure III.D.10. In bright field, the lamellae appear as continuous structures, whereas the dark field micrograph shows individual crystallites about 150 angstroms in width by 450 angstroms in length.

Figure III.D.14 shows a lamellar region of a PBT spherulite, very similar in appearance to Takahashi's PPTA lamellae. A fine structure running perpendicular to the lamellae can be seen to run across the tear in the film. For the sake of comparison, Figure III.D.15 shows a "grassy mat" prepared by rapid coagulation of an isotropic PBT/MSA solution into water, similar to what Minter reported for PBO (5).

One other feature of the PBT lamellae spherulites is that electron diffraction down the c axis has been observed for the first time (e.g. Figure III.D.16). The angle (γ) between the e1 and e2 reflection is about 109 degrees which is not consistent with the monoclinic unit cell with γ equal

to 95.2 degrees proposed by Roche (18). The e3 and e4 reflections are also present, but very weak: e3 at an angle of about 20 degrees from the e2 reflection and e4 being the second order e1 reflection.

2. Discussion

Conclusive proof for the existence of PBT crystal solvates has been presented. The melting transitions observed by DSC and optical microscopy, coupled with the X-ray diffraction pattern of the anisotropic solid, show that a crystalline solid(s) containing both polymer and solvent is (are) formed in this system. The existence of two strong melting transitions and a weaker third transition, all observed both by DSC and optical microscopy, give evidence for the existence of at least one and probably two or three crystal solvates.

Upon removal of the solvent, the optically negative crystal solvate spherulites remain optically negative. This is indicative of retention of the gross morphology upon transformation from crystal solvate to crystalline polymer. The crystalline polymer is highly ordered as revealed by observation under the electron microscope. It seems reasonable that the existence of lamellae in the crystalline polymer point to the existence of lamellar forms in the crystal solvate spherulites.

Examination of the electron diffraction patterns obtained from the PBT spherulites reveals a highly textured morphology. The existence of the individual crystallites in the dark field micrograph of the continuous lamellae in Figure III.D.10 supports this. Specific reasons for why the lamellae are broken by sections in the Bragg condition and out of the Bragg condition are not understood. It is, however, a feature that is not exclusive to PBT, but is also

found in polyethylene (20) and PPTA (6). Whether or not this is related to the 100 angstrom striations observed in Figure III.D.14 is not clear. The sample preparation of the electron microscopy grids involved the placing of the crystal solvate in equilibrium with an isotropic solution into water. Since rapid coagulation of PBT solutions gives rise to a fibrillar mat, these striations may be a result of the coagulation of the remaining isotropic solution. However, they run more or less parallel to each other and are not randomly oriented as they would be in a coagulated film. One thing is clear: the final morphology of PBT is highly path dependent. Very slow diffusion of limited amounts of water leads to lamellar crystal solvate spherulites, which, when washed, leave crystalline lamellar PBT spherulites. Very rapid addition of copious amounts of water to PBT solutions yields fibrillar polycrystalline mats of PBT.

The phase behavior of this system is consistent with the schematic given by Iovleva. Because there probably exist at least two crystal solvates, however, the schematic must be modified slightly. The phase boundaries of the chimney region for PBT in MSA were obtained by Tsai (21). Proper adjustment for the different MW they used shifted the chimney to the right for our study according to the relationship $V2^* = 8/x(1-2/x)$, where x is the aspect ratio and $V2^*$ is the characteristic concentration for the appearance of the chimney region. The observation of melting at 90 degrees C, together with nematic to isotropic clearing at elevated temperatures, indicates the chimney region occurs at higher temperatures than the crystal solvate and therefore nematic solutions can occur at equilibrium. However, the fact that the higher melting crystal solvates melt into isotropic solutions indicates that the chimney region curves and crosses the crystallization curves.

Ciferri and Krigbaum's theoretical work supposes an equilibrium with crystalline polymer. Their treatment is even more applicable to polymeric systems with the inclusion of crystal solvates. Lower melting transition temperatures and heats of fusion would be true of crystal solvates as compared with crystalline polymer. We have shown here that a treatment of the phase behavior by superposition of liquid-liquid and liquid-crystal phase diagrams helps to explain the observations in the PBT/MSA.H₂O system.

Understanding of this type of phase behavior can help to explain some of the experimental observations in the literature. Sasaki et al., have studied the PBLG/BA system (22). They have observed two gels, A and B, of different stoichiometric polymer/solvent ratios. Experimentally, the B type gel is obtained by repeated quenching from 60 degrees C to below 48 degrees C. This puts the system in an unstable state, with regard to the equilibrium crystal or crystal solvate, but also with respect to the liquid-liquid phase diagram. Liquid-liquid phase separation is kinetically favorable and gives an anisotropic solution of composition that must be greater in polymer than that of the crystal solvate, not to precisely the crystal solvate composition as claimed. This is unstable with respect to crystalline polymer and crystal solvate, so phase separation to these two solid forms occurs. Heating to 60 degrees C melts the crystal solvate while the crystalline polymer retains its solid form. Quenching again gives the same behavior of liquid-liquid phase separation followed by solid-solid phase separation of the anisotropic solution. Thus B gel grows at the expense of A gel. The observations of Sasaki et al., are more easily interpreted using this type of treatment of phase behavior.

Inclusion of crystal solvates in the Ciferri-Krigbaum phase relationship enables significantly better understanding of the experimental observations in the present PBT work, as well as in other systems such as PBLG/BA.

3. Conclusions

Growth of crystal solvates in the PBT/MSA system has been accomplished for the first time through the diffusion of water into the system. Identification of the solid as crystal solvate was accomplished by diffraction and thermodynamic measurements. In this way, evidence for the existence of at least one and possibly two or three crystal solvates has been obtained.

Upon observation under an optical microscope negative spherulites from this system were observed. The tangential orientation of the rigid PBT chains in the spherulites indicated by the optical microscope were confirmed using an electron microscope for both direct visualization and diffraction studies of residual dried PBT.

The crystalline PBT left as a residue upon removal of the acid solvent was also investigated. We observed lamellae whose thickness corresponds closely with the molecular length of the PBT used. The path dependent morphology of these samples was discussed and texturing of the PBT was described. For the first time a c axis projection electron diffraction pattern is obtained and reported. This represents the first significant departure from the unit cell obtained by Roche et al., and points to the probability of polymorphism for PBT.

Phase behavior after the Ciferri and Krigbaum approach is investigated and a pseudo-binary schematic phase diagram for the PBT/MSA.H₂O system is presented.

E. Future Work

The work that has been presented here, coupled with some preliminary observations noted below, suggests several avenues for subsequent investigation.

The unit cell of PBT previously obtained by Roche, et al., (18) was obtained by fiber diffraction perpendicular to the chain axis. Calculations from the intensities of the equatorial and layer line reflections were used to obtain the value for gamma of 95.2 degrees (18). Attempts by Minter to stack films and view the c axis by x-ray diffraction were inconclusive (5). No electron diffraction data has previously been obtained viewing down the c axis. The low MW of the PBT used in this study, along with the path of crystal formation, allowed this type of diffraction data to be obtained (e.g. Figure III.D.16). The difference in sample history is consistent with polymorphism. However, the reflections are not sharp enough to allow determination of gamma closer than plus or minus 5 degrees. We expect that through further study of crystalline PBT crystallized through the crystal solvate intermediate, better diffraction data can be obtained directly. This data, along with data from tilting about the c axis should give a well-defined unit cell and crystal structure for PBT crystallized in this way.

While, generally, solvent was washed out of the samples used in electron microscopy, occasionally diffraction patterns were obtained that were clearly not PBT, but rather a crystal solvate of PBT (e.g. Figure III.E.1). Further work along these lines would enable the crystal structure of the crystal

solvate to be determined, provided the stoichiometric ratio of PBT to MSA was also ascertained. Since more than one PBT/MSA crystal solvate is believed to exist, it would be useful to ascertain the crystal structure of each type.

Characterization of the polymorphs of the crystal solvate would be helpful in knowing if, after washing, the residual PBT also exhibits polymorphism. Growth of PBT/MSA crystal solvates includes growth from isotropic, anisotropic and biphasic regions (e.g. Figure III.E.2). The path dependency of the morphology could be investigated by examining the crystal solvates grown from each phase.

It was also observed by optical microscopy that PBT dissolved in PPA and very slowly precipitated in ortho phosphoric acid produced an orange solid that melted at 70 degrees C into an isotropic solution. Upon standing it was observed to crystallize from the outside of the cover slip in with the passage of time and corresponding diffusion of water.

An unexplained observation of the PBT/PPA system was also made. When this orange solid was placed on a glass slide, covered with a cover slip, and then placed onto a preheated (200 degrees C) hot stage of an optical microscope, melting to an isotropic solution followed by rapid nucleation and growth of spherulites was observed. Whether this is due to a change in the solvent, PPA, or to some more complicated phase is not known.

One further extension of this work would be to investigate poly(p-phenylene benzobisoxazole) (PBO) to see if it also gives rise to crystal solvates. The unit cell of PBO has not yet been determined and crystallization of low MW PBO through the crystal solvate intermediate may provide a straightforward means of determining it. It now seems that PBO may be at least as useful as PBT as a high-modulus high-strength material and investigations of PBO could prove to be singularly important.

References

1. H. Sobue, H. Kiessig and K. Hess, Z. Physik. Chem. B43, 309 (1939).
2. M.M. Iovleva and S.P. Papkov, Vysokomol. soyed. A24, 233 (1982). Translated in Polym. Sci. USSR, 24, 236 (1982).
3. M.M. Iovleva, V.N. Smirnova, Z.S. Khanin, A.V. Volokhine and S.P. Papkov, Polym. Sci. USSR. 23, 2048 (1981).
4. C.R. Crosby, III, N.C. Ford, Jr., F.E. Karasz and K.H. Langley, J. Chem. Phys. 75, 4298 (1981).
5. J. Minter, Ph.D. Dissertation, University of Massachusetts, 1982.
6. T. Takahashi, H. Iwamoto, K. Inove and I. Tsujimoto, J. Polym. Sci., Polym. Phys. Ed. 17, 115 (1979).
7. V.A. Platonov, Diss. Cand. Chem. Sci., NPO, Khimvolokno, Mytishi (1978).
8. M.M. Iovleva, S.I. Bandvivan, N.I. Ivanova, V.A. Platonov, L.P. Mil'Kova, Z.S. Khonim, A.V. Volokhina and S.P. Papkov, Vysolomol. soyed. B21, 351 (1979).
9. L. Onsager, Ann. N.Y. Acad. Sci. 51, 627 (1949).
10. A. Ishihara, J. Chem. Phys. 19, 1142 (1951).
11. P.J. Flory, Proc. Royal Soc. London, Ser. A 234, 73 (1956).
12. A. Ciferri and W.R. Krigbaum, Mol. Cryst. Liq. Cryst. 69, 273 (1981).
13. K.H. Gardner, R.R. Matheson, P. Avakian, Y.T. Chin, T.D. Gierke and H.H. Yang, J. Polym. Sci., Polym. Phys. Ed. 21, 1955 (1983).
14. S. Russo and W.G. Miller, Macromolecules 17, 1324 (1984).
15. M. Panar, P. Avakian, R.C. Blume, K.H. Gardner, T.D. Gierke and H.H. Yang, in press.
16. M.G. Dobb, D.J. Johnson and B.P. Saville, J. Polym. Sci., Polym. Phys. Ed. 15, 2201 (1977).
17. J.F. Wolfe, B.H. Loo and F.E. Arnold, Macromolecules 14, 915 (1981).
18. E.J. Roche, T. Takahashi and E.L. Thomas, ACS Symposium Series 141, 303 (1981).

19. S. Allen, Ph.D. Dissertation, University of Massachusetts, 1983.
20. E.L. Thomas, unpublished data.
21. H. Tsai, Ph.D. Dissertation, Carnegie-Mellon University, 1983.
22. S. Sasaki, K. Tokuma and I. Uematsu, Polymer Bulletin 10, 539 (1983).

TABLE II.D.2
MELTING BEHAVIOR OF PBT/MSA.H₂O CRYSTAL SOLVATES

	<u>T1</u>	<u>T2</u>	<u>T3</u>
Optical Microscopy	90-100	135-200	varied: 200-300
DSC	90-100	140-195	220-245

(All tempertures in degrees Celsius)

TABLE II.D.2
COOPERATIVE DIFFRACTION OF PBT FIBER
AND CRYSTAL SOLVATE

<u>PBT Fiber</u>	<u>PBT Crystal Solvate</u>
12.45 m	12.45
5.9 e	7.45
3.54 e	5.2
3.18 e	4.5
2.94 e	4.2
	3.9
	3.6
	3.3
	2.6

m = meridional
e = equatorial

(All values of d spacings in angstroms)

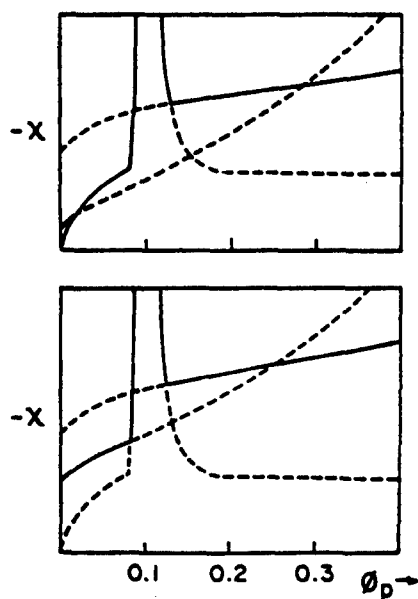


Figure III.B.1

Superposition of liquid-liquid and solid-liquid phase diagrams. Top diagram is for a crystal having smaller melting transition temperature and heat of fusion; bottom diagram is for larger values.

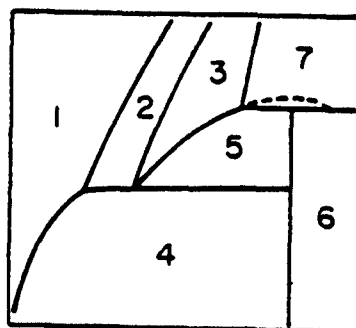


Figure III.B.2

Schematic phase diagram for rigid-rod polymer with the inclusion of a crystal solvent. (1) isotropic solution, (2) isotropic solution plus anisotropic solution, (3) anisotropic solution, (4) isotropic solution plus crystal solvate (5) crystal solvate plus crystalline polymer, (6) crystalline polymer plus anisotropic solution, (7) crystalline polymer plus anisotropic solution.

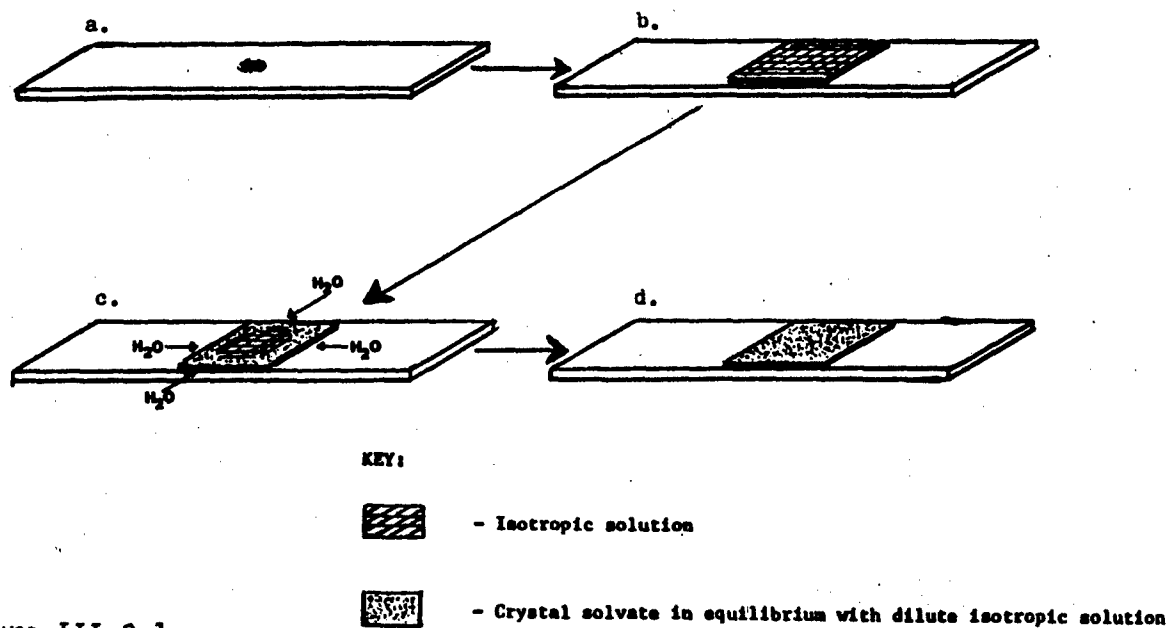


Figure III.C.1

a. Drop of PBT/MSA solution is put on a clean glass slide, b. cover slip is placed over drop, c. water diffusing into the solution induces growth of crystal solvate, d. crystal solvate is fully grown.

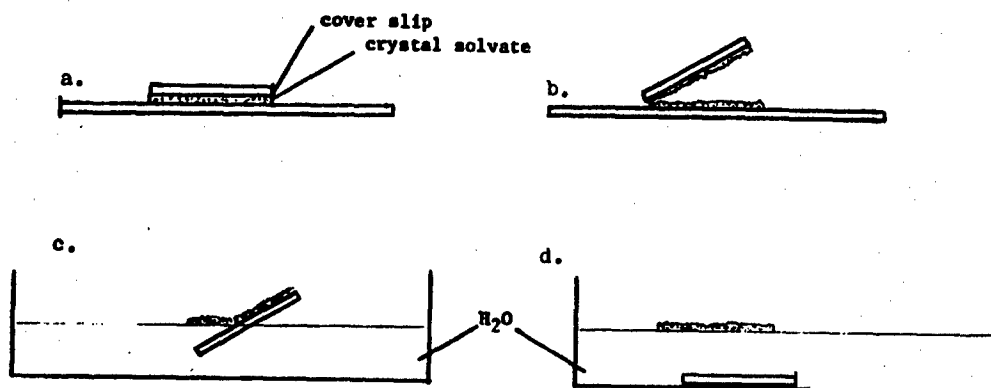


Figure III.C.2

a. Cover slip, crystal solvates, and glass slide, after heating at about 150°C, b. cover slip is split off, c. crystal solvate floated off onto deionized water, d. crystal solvate ready to be picked up with electron microscope grids.

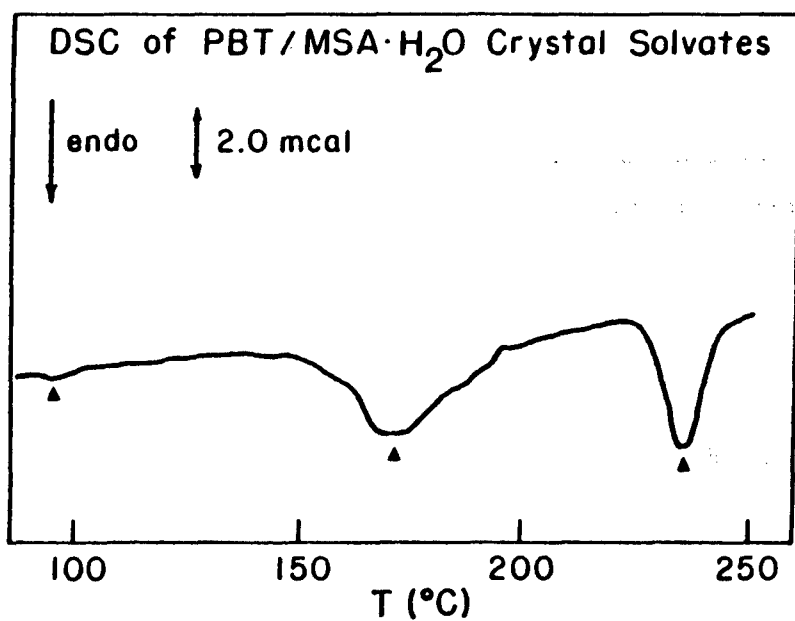


Figure III.D.1

Differential scanning calorimeter trace of PBT/MSA·H₂O crystal solvates.

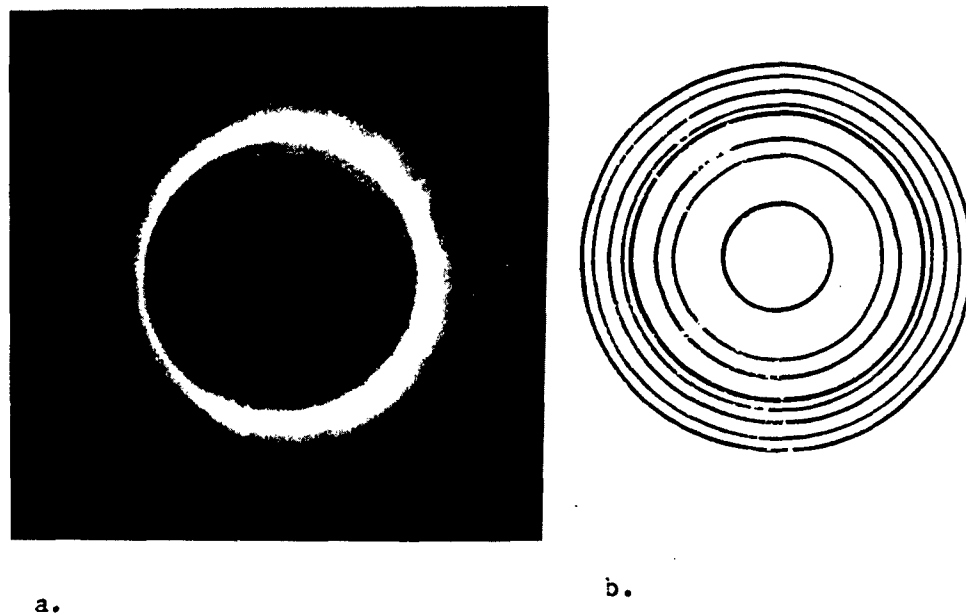


Figure III.D.2

a. Statton flat film X-ray diffraction of PBT/MSA·H₂O, b. schematic of X-ray pattern.

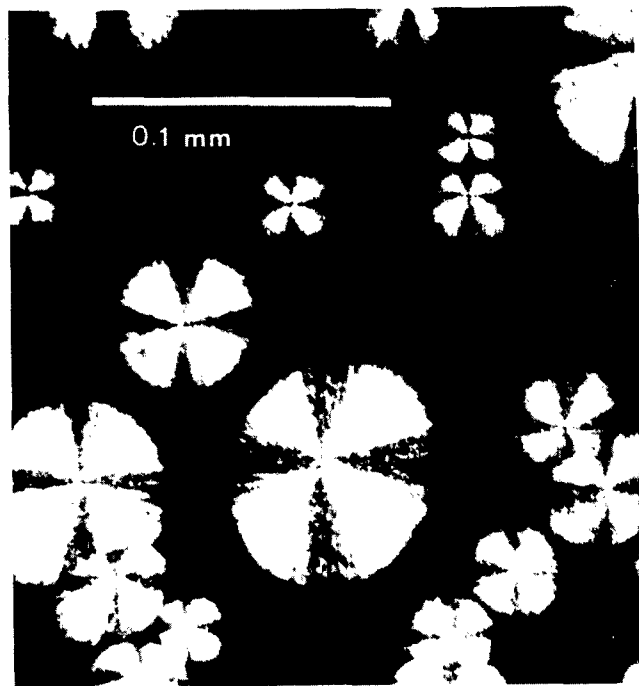


Figure III.D.3

Typical Maltese cross extinction pattern of PBT/MSA.H₂O crystal solvate spherulites viewed under crossed polars in an optical microscope.

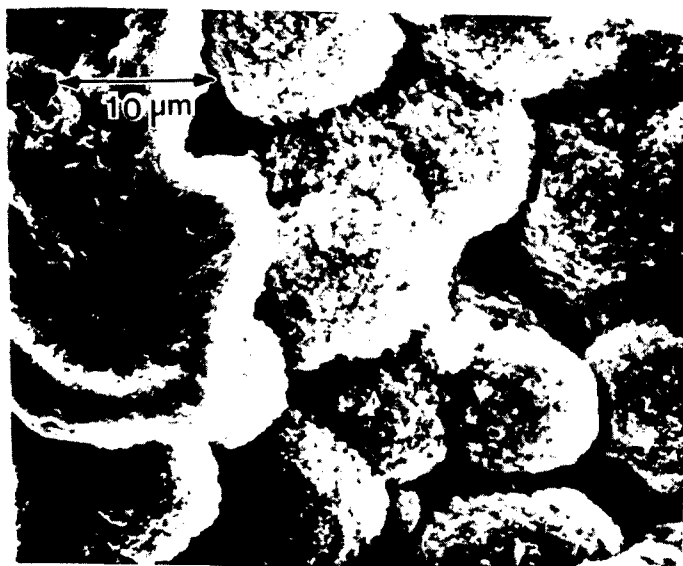


Figure III.D.4

Scanning electron microscope photograph of PBT/MSA.H₂O spherulites having been washed in copious amounts of acetone and dried.

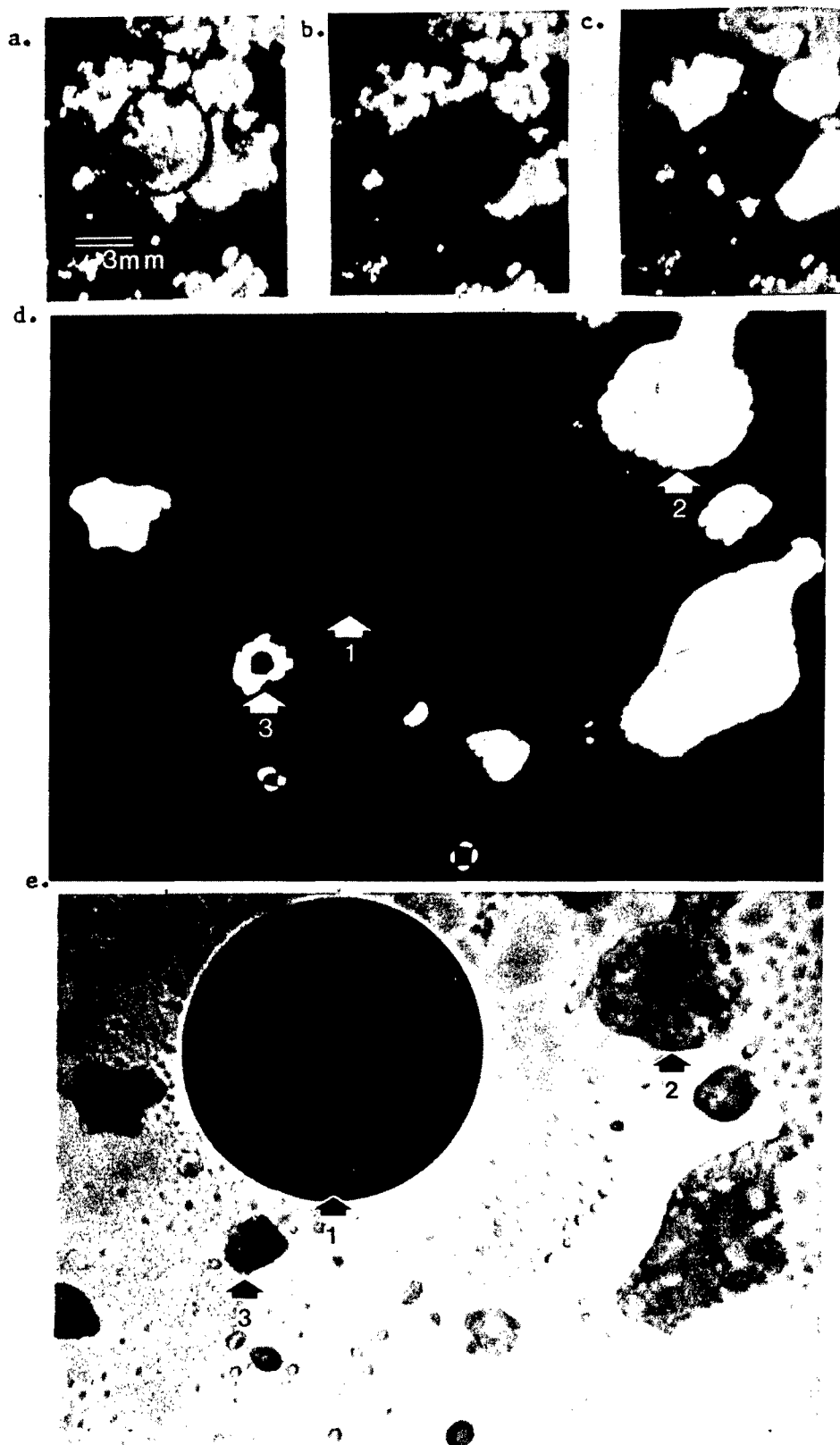


Figure III.D.5

Optical micrographs showing melting of crystal solvates. a. at 27°C, b. at 92°C, c. at 94°C, d. and e. at 117°C. Note isotropic (1), anisotropic (2) and biphasic (3) liquid domains at 117°C equilibrium.

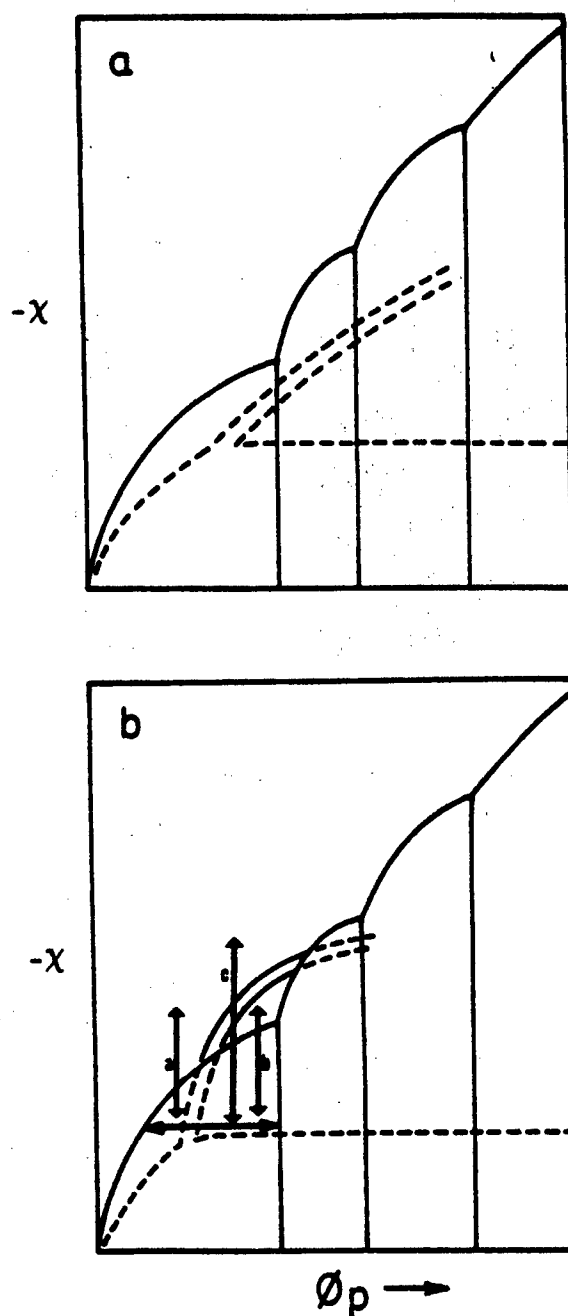


Figure III.D.6

a. Superposition of liquid-liquid and solid-liquid phase diagrams with the chimney region inaccessible at equilibrium, b. with chimney region partially accessible at equilibrium.

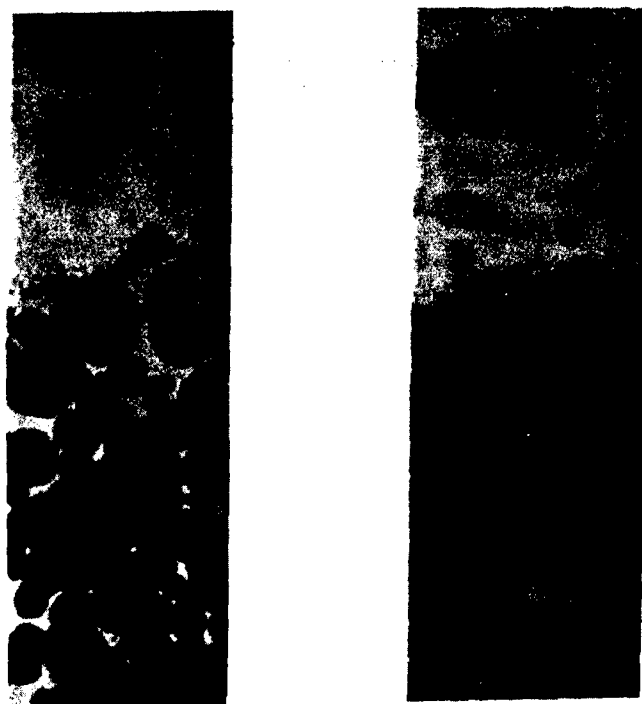


Figure III.D.7

Crystal solvates growing from metastable nematic liquid into equilibrium state of crystal solvate plus isotropic liquid.



Figure III.D.8

A crystal solvate spherulite growing from a nematic solution.

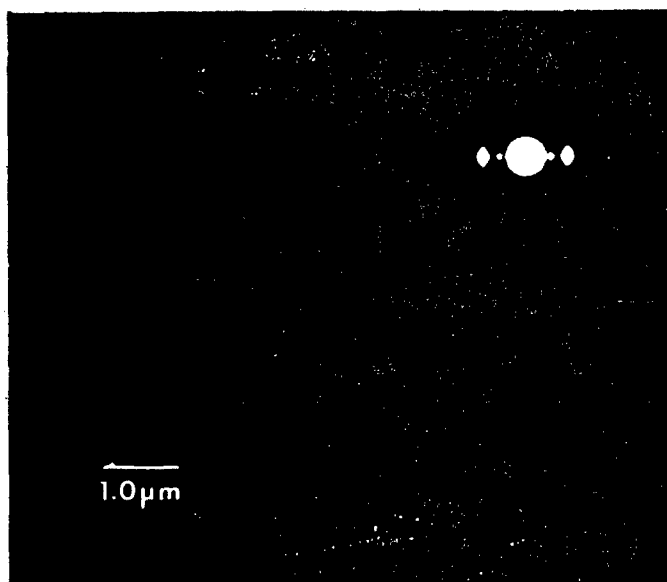


Figure III.D.9

PBT lamellae remaining after solvent removal and drying. Electron diffraction (inset) reveals the chain orientation is perpendicular to the lamellae.

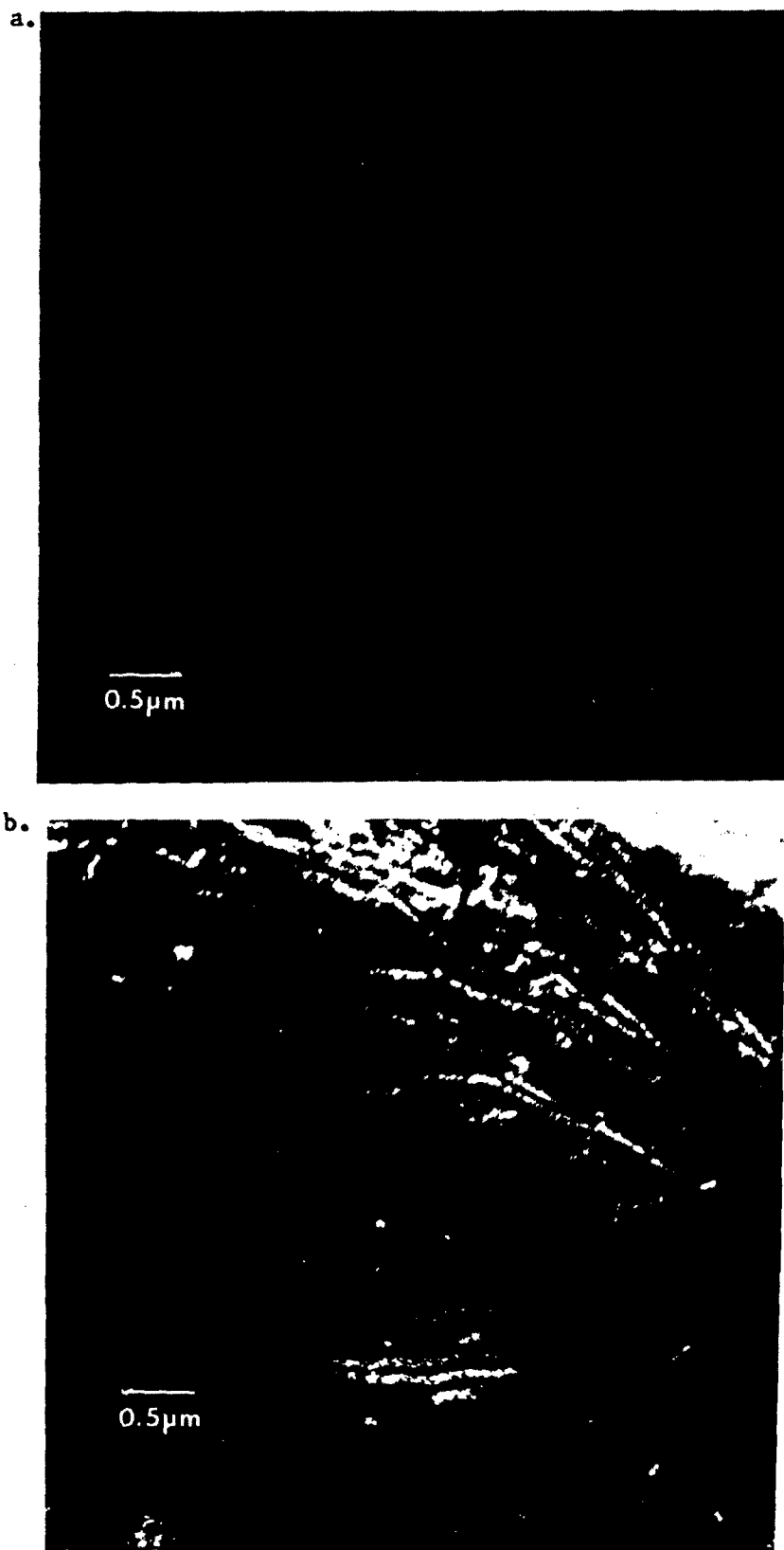


Figure III.D.10

Bright field/dark field pair (a and b respectively) showing lamellae and fracture paths of lamellar region of PBT.

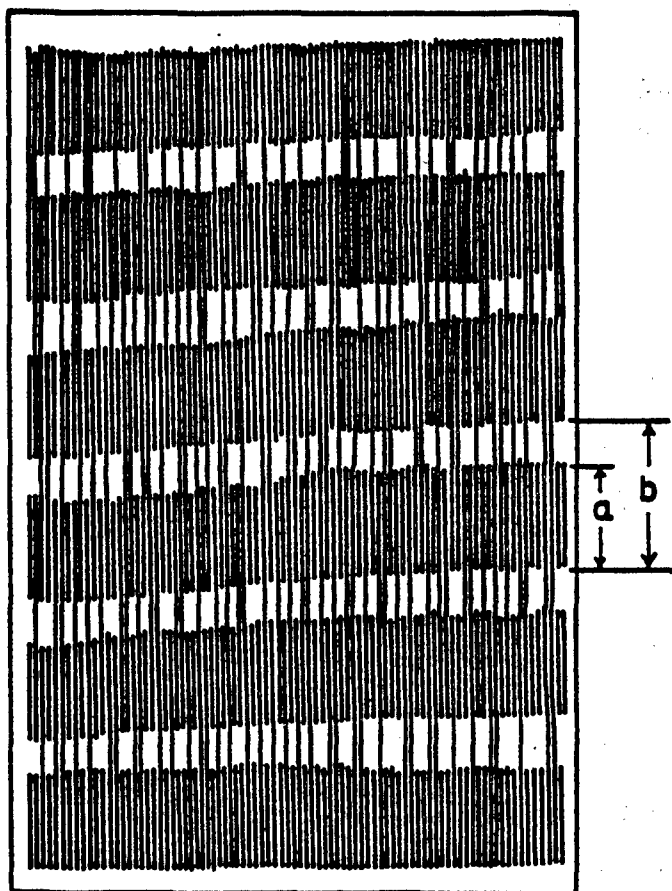


Figure III.D.11

Schematic of proposed lamellar structure of PBT. a. corresponds to lamellar width, b. corresponds to long period.

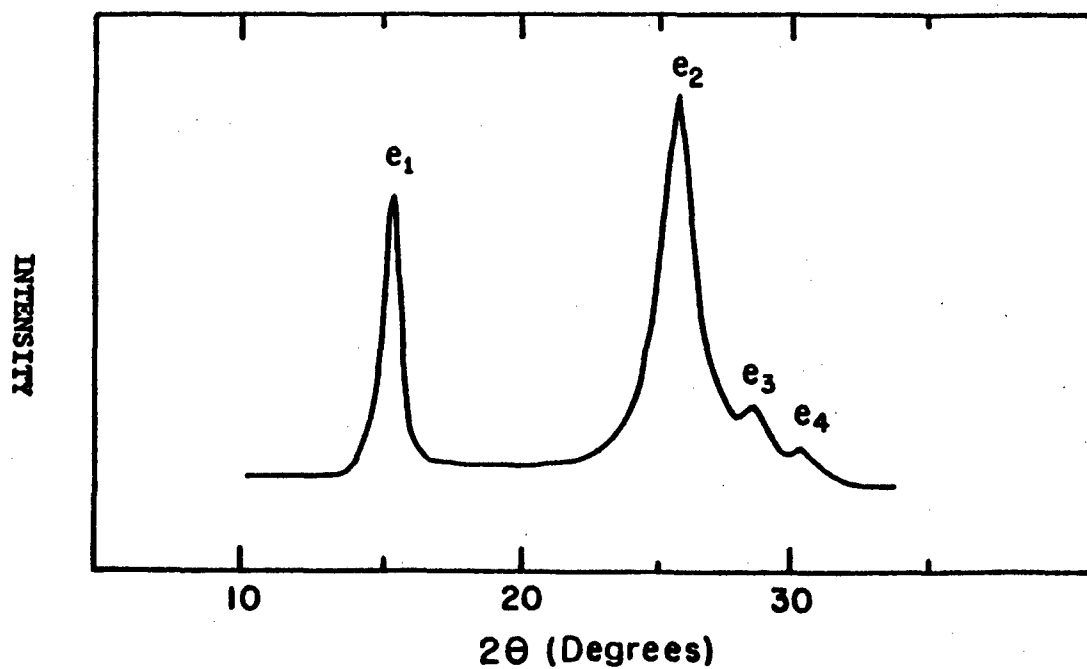


Figure III.D.12

Equatorial 2θ scan of PBT fiber.

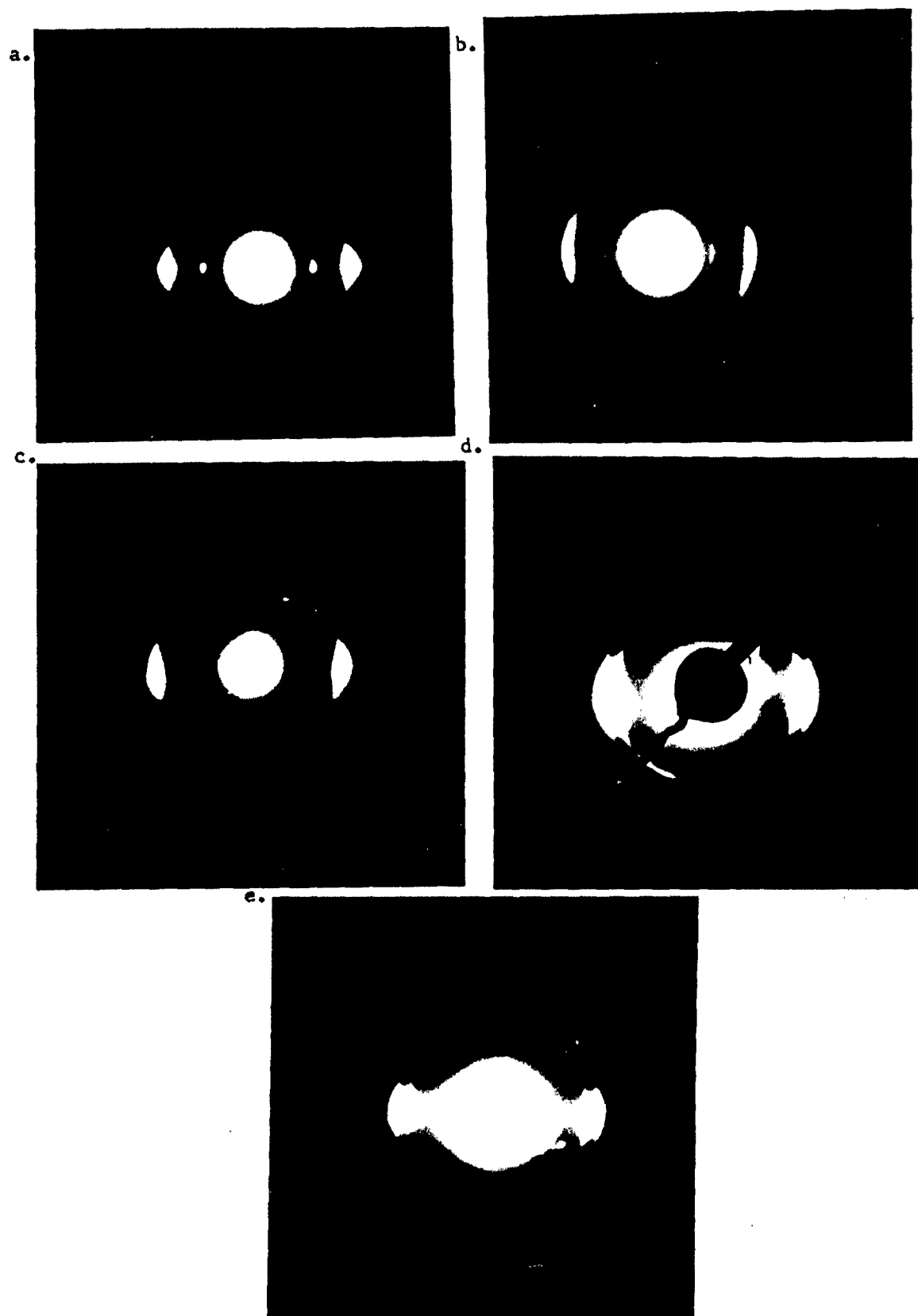


Figure III.D.13

Electron diffraction data revealing texturing in PBT. a. e1 - e4 all present in typical fiber symmetric intensities, b. e1 and 32 only, c. e2 only, d. e2 and e3 only with e2 being more intense, e. e2 and e3 only with e3 being more intense.

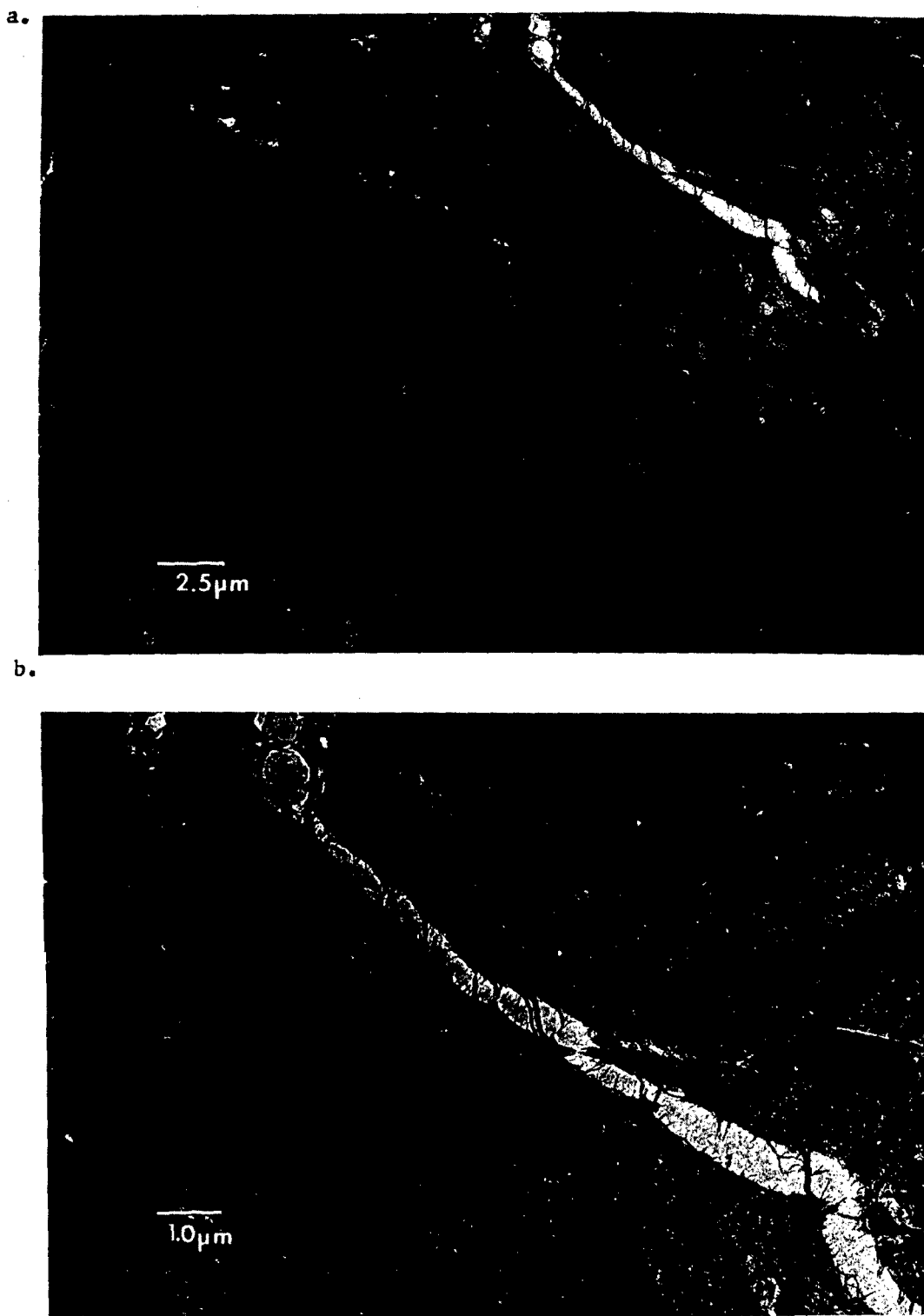


Figure III.D.14

Bright field electron micrographs of lamellar PBT. a. sheaf like structures readily apparent and b. higher magnification of a. Note fine 100 angstrom cross-hatching perpendicular to lamellae.

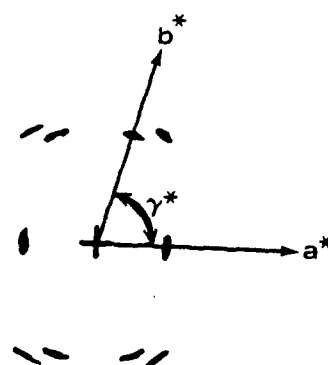


Figure III.D.15

Bright field image of "grassy mat" formed by coagulation of isotropic solution.



a.



b.

Figure III.D.16

a. electron diffraction of the a b plane of a twinned crystal. C axis is perpendicular to the page, b. schematic of diffraction pattern.

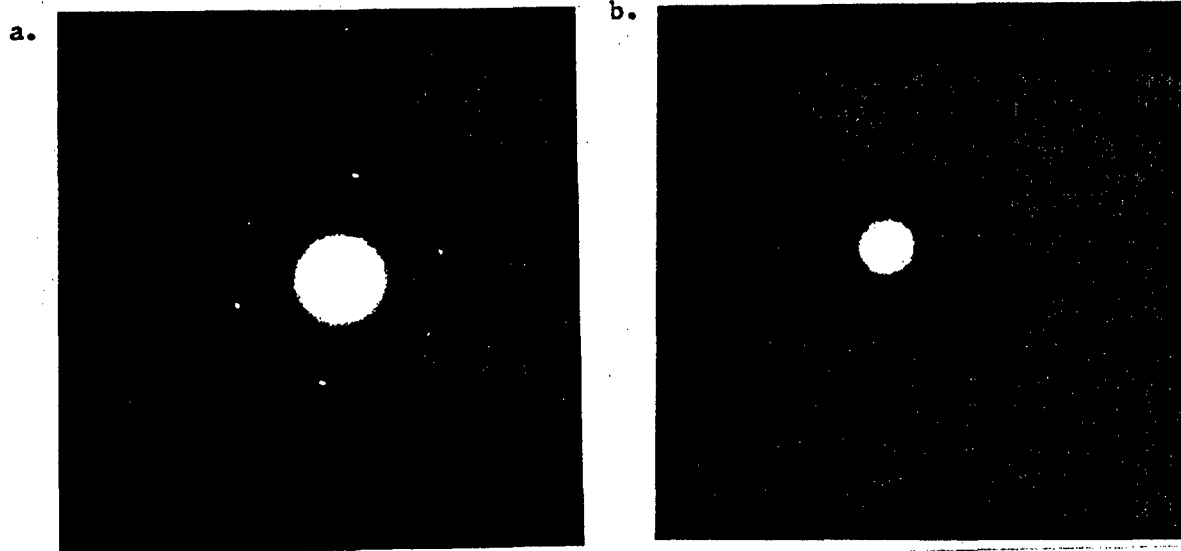


Figure III.E.1

Examples of crystal solvate diffraction. Pattern a has the e2 PBT arc superimposed upon it.

a.



b.



c.

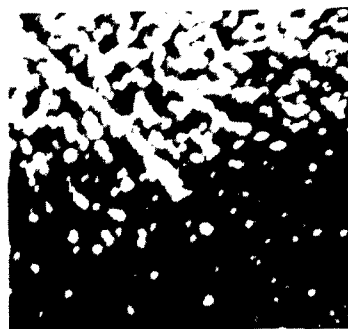
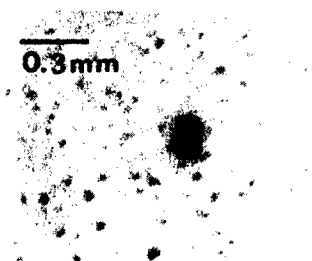


Figure III.E.2

Crystal solvate growth from a. isotropic, b. anisotropic and c. biphasic solutions. Left: analyzer removed; Right: polarizer and analyzer crossed.

SECTION IV: SPECTROSCOPIC ANALYSIS OF POLY(p-PHENYLENE BENZOBISTHIAZOLE) FILMS

A. Introduction

Fibers of rod-like polymers usually exhibit very high mechanical modulus and strength and, in fact, these values may exceed those for metal on a per weight basis (1). The molecular origin of the properties achieved is in the rigidity of the chain backbone commonly found for this class of polymers. This lack of conformational freedom significantly reduces the possibility of rotation about single bonds, producing effectively straight chain segments, and eliminates the degree of freedom which lowers the mechanical properties. Some of these rigid chains form lyotropic liquid crystals. The isotropic to anisotropic transition depends strongly on concentration, molecular weight, and temperature (2,3). From processing considerations, it is advantageous to spin fibers or extrude bulk items from the anisotropic state. This complicated process involves several steps: 1) dissolution of the polymer in a suitable solvent, 2) extrusion in the anisotropic state into a coagulating bath, 3) washing and neutralization, and 4) post-processing treatments. An interesting polymer in this class, poly(p-phenylene benzobisthiazole) (PBT), has been brought to our attention. The highly oriented fibers obtained from this polymer by following the processing procedure described above exhibit extremely high mechanical properties in terms of modulus and strength (4). The improvement in properties is particularly evident after annealing under tension (4,5). After this post-processing treatment, the sample color changes (6), the lateral dimension of the

crystallites increases (5), chain segment orientation improves (5), and a portion of the sample may degrade (7). Poly(p-phenylene benzobisthiazole) is only soluble in some of the strongest acids, such as polyphosphoric acid, chlorosulfonic acid, methane sulfonic acid, and 100% sulfuric acid. Since removal of the acid during the coagulation and washing is a diffusion process, and because of the inhomogeneous morphology usually found for this type of polymer (8), residual acid and water often remain in the processed fibers. The presence of residual acid and water in the post-processing sample is of obvious interest, not only because it influences the perfection of chain packing and interacts with the matrix material used for composites, but it may also initiate unexpected chemical reactions with the polymer during post-processing thermal treatment, consequently leading to crosslinking or degradation.

The principal aim of this spectroscopic analysis is to measure the amount and the environment of residual acid and water molecules in these processed samples. Infrared spectroscopy provides a convenient and effective method to determine the concentration of acid or water in a sample. Beer's law relates the absorbed infrared band intensity to the concentration of a constituent by the equation:

$$A = \ln \frac{I_0}{I} = abc \quad (1)$$

where A equals the absorbance of the constituent, I_0 equals the radiation intensity impinging on the sample, I equals the radiant intensity transmitted by the sample, a equals the absorption coefficient of the constituent at a particular frequency, b equals the path length, and c equals the concentration of the constituent in the sample. If the absorption coefficient and the sample pathlength are known, characteristic band absorbance can be converted to concentration.

In addition to determining concentration, we are quite interested in clarifying the location of the acid and water molecules. Attenuated total reflectance spectroscopy allows us to sample a specimen at controlled depths. Our results are reported here.

B. Experimental

Fourier transform infrared (FTIR) spectroscopy provides a very reliable intensity (absorbance) measurement. All of our infrared spectra were taken on a Nicolet 7199 FTIR spectrometer, except for the attenuated total reflectance (ATR) measurements, which were taken on an IBM-98 evacuable FTIR spectrometer. With this IBM instrument, the elimination of any trace of water in the beam path greatly increases the ability of the spectrometer to measure low-absorbing species accurately. The attenuated total reflectance attachment was purchased from Harrick Scientific. This attachment is quite flexible, allowing us to select a continuous range of incident angles. In order to vary the depth of penetration further, both KRS-5 and Ge crystals were used. When necessary, a demountable liquid cell, also purchased from Harrick Scientific, was used. The heating cell used was built in this laboratory. The highest temperature that

can be achieved is 415°C under inert atmosphere. All spectra were recorded with 2 cm⁻¹ band resolution, and 100 to 200 scans.

The two PBT films used in this study were furnished by Celanese Research Co. The first sample, S₁, was dried at room temperature, has a denier value of 380, and is 4.2 mm in width. The second sample, S₂, was dried at 109°C, has a denier value of 1570, and is 8.5 mm in width. Both of these films were used in the study to characterize residual acid and water, but only the S₁ film was studied for post-processing microstructural changes. Thermal annealing was carried out at the University of Massachusetts under the conditions described in reference 9. The polyphosphoric acid (PPA) was purchased from Sigma. It contains 82-86% of P₂O₅. Although most of the PBT samples are essentially insoluble after processing, they can be swollen by soaking in polyphosphoric acid.

A typical transmission infrared spectrum obtained for a poly(p-phenylene benzothiazole) film is shown in Figure IV.B.1. Polarized spectra are shown in Figures IV.B.1b and IV.B.1c. The spectra of S₁ and S₂ films are very similar. The only noticeable difference is that the broad water band appears in the spectrum of the first sample but not of the second.

C. Results and Discussion

A comparison of the spectra of the as-prepared film with a PPA-swollen film demonstrates conclusively that the medium to strong bands at 2850, 2250, and 1005 cm^{-1} can be associated with PPA. Their intensities increase with swelling time. The difference spectrum can be compared to the pure acid spectrum, as shown in Figure IV.B.2. After thermal annealing, some of the infrared active bands of PBT exhibit both frequency and shape changes, causing some sharp features to be superimposed on the broad acid bands in the difference spectrum. The absorption coefficient of characteristic PPA bands can be calculated from their absorbance when measured with a liquid cell of well defined path length. In this case the path length b is $6\text{ }\mu\text{m}$. In our study concentration is expressed in terms of volume percentage, that is, a pure acid has 100% by volume concentration. From our measurements, the absorption coefficients of 2850 and 1005 cm^{-1} are then calculated to be $0.13\text{ }\mu\text{m}^{-1}$ and $0.2\text{ }\mu\text{m}^{-1}$ respectively.

The accuracy of the acid concentration determination within PBT films depends greatly on the film thickness measurements which can be taken by two different methods. The first, simply using a micrometer, is easy to conduct, but only reliable for thicker samples. A second method, Fizeau fringes (10), is suitable for films thinner than $10\text{ }\mu\text{m}$. In addition, the sample thickness can also be calculated from its denier value and crystalline density. The density of PBT film measured by pycnometer is 1.5 g/cm^3 (4), whereas the calculated

value from a proposed unit cell ranges from 1.69 to 1.71 g/cm³, depending on the unit cell model (11). We used $\rho = 1.5$ g/cm³ in our calculations. The thicknesses calculated this way are in good agreement with the Fizeau fringe values (Table IV.B.1), although both values deviate from the micrometer measurements. Part of the problem in thickness measurements by micrometer can be attributed to the thicker edges of each sample. A diagram of the sample cross section for an S₁ film is shown in Figure IV.B.3. This feature may be due to non-uniform sample contraction during the coagulation process.

The absorbance measured at 2850 cm⁻¹ of the S₂ film is 0.17. With the absorption coefficient measured for PPA, from Beer's law, we determined the acid content in the film to be 9.3% by volume. For the S₁ film, the amount of acid was determined to be 6.2% by volume. Despite the substantial amount of washing commonly used in processing, our measured values demonstrate that the residual acid in such films is considerable.

The band observed at approximately 3300 cm⁻¹ in the spectrum of the S₁ film (Figure IV.B.1a) is assignable to the OH stretching vibration of water molecules. This band does not appear in the spectrum of the S₂ film, indicating that drying at 109°C is sufficient to remove water introduced during the coagulation and washing cycles. The absorption coefficient of the water band, a , is related to the imaginary part of the refractive index, n_i , by $a(\lambda) = 4\pi n_i(\lambda)$. For water at approximately 3300 cm⁻¹ n_i is 0.29 (12). Therefore, a is 1.24. Using the same calculation employed to determine the acid concentration, the water content in the S₁ film was found to be 1.1% by volume. It is interesting to note that this water concentration is much lower than the acid content.

In addition to concentration determination, we are also quite interested in clarifying where the acid or water molecules are located. From polarized spectra it is interesting to note that the dichroic ratio of the water band at 3300 cm^{-1} is 1.9 while that of PPA at 2850 cm^{-1} is 1.03. An isotropic sample should have a dichroic ratio of 1.0. The high dichroic ratio of the water molecules suggests that they are packed in a highly oriented fashion in the film. Therefore, it is not possible to assign the location of the water molecules only to the macrovoids introduced during the coagulation cycle. Our data seem to suggest that the water molecules are packed in between the PBT molecules or fibrils. The nearly isotropic value measured for the acid does not necessarily mean that acid molecules are completely random in orientation. Even for a uniaxially oriented system, if the transition moment of the vibrational band forms an angle of 55° with respect to the extrusion direction, the dichroic ratio measured will be 1.0.

Because of the processing conditions used, we feel there may be substantial differences in the microstructure between the film surface and the inner bulk, as suggested earlier for poly(p-phenylene terephthalate) (8). Attenuated total reflectance (ATR) spectroscopy is often used to obtain surface information. The depths that this technique can monitor depend on the frequency of the incident radiation, the refractive index of the sample, the internal reflectance element (IRE), and the incident angle (13):

$$d_p = \frac{\lambda}{2\pi n_{IRE} [\sin^2 \theta - (\frac{n}{n_{IRE}})^2]^{1/2}} \quad (2)$$

where d_p is the depth of penetration for which the electric field strength has decreased to $1/e$ of its value at the surface; n is the refractive index of the film, n_{IRE} is the index of refraction of the reflecting element, θ is the incident angle, and λ is the wavelength. In the case of uniaxially extruded films, a large degree of optical anisotropy is exhibited due to the molecular orientation such that the refractive index along the extrusion axis (n_{\parallel}) is higher than that perpendicular to the same axis (n_{\perp}). As a first order approximation, if we use a linear polarized transverse magnetic (TM) wave as the incident beam with the extrusion axis either in the incident plane or perpendicular to it, the depth of penetration then depends on n being n_{\parallel} or n_{\perp} , respectively. For PBT film S₂, n_{\parallel} and n_{\perp} were measured to be 2.52 ± 0.04 and 1.64 ± 0.04 respectively (we will discuss the measurement later).

For a 45° incidence angle, using a germanium crystal as the internal reflecting element, we have $d_{p\parallel} = 0.43 \mu\text{m}$ or $0.38 \mu\text{m}$ at 2850 cm^{-1} or 3300 cm^{-1} respectively for $n_{\parallel} = 2.52$; $d_{p\perp} = 0.24 \mu\text{m}$ or $0.21 \mu\text{m}$ at 2850 cm^{-1} or 3300 cm^{-1} for $n_{\perp} = 1.64$. It should be emphasized, however, that if a quantitative evaluation of acid or water concentration as a function of thickness is needed, the effective thickness, d_e , must be used, not the depth of penetration (14). In some cases d_e and d_p can be similar; in other cases they differ significantly. Therefore, the depth we are studying can be as deep as $1.28 \mu\text{m}$ ($d_{e\parallel}$) for $n_{\parallel} = 2.52$. Therefore, the spectra obtained by the ATR technique is truly representative of the surface structure in our samples.

The spectra obtained with the ATR technique showed no trace of acid bands in the first $0.24 \mu\text{m}$ layer of the S₁ film. But water bands (3300 cm^{-1}) do

appear at this depth (Figure IV.B.4). From the observed absorbance and the calculated absorption coefficient of water at this frequency, we estimate there is 23% water by volume in the region from the surface to a depth of 0.21 μm , if Beer's law is applied. The comparison between the reflection (surface) and transmission (bulk) spectra suggests that water is mostly concentrated in the skin of the film while PPA is located in the core. We also noticed that the as-prepared S_2 film does not show any water trace by the transmission method, whereas the S_1 film does. The difference between the two films is in their preparation; the S_2 sample was dried at the fairly high temperature of 109°C, the S_1 sample was dried at room temperature. After heating the S_1 film to 110°C in vacuo for 1 hour, its spectrum also showed no evidence of the water band. And if this dried film is left in the open air for a few days, water bands will reappear.

Wide angle X-ray scattering data of annealed PBT films show a well defined lateral spacing between PBT molecules, from which the unit cell was deduced (11). Therefore, it is difficult to imagine PPA molecules uniformly packed with PBT molecules. A possible picture is that PBT molecules form aggregates or fibrils and the residue acid is packed between these aggregates or fibrils.

From both fundamental and practical considerations the presence of significant amounts of residual acid is troublesome. From past studies, residual acid is difficult to remove (5). In our study, films boiled in distilled water for more than two weeks still exhibit evidence of acid. Application of a weak base (NH_4OH) or a strong base (NaOH) was not effective in neutralizing the acid. Since the apparent acid exists in the core region of the film, it is difficult

for either water molecules or base molecules to diffuse through the skin region inward. On the other hand, the densely packed skin prevents the acid molecules from diffusing out. From spectroscopic analysis, it is clearly evident that the high temperature annealing can remove most of the residual acid. The spectrum of S_1 film after annealing at 415°C in the presence of nitrogen are shown in Figure IV.B.5. Characteristic PPA bands disappeared after annealing for 30 min. Actually, even with heating to 300°C one can reduce the acid content significantly. Although heating at even more elevated temperatures is more efficient in removing acid, there are definite alterations in the spectrum accompanying the diminishing of the acid bands. The PBT bands at 837 cm^{-1} and 605 cm^{-1} intensify without changes in either frequency or shape after annealing. These spectroscopic changes arise from the microstructural changes of PBT molecules.

Because of its simplicity, birefringence has often been used to estimate segmental orientation, since the index of refraction can be very different for the direction perpendicular to the chain axis, n_\perp , versus the parallel one, n_\parallel . Our infrared spectroscopic measurements provide one possibility to obtain n_\parallel and n_\perp .

The high birefringence of PBT is mainly due to the high degree of orientation of polymer chains in the film. For highly birefringent material, a light with polarization parallel to the optical axis will experience a different refractive index from a light polarized perpendicularly to the same axis. The relative magnitude of the index of refraction depends very much on the polarizability of the molecule, that is the electron binding force. A strong binding force corresponds to low polarizability, therefore a low refractive index. The

exact relationship is usually expressed by the Lorentz-Lorenz equation (10):

$$\frac{n^2 - 1}{n^2 + 2} = \frac{4\pi}{3} \frac{N_A \rho}{M} \alpha \quad (3)$$

where ρ is the sample density, α the polarizability tensor, N_A Avagadro's number, and M the molecular weight. According to Bhaumik's calculation (15), the polarizability along the chain axis has the highest value. Since PBT chains have a uniaxial geometry in the film (5), the refractive index along the extrusion axis has a higher value than the ones along the transverse direction. However, the refractive index varies with orientation. Its value should then be expressed in terms of average polarizability:

$$\frac{n^2 - 1}{n^2 + 2} = \frac{4\pi}{3} \frac{N_A \rho}{M} \langle \alpha \rangle \quad (4)$$

where $\langle \alpha \rangle$ is the α averaged for all possible orientations. In the first order of approximation, poly(p-phenylene benzobisthiazole) film is assumed to possess a perfect uniaxial orientation and the contribution to the polarizability from the intermolecular interaction is small, the refractive index along each principal axis of the polarizability tensor can be expressed as

$$\frac{n_i^2 - 1}{n_i^2 + 2} = \frac{4\pi}{3} \frac{N_A \rho}{M} \alpha_{ii} \quad i = x, y, z \quad (5)$$

where α_{ii} is the polarizability component along the i th axis. The principal polarizability components α_{ii} were calculated by Bhaumik and his coworkers by means of the bond additivity method (15). In their calculation, the chain axis was taken to be the y axis and the plane of the phenylene ring lies in the x - y plane with the heterocyclic ring tilted away from this plane at an angle of

23.2°. The calculated results are $\alpha_{xx}=37.5 \text{ Å}^3$, $\alpha_{yy}=41.7 \text{ Å}^3$, and $\alpha_{zz}=23.3 \text{ Å}^3$. Substituting these values into the Lorentz-Lorenz equation, the indices of refraction along the three axes are $n_x=2.11$, $n_y=2.31$, and $n_z=1.58$ for $\rho=1.5 \text{ g/cm}^3$. A similar calculation was carried out by Hamza and Sikorski for poly(p-phenylene terephthalamide) (16). They found $n_{\parallel} = 2.199$ and $n_{\perp} = 1.742$. However, their measured values are $n_{\parallel}=2.267$ and $n_{\perp}=1.605$ for Kevlar 49 (16).

In addition to the theoretical calculation, the index of refraction in the infrared region can be measured by the ATR technique. Even with this technique there are several methods that can be used to obtain the optical constants of a material (17). We followed the method outlined by Mirabella (18). His method is based on the fact that the ATR spectra will "degenerate" to dispersion curves when the incident angle reaches the critical angle. By examining the bandshapes of spectra at various incident angles, one can determine the critical angle for the sample and, therefore, the refractive index. This method is believed to be quite sensitive (18). Figure IV.B.6 shows the spectra in the $1000\text{--}1400 \text{ cm}^{-1}$ region of a PBT S_2 film on a KRS-5 crystal as a function of incident angle. Notice that, for the n_{\parallel} measurements, by examining the lower frequency side of each band, the spectra degenerate to dispersion curves between 45° and 42.1° , indicating that the critical angle lies very close to 43.7° (Figure IV.B.6), while there is a substantial difference between n_{\parallel} and n_{\perp} , the n_{\perp} measurement was carried out using a KRS-5 IRE crystal, and the n_{\parallel} measurement was carried out using a GE element. For the n_{\parallel} measurement the critical angle is 38.94° . Thus $n_{\perp}=1.64 \pm 0.04$ and $n_{\parallel}=2.52 \pm 0.04$. Even though we have corrected for the non-normal incidence of the incident beam, some uncertainty due to the convergence

of the incident beam used and the error in the angle measurement still exists and is given above.

The same measurements done on the heat-tension treated film show $n_{\parallel}=1.61 \pm 0.03$ and $n_{\perp}=2.60 \pm 0.03$. Although the values for the heat-tension treated samples are essentially the same as those for the S_2 film (within the range of uncertainty) the higher value in n_{\parallel} and lower value in n_{\perp} are persistently recorded. This feature is consistent with the higher molecular orientation reported for the heat-tension treated material (9). The birefringence $n=n_{\parallel}-n_{\perp}$ in the infrared region is calculated to be 0.88 ± 0.04 , a value smaller than the 1.5 suggested by Berry (19).

In our analysis, the PBT molecules were assumed to be cylindrically symmetrical. The actual structure deviates from this assumed one in that uniplanar orientation may exist (20). However, our calculated values are surprisingly close to the measured ones ($n_y=2.31$ versus $n_{\parallel}=2.52$ and $n_x=2.11$ or $n_z=1.58$ versus $n_{\perp}=1.64$). The intermolecular field may perturb the single chain polarizability. These perturbations should affect the transverse polarizabilities in the x and z directions much more so than along the chain axis. This may explain the much higher agreement between the calculated and experimental values of n_y than for those of n_x or n_z .

D. Conclusions

By using the attenuated total reflectance technique in conjunction with commonly employed transmission infrared spectroscopy we were able to determine quantitatively the residual water and acid content in poly(p-phenylene benzobisthiazole) films. It is surprising that the volume fraction of water molecules can be so high in the first 0.21 μm layer. Also, post-processing annealing, even with very moderate temperatures, can remove the water effectively. The acid was found mainly in the interior of the film. This is not surprising due to the fact that acid removal during coagulation and washing and neutralization after coagulation are essentially diffusion processes. The "skin" first formed during the initial stage of coagulation provides a fairly high barrier for the acid molecules to move outward and the water or base molecules to move inward. We have also shown that post-processing annealing with high temperatures can remove acid as well. But films exposed to such high temperature treatment do show new spectroscopic features suggesting that the polymer structures have been altered. Using the absorbance values measured by infrared irradiation, the birefringence of poly(p-phenylene benzobisthiazole) has been determined to be 0.88 ± 0.04 in the infrared region, a value much smaller than previously suggested, but close to that of poly(p-phenylene terephthalate).

References

1. W.B. Black, Ann. Rev. Mater. Sci. 10, 311 (1980).
2. P.J. Flory, Proc. Roy. Soc. of London, A234, 60 (1956).
3. Ibid, p. 73.
4. S. Allen, Ph.D. Dissertation, University of Massachusetts, 1983.
5. J.R. Minter, K. Shimamura and E.L. Thomas, J. Mater. Sci. 16, 3303 (1981).
6. J.A. Odell, A. Keller, E.D.T. Atkins and M.J. Miles, J. Mater. Sci. 16, 3309 (1981).
7. J.F. Wolfe, B.H. Loo and F.E. Arnold, Macromolecules 14, 915 (1981).
8. M. Panar, R. Avakian, R.C. Blume, K.H. Gardner, T.D. Gierke and H.H. Yang, J. Polym. Sci., Polym. Phys. Ed. 21, 1955 (1983); R.J. Morgan, C.O. Pruneda and W.J. Steele, J. Polym. Sci., Polym. Phys. Ed. 21, 1757 (1983).
9. E.L. Thomas, R.J. Farris and S.L. Hsu, "Mechanical Properties vs. Morphology of Ordered Polymers," Technical Report AFWAL-TR-80-4045, Volume IV. (1983).
10. M. Born and E. Wolf, "Principles of Optics," Pergamon, Oxford, 1980.
11. J.R. Minter, Ph.D. Dissertation, University of Massachusetts, 1982.
12. A.N. Rusk and D. Williams, J. Opt. Soc. Am. 61(7), 895 (1971).
13. N.J. Harrick, "Internal Reflection Spectroscopy," Ossining, New York: Harrick Scientific Corporation, 1979.
14. F.M. Mirabella, Jr., J. Polym. Sci., Polym. Phys. Ed. 21, 2403 (1983).
15. D. Bhaumik, H.H. Jaffe and J.E. Mark, Macromolecules 14, 1125 (1981).
16. A.A. Hamza and J. Skorski, J. Macroscopy 113(1), 15 (1977).

17. B. Crawford, T.G. Groplen and D. Swanson in "Advances in Infrared and Raman Spectroscopy," Vol. 4, R.J.H. Clark and R.E. Hester, Eds., Hayden, London, 1978.
18. F.M. Mirabella, Jr., J. Polym. Sci., Polym. Phys. Ed. 22, 1283 (1984).
19. G.C. Berry, "Physical Chemical Properties of Aromatic Heterocyclic Polymers," Technical Report AFWAL-TR-71-Part VII, 1977.
20. C. Chang and S.L. Hsu, to be published.

TABLE IV.B.1

PROPERTIES OF SAMPLE FILMS

		<u>S₁</u>	<u>S₂</u>
Drying temperature		room temperature	109°C
Denier (g/9000 m)		380	1570
calculation(a)		6 μm	14 μm
Thickness	Fizeau fringes	6 \pm 1 μm	12 \pm 4 μm
	micrometer	13 μm	18 μm

(a) Density was taken to be 1.5 g/cm³.

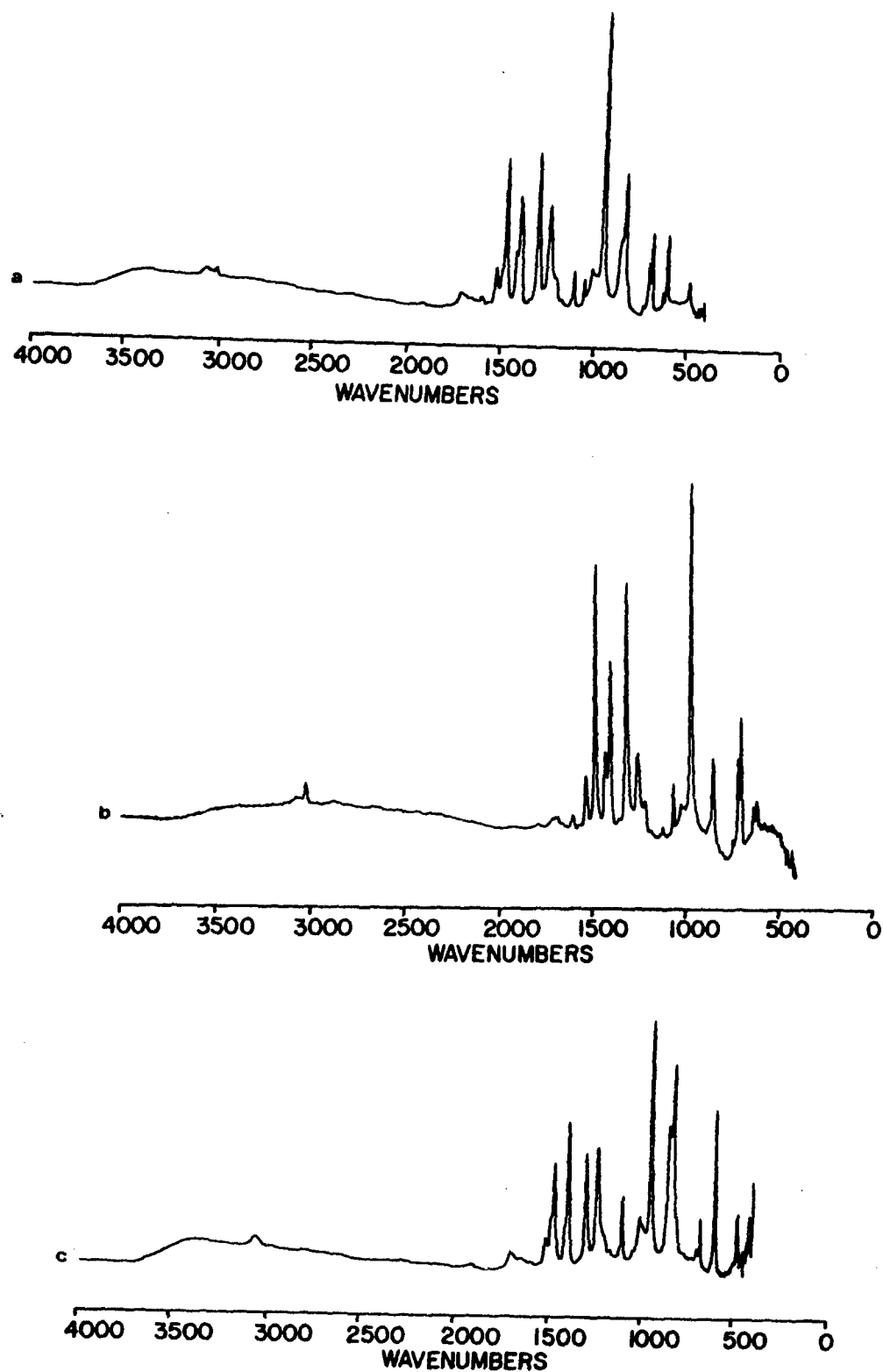


Figure IV.B.1

The infrared spectra obtained for the poly(p-phenylene benzobisthiazole) film S₁; a) obtained using unpolarized irradiation; b) spectrum obtained using irradiation polarized parallel to the extrusion (chain) direction; c) spectrum obtained using irradiation polarized perpendicularly to the chain axis.

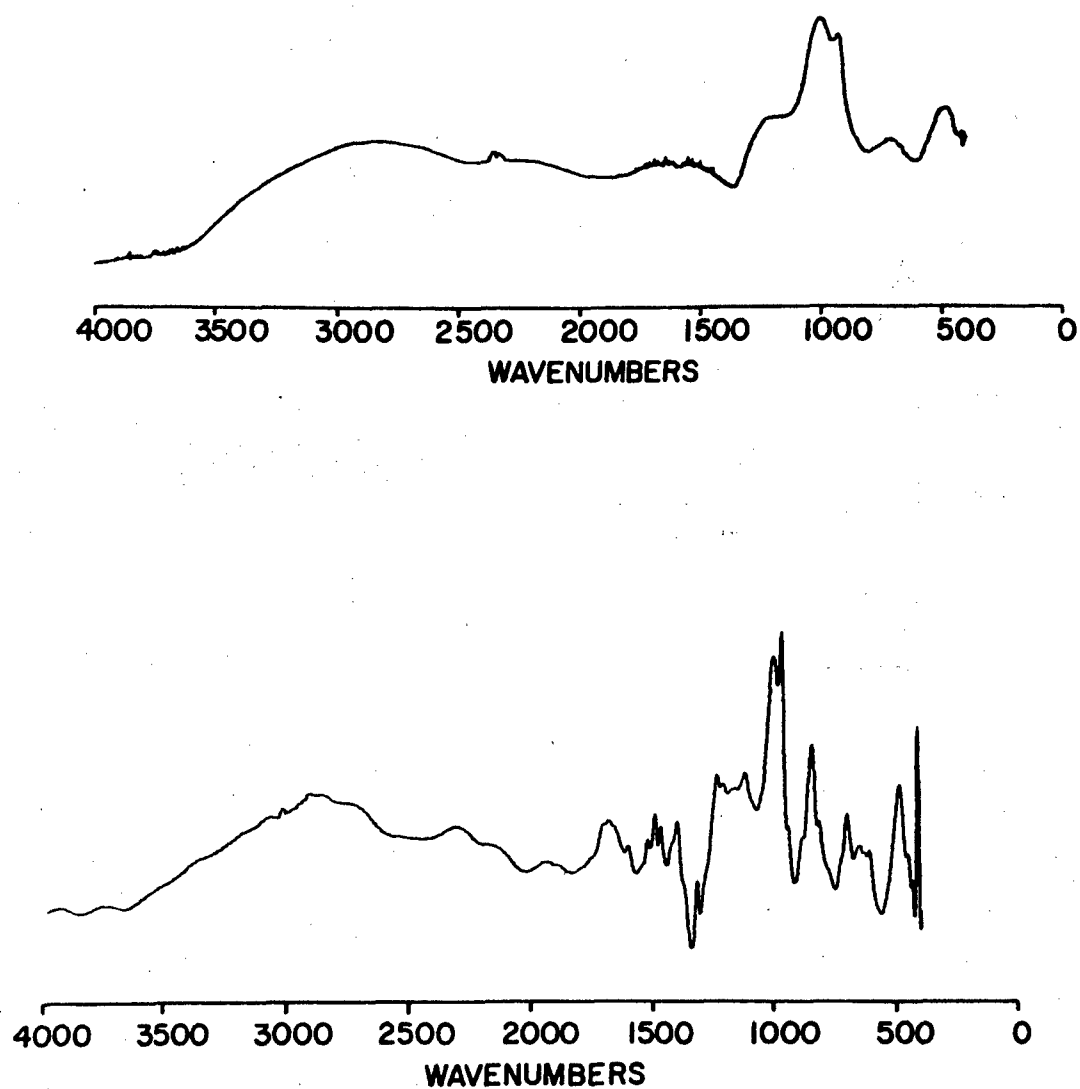


Figure IV.B.2

a) Infrared spectrum of pure polyphosphoric acid, b) difference spectrum between an as-prepared film and an annealed film. For the sake of clarity, the y axis of this spectrum has been expanded.

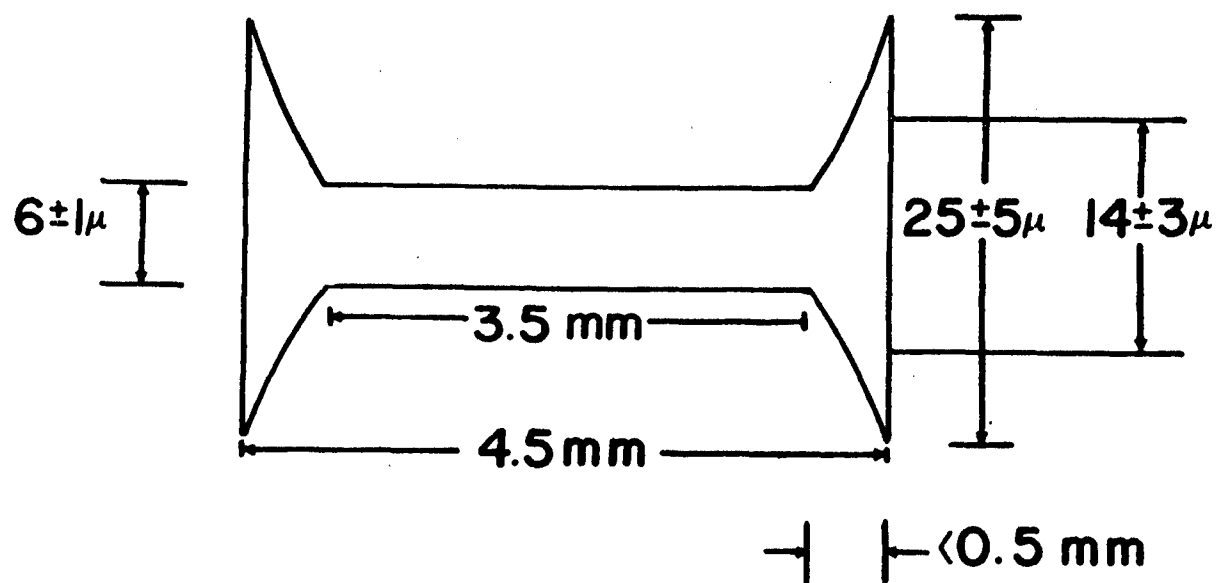


Figure IV.B.3

Schematic drawing of a S_1 film cross section.

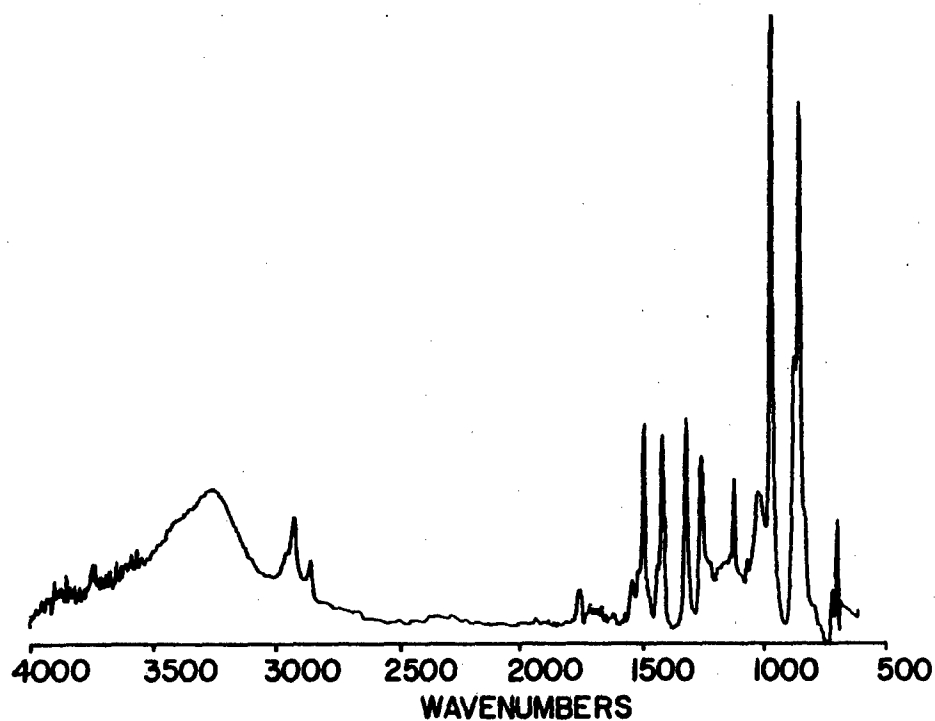


Figure IV.B.4

Infrared spectrum obtained for the poly(p-phenylene benzobisthiazole) film S₁ using attenuated total reflectance technique. Germanium crystal was used with an incident angle of 45°.

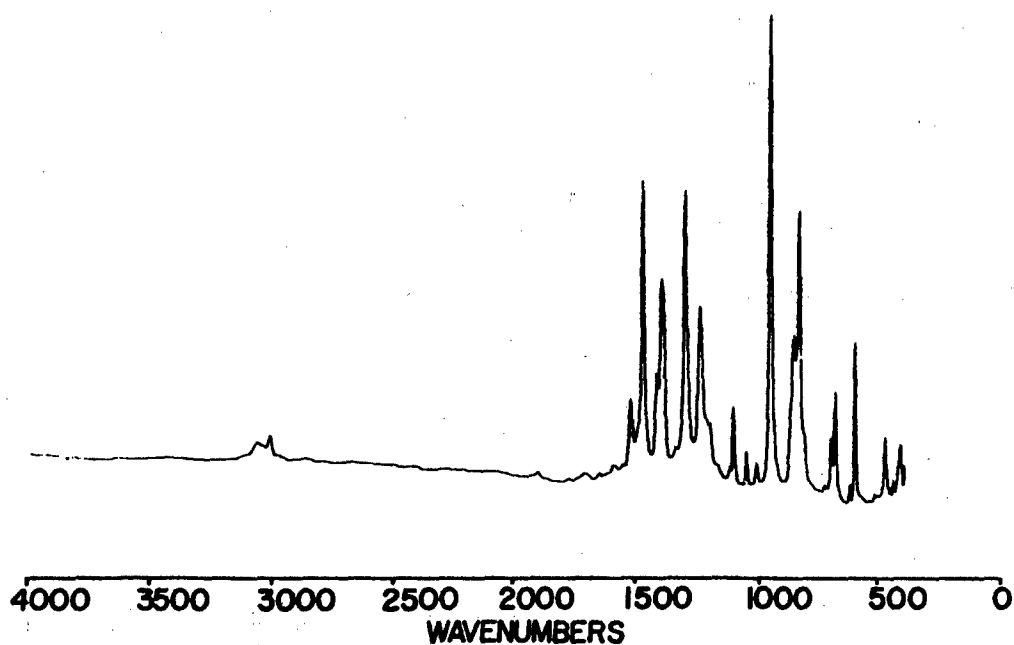


Figure IV.B.5

Infrared spectrum obtained for the poly(p-phenylene benzobisthiazole) film annealed at 415°C under tension.

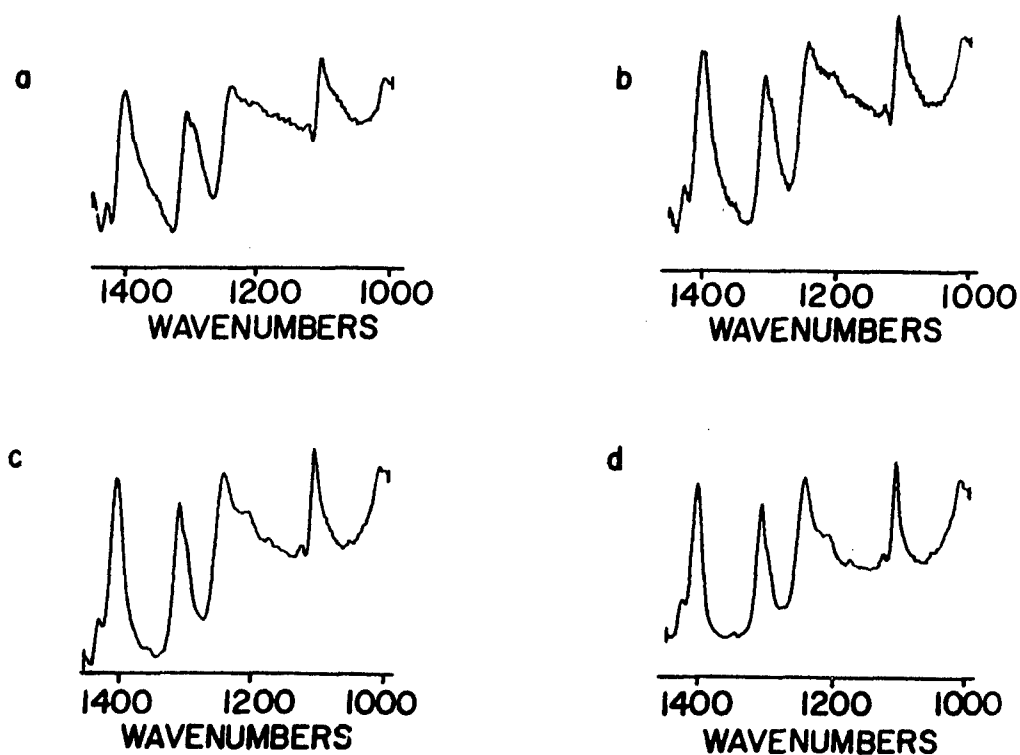


Figure IV.B.6

ATR spectra of PBT film on KRS-5 as a function of angle of incidence θ = a) 42.1° , b) 42.9° , c) 43.7° , and d) 45° . This is done by using TM wave and the extrusion axis oriented perpendicular to the incident plane.

SECTION V. TEMPERATURE AND STRAIN RATE DEPENDENCE OF THE DEFORMATION BEHAVIOR OF POLY(PARAPHENYLENE BENZOBISTHIAZOLE)

A. Summary

The mechanical properties of PBT films feature an interesting temperature and strain rate dependence. The elastic modulus and yield behavior have been studied over a wide temperature range from 30°C to 650°C. The onset of a structural reorganization is observed at about 300°C. The dependence of yield stress on strain rate at different temperatures was examined in terms of the Eyring theory of an activated rate process. We found that the stress activation volume varies with temperature. The overall elastic-plastic behavior as a function of temperature and strain rate was interpreted in terms of a previously suggested model that incorporates residual stresses in a rigid rod-like polymer. Enhancement of modulus was also observed due to deformation of the films under elevated temperatures, where better molecular orientation and lateral ordering are achieved.

B. Introduction

Poly-(p-phenylene benzobisthiazole) (PBT) is a wholly aromatic, extended chain, rigid rod-like polymer. It can be processed into fibers and thin films of high modulus, high strength and good thermal stability [1-4]. The structure of PBT has been reported as well aligned rods packed in a two-dimensional net with translational displacements along the chain axis [5]. The morphological features and mechanical properties of PBT films before and after heat treatment are discussed in a recent communication [6], where the elastic-plastic behavior of the material is accounted for by a nonuniform residual stress distribution. The tension heat treatment enhances greatly the axial modulus and strength. Straightening of buckled macrostructure regions was observed by scanning

electron microscopy. A more detailed model incorporating the residual stresses introduced during coagulation of a rod-like structure has been developed to interpret the effectiveness of tension heat treatment in case of PBT fibers [4]. The overall sample orientation improvement and lateral crystallite size increase from tensioned heat treatment has been detected by means of WAXS in both fibers and films [6-9].

The primary emphasis of previous studies was focused on the deformation behavior and morphological aspects evaluated before and after heat treatment. Limited data are available on the mechanical properties of PBT fibers, measured at high temperatures. An interest arose to follow the mechanical properties and failure mechanism as a function of temperature and strain rate. Tensile deformation as a material response to temperature and loading rate is of great theoretical and technical interest.

The experimental part of the work reported below includes the following: determination of the temperature dependence of tensile modulus, yield stress and ultimate properties of PBT film by means of short-term isothermal tests, evaluation of the effect of annealing on the modulus changes on the return cycle (cooling); measurements of the yield stress as a function of strain rate at different temperatures and thermal stress analysis for the samples subjected to successive heating. The data obtained indicate that as-extruded PBT films undergo a structural transition in the temperature range close to 300°C which changes the character of the tensile and stress-relaxation behavior.

C. Experimental Details

1. Material

The PBT films used in this study were obtained from Celanese Research Corporation. Films were extruded through a dry-jet wet spin apparatus from PBT solution in polyphosphoric acid (9.2% solids) into a water coagulation bath. Deionized water was used as a washing bath. The measured denier was 416 and final width of the air-dried (without tension applied) samples was 4.5mm.

2. Tensile Tests

The tensile tests were performed on a Instron Testing Machine with strain rates from $0.04 \times 10^{-3} \text{ sec}^{-1}$ to $8.33 \times 10^{-3} \text{ sec}^{-1}$ and over a range of temperature from 30°C to 675°C in nitrogen atmosphere. Test samples of gauge length 200 mm were aligned inside a tubular oven parallel to the axis of the jaws of an Instron machine. Free ends of the samples mounted on the paper tabs were gripped outside of the oven. Room temperature air was blown onto the jaws in order to minimize the machine compliance due to heating. Samples were conditioned for 5 minutes at each temperature prior to each test.

3. Oven Construction

Figure V.C.1 shows a schematic diagram for the oven used as environmental chamber. It consists of two coaxial silica cylinders. Heating wires were wrapped on the surface of the inner cylinder. The outer cylinder was insulated with asbestos and covered with a metal jacket. The oven was provided with two

gas inlets. Nitrogen gas was purged into the upper inlet at a rate of 4 liters/min during the heating and 20 liters/min when cooling was required. The gas circulates around the wiring in the space between two tubes and enters the specimen chamber through the lower inlet in the inner cylinder.

Nitrogen gas circulation suppresses the oxidation process of the polymer and regulates the heating and cooling of specimen chamber. The upper and lower ends of the oven were sealed with asbestos covers such that only two small ports were left to allow sample insertion. A removable flattened metal tube was used to avoid sample damage during this insertion. A platinum RTD thermocouple was placed near the sample surface in the middle of the oven. Temperature control and regulation was provided by means of a rheostat. The temperature gradient along the oven, from the middle to the ends, was measured as $-0.34^{\circ}\text{C}/\text{mm}$ at 100°C and $-1.1^{\circ}\text{C}/\text{mm}$ at 700°C .

4. Force-Temperature Experiment

Using the previously described equipment, the stress changes in the sample could be followed over a temperature range of 30°C - 650°C . A heating rate of $11^{\circ}/\text{min}$ with a variation $\pm 3^{\circ}/\text{min}$ was controlled manually.

D. Results and Discussion

1. Stress-Strain Behavior

The PBT films possess an elastic-plastic type of deformation at test temperatures from 30°C and up to 550°C . The departure from linear elastic behavior and influence of tension heat treatment on the deformation behavior has been

previously discussed in terms of structural irregularities and internal stresses introduced during processing. The plasticising effect of any residual solvent also has to be taken into consideration [10]. More careful examination of this matter is in progress and will be reported in a future communication [20].

Representative stress-strain curves, for different temperatures, obtained at the same strain rate ($0.08 \times 10^{-3} \text{ sec}^{-1}$) are shown in Figure V.D.1. We observed that the portion of the apparent plastic deformation gradually increased at the expense of an elastic one in the 30°C-300°C region. The reverse was observed when the temperature was further increased. The material became stiffer again and showed a dominant elastic behavior. The stress-strain dependence at 580°C and above appeared to be completely linear.

The dependence of ultimate stress and strain, yield stress and elastic modulus on the temperature was derived from the stress-strain curves. The value of the highest stress was taken as the ultimate strength σ_F . The ultimate strain ϵ_F corresponds to the elongation at the breaking point with the Young's modulus E calculated from the slope of the initial linear region of the stress-strain curve. The yield point was estimated from the intersection of two tangent lines [11].

The mean value of $\epsilon_F(T)$, $\sigma_F(T)$, $\sigma_y(T)$ and $E(T)$ are plotted in Figure V.D.2 as ratios of the characteristic values obtained at room temperature. According to these data PBT can be regarded as an interesting thermally stable polymer, whose strength hardly changes up to 450°C. The fact that ultimate strength does not decrease in this region may indicate a more efficient straightening of the buckled elements during the testing at higher temperatures, causing an internal

stress redistribution with resulting changes in the spectrum of the defects responsible for the specimen failure. The observation of the sample surface changes seems to confirm this suggestion. The surface appeared to be smooth and glossy after the testing in contrast to that of the manufactured film.

The lowering of strength starting from 450°C was accompanied by a color change from yellowish to metallic blue which progressively increases, until decomposition (above 650°C) where the material became black and lost most of its mechanical properties. The considerably lower temperature of degradation than observed by DSC and DTA [20] is very likely due to thermo-oxidation because of the presence of oxygen in the testing environment.

On the basis of the strain prior to fracture [12] two transitions can be identified: a "brittle-ductile" transition taking place at temperature range up to 200°C and reverse "ductile-brittle" transition occurring above 300°C. The best drawing properties were observed in the temperature region of 180°C-350°C where a nice smooth surface finish was developed during the test. This is consistent with the behavior during the loading-unloading cycles (see following discussion in corresponding section). Above 500°C the typical brittle fracture resulted in a uniform breakage in the middle of the specimen (e.g. samples H and I in Figure V.D.3). In this region the polymer behavior is noticeably effected by the degradation process as it can be clearly seen on the curve corresponding to the temperature dependence of elastic modulus. These data suggest that the temperature range studied can be divided into three regions. In the first region (30°C-300°C) the modulus of PBT decays with the temperature similar to that of other polymers. Since lateral interactions decrease with temperature the

deformation process is facilitated at higher temperature and larger material compliance is observed. The modulus reaches its minimum value (50% of that at ambient temperature) at 300°C. The second region is characterized by steady enhancement until the modulus reaches a new maximum (about 75% of the initial value) at 575°C. The following deterioration of the mechanical properties is most likely due to thermal degradation.

According to a previous model for PBT fibers and films based on the existence of overstressed buckled elements in the structure, the modulus of such a material will be governed by the degree of straightening of these elements. It is logical to assume that unbuckling requires a smaller applied force when the temperature is raised. The yield stress varies in this manner over the region of 30°C-300°C and passes through a minimum in the region of 250°C-400°C. Higher stresses are required for plastic deformation at temperatures above 400°C, since the material becomes stiffer. This suggests that the motion of the structural units becomes more restricted due to changes in the internal structure. Apparently the five minutes of thermal conditioning employed (essentially a short term nontensioned heat treatment) is sufficient to produce these changes. At higher temperatures these structural changes dominate over the softening effect of temperature. The ratio of the yield stress to modulus, which is essentially the strain at yield, also changes with the temperature. The value of 0.005 calculated at room temperature is much smaller of that for typical polymers (0.025 [13-15]) most likely due to the perfection of the chain alignment.

2. Heating-Cooling Experiment

Figure V.D.4 shows the variation of the modulus as a function of temperature upon cooling. In this experiment, samples were annealed for 5 minutes at 190°C (curve B) and 575°C (curves C and D) then the temperature was lowered and tensile tests were carried out (after conditioning for an additional 5 minutes at each test temperature). The lowest curve (A) is the same as in Figure V.D.2 for comparison. The path of return cooling curves is different to that of the heating. The modulus steadily increases upon cooling. After untensioned annealing at 575°C the performance of PBT can be improved in such a way that at 350°C the modulus is equal to over 80% of that of initial sample at 30°C , and exceeds the initial value by 20% when completely cooled (data on the curve C).

The difference between the three cooling curves is due to different measuring procedures employed. While curve C was constructed according to the mean values obtained at each temperature for a number of samples, curves B and D represent the measurements done on single specimen throughout the entire temperature range. Much higher values of modulus are achieved upon cooling due to strain cycling (work hardening) effect for these multiply tested specimens as reflected in curve D. Curve B (cooling) is likely to be analogous to the first part of curve A (heating to 190°C). The deviation in modulus values observed can be accounted for the same effect of work hardening. These observations suggest structural changes are initiated in the vicinity of 300°C .

It is also interesting to compare the elastic modulus changes upon heating and cooling for different types of polymers. The experimental data for three

selected polymers are combined in Figure V.D.5. Curve A shows the behavior of PBT, while curves B and C represent methyl cellulose (MC) and polymethylmethacrylate (PMMA), respectively [16]. The rate of the modulus decrease with temperature is highly dependent on molecular backbone stiffness. In the case of flexible chains (PMMA) the transition is considered as a glass-rubbery state transition and overall deformation achieved during the tensile test is fully recoverable. In contrast plastic deformation accumulates upon heating for MC and PBT. The noticeable irreversible increase in the modulus of MC measured above 200°C is accounted for the development of crystallinity in a previously amorphous polymer. PBT is characterized as a single phased material [9], and it seems that the changes in its structure follow a similar path overall general perfection of molecular order.

3. X-ray Data

The irreversible changes of structure with heat treatment of PBT could be detected by means of X-ray diffraction. WAXS flat film patterns for PBT films tensioned (during the tensile test) at different temperatures (30°C; 370°C and 650°C) are compared in Figure V.D.6. It is evident that for higher temperature a lower azimuthal spread of the major equatorial reflections is observed. This is associated with significant increase in the axial orientation. There is also an increase in extent and perfection of the lateral molecular order as observed from the decreased radial breadth of the same reflections. Increase in the lateral "crystallite" size accompanied by a simultaneous overall orientation

improvement has been previously suggested on the basis of study of the heat treatment on PBT fibers and films [4,7,9]. These morphological changes are substantially enhanced when tension is applied during heat treatment and results in greater improvement of mechanical properties of PBT as shown in Allen's work [9]. Accumulation of plastic deformation during the multiple tests on the same sample leads to higher modulus value achieved upon the cooling in our experiment (compare curves C and D in Figure V.D.4).

4. Work-hardening Effect

A separate series of experiments consisted of tensioning PBT films for a number of cycles at various temperatures. Typical data are represented in Figure V.D.7. The ratio of modulus after cycling to the initial modulus (E_c/E_o) is strongly dependent on the temperature and tension applied. The most efficient work hardening effect was observed in the temperature region corresponding to the extremum of the dependence $E(T)$, $\epsilon_f(T)$ and $\sigma_y(T)$. The modulus may reach 100% or higher with the number of cycles required relatively small (3-7) and dependent on the temperature and the load amplitude.

E. Activation Volume

It would be interesting to know whether appreciable changes in activation volume occur as the polymer changes its state. Different experimental methods for estimating the activation volume have been recently reviewed [17]. A method which employs a series of constant strain-rate tests is most appropriate for our investigation.

Stress-strain characteristics of PBT were obtained at different strain rates and different temperatures (30°C, 160°C, 305°C and 450°C). The experimental curves for 30°C and 160°C are given in Figure V.E.1. The yield stress is plotted as a function of logarithmic strain rate in Figure V.E.2. The data show that the yield stress depends strongly on the strain rate at room temperature whereas the dependence is very small at 305°C and 450°C. At these temperatures the material is seen to pass into a state where the yield process becomes almost time independent.

The observed linearity of the dependence of the yield stress on the strain rate (or time) at constant temperature can be described by the Eyring theory which deals with an activated rate process [18]. The Eyring equation for an activated rate process can be written in terms of strain rate and temperature as

$$\dot{\epsilon} = \dot{\epsilon}_0 \exp - \left(\frac{\Delta U - \sigma_y V^*}{kT} \right) \quad (1)$$

where $\dot{\epsilon}_0$ is a constant, ΔU is the activation energy for an activated-rate process, σ_y is the yield stress, V^* is the stress activation volume, k is the Boltzmann constant and T is the absolute temperature. This equation implies that stress at yield and the logarithm of strain rate have a linear relationship with a slope given by

$$\frac{\partial \sigma_y}{(\partial \ln \dot{\epsilon})_T} = \frac{kT}{V^*} \quad (2)$$

Figure V.E.3, shows the calculated values of the stress activation volume V^* plotted as a function of test temperature. A relatively small increase of the activation volume with test temperature is observed in the lower temperature range. There is, however, a rapid increase in V^* for test temperature at 300°C and above. Above approximately 300°C the activation volume is nearly independent of temperature. The activation volume estimated for temperatures above 300°C is approximately an order of magnitude higher than that estimated for temperatures below 150°C .

1. Extension-Contraction

In this experiment, axial stress was constantly monitored as the temperature was raised from ambient to 650°C , while the length of specimen was held constant. We found that a measurable shrinkage force is developed at a very early stage of heating even with no initial constraint (Figure V.E.4, curve A). The force reaches a maximum at approximately 80°C and decays to zero at about 150°C . In this region, a continuous elongation of the film occurs. With increased temperature a very rapid increase in the retractive force occurs at about 600°C . Results obtained on the preloaded samples follow a similar trend except that the initial shrinkage force has been over-balanced by a higher applied stress on the sample. The temperature of the recovery (full release of the applied stress), the temperature where new contraction starts and the temperature for the maximum of the shrinkage force are strongly dependent on the pre-loading regime (see Figure V.E.5). The rate of contraction at high temperatures indicates the intensity of the structural reorganization, the latter can be

manipulated by the applied temperature and/or tension within the limits of material strength and thermal stability. A combination of 150-200 MPa tension at 630°C-670°C was found optional on the basis of systematic study for PBT fiber heat treatment [9].

Although the interrelationship between applied force, temperature and sample shrinkage is evident, the mechanism of the sample extension-retraction behavior with heat treatment remains unclear. Generally the changes in the material properties under the influence of heating and tension are certainly related to straightening of the buckled segments of the microfibrils and further perfecting of structure. The observed modulus increase with the higher test temperature also may suggest a densification mechanism (loss of microvoids) in analogy with plastically deformed carbon fibers [22]. More advanced discussion is difficult because it is hard to separate all the effects including the influence of residual solvent found in starting material [10].

F. Conclusion

The deformation behavior of poly(p-phenylene benzobisthiazole) films which consist of a fibrillar structure composed of highly oriented rod-like molecular bundles was studied as a function of temperature and strain rate. Both the tensile modulus and yield stress show a similar temperature dependence. They decrease slowly under the influence of increasing temperature to minimum values around 300°C; and after then they start to increase with the test temperature. Upon cooling the elastic modulus of PBT films, annealed at 600°C, increases with

decreasing test temperature. The considerable enhancement of modulus is similar to that produced by tensioned heat treatment.

Cyclic deformation and tensioned heat treatment of PBT films improve the overall orientation and the lateral ordering of the structure which consequently enhances the strength and modulus. The interrelationship between tension and temperature is such that similar results may be achieved by either variable within the limits of the material strength and thermal stability.

The yield stress of PBT increases linearly with the strain rate at a chosen test temperatures. This behavior can be modeled in terms of a single activated rate process. The stress activation volume for the deformational processes calculated from the Eyring rate theory showed a rapid 10 fold increase in the region of 150-300°C to a constant activation volume at higher temperatures. The stress at break of the PBT films remained nearly unchanged over a considerable temperature range (up to 500°C), which indicates good strength at high temperatures. The strain at break showed a temperature dependence with a maximum, around 300°C, which may be considered as an optimum temperature for ductile behavior.

Tensioned PBT films showed an expansion-contraction behavior upon successive heating, associated with mobility changes of structural elements in the polymer system which leads to an irreversible change in thermomechanical properties.

References

1. F.E. Arnold and R.K. Van Dusen, J. Appl. Polymer Sci. 15, 2035 (1971).
2. S.R. Allen, A.G. Filippov, R.J. Farris, E.L. Thomas, C.P. Wong, G.C. Berry and E.C. Chenevey, Macromolecules 14, 1135 (1981).
3. S.R. Allen, A.G. Filippov, R.J. Farris and E.L. Thomas, J. Appl. Polym. Sci. 26, 291 (1981).
4. "The Strength and Stiffness of Polymers," ed. A.E. Zachariades and R.S. Porter, 359, Marcel Dekker, New York, 1983.
5. E.J. Roche, T.T. Takahashi and E.L. Thomas, American Chemical Society Symposium Series, "Fiber Diffraction Methods," 141 (1980).
6. L. Feldman, R.J. Farris and E.L. Thomas, J. Mater. Sci., to be published.
7. J.R. Minter, K. Shimamura and E.L. Thomas, J. Mater. Sci. 16, 3303 (1981).
8. J.A. Odell, A. Keller, E.D.T. Atkins and M.J. Miles, J. Materl. Sci. 16, 3309 (1981).
9. S.R. Allen, R.J. Farris and E.L. Thomas, to be published.
10. C. Chang and S.L. Hsu, to be published.
11. I.M. Ward, J. Mater. Sci. 6, 1397 (1971).
12. N. Brown and I.M. Ward, J. Mater. Sci. 18, 1405 (1983).
13. B. Hartman and R.F. Cole, Polym. Eng. Sci. 23, 13 (1981).
14. N. Brown, Mater. Sci. Eng. 8, 69 (1971).
15. Z.D. Jastrzebski, "The Nature and Properties of Engineering Materials," Wiley, New York, 1959.
16. S.K. Zakharov, N.A. Dolotova, G.A. Petropavlovskii, G.G. Vasileva, L.K. Feldman (ne. Yakovenko), E.V. Kuvshinskii, Khimia Drevesiny 4, 26 (1977).
17. J.R. White, J. Mater. Sci. 16, 3249 (1981).

18. P.D. Coats and I.M. Ward, J. Mater. Sci. 13, 1957 (1978).
19. E.L. Thomas, R.J. Farris and S.L. Hsu, AFWAL-TR-80-4045, "Mechanical Properties vs. Morphology of Ordered Polymers," Volume V. (1983).
20. L. Feldman, C. Chang, et al., to be published.
21. T.E. Brady and G.S.Yeh, J. Appl. Polym. Physics 42, 12, 4622 (1971).
22. G.E. Mostovoi, L.P. Kobets and V.I. Frolov, Mechanics of Composite Materials 15, 1, 20 (1979).

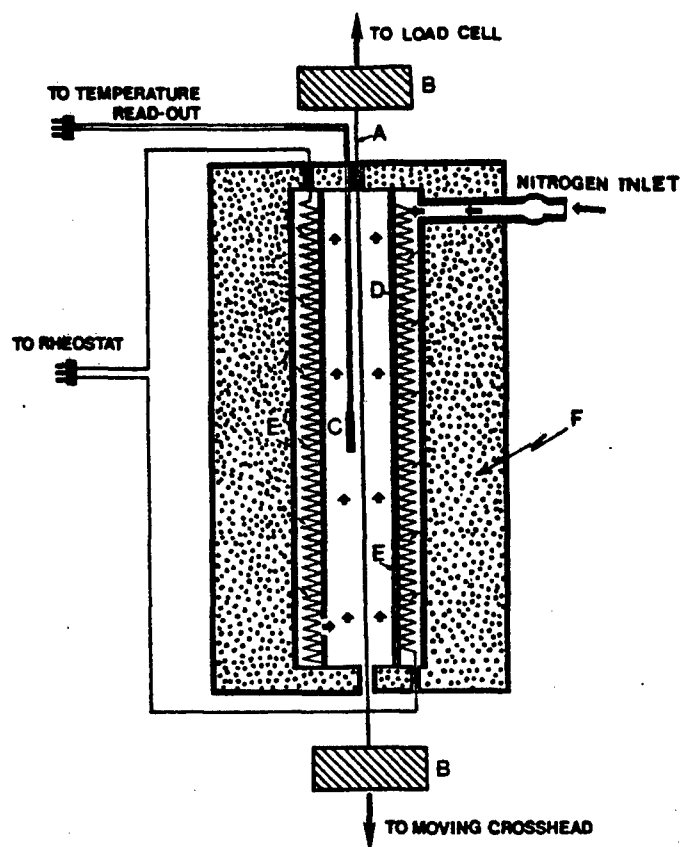


Figure V.C.1

Schematic of the test arrangements; A-sample; B-clamps of the testing machine; C-thermocouple; D-heating wire; E-thermoresistant glass; F-insulation.

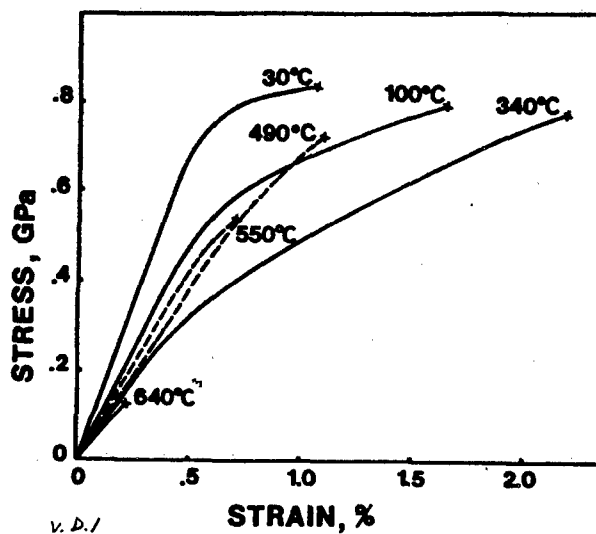


Figure V.D.1

Stress-strain curves at various temperatures for PBT film at a strain rate $0.08 \times 10^{-3} \text{ sec}^{-1}$.

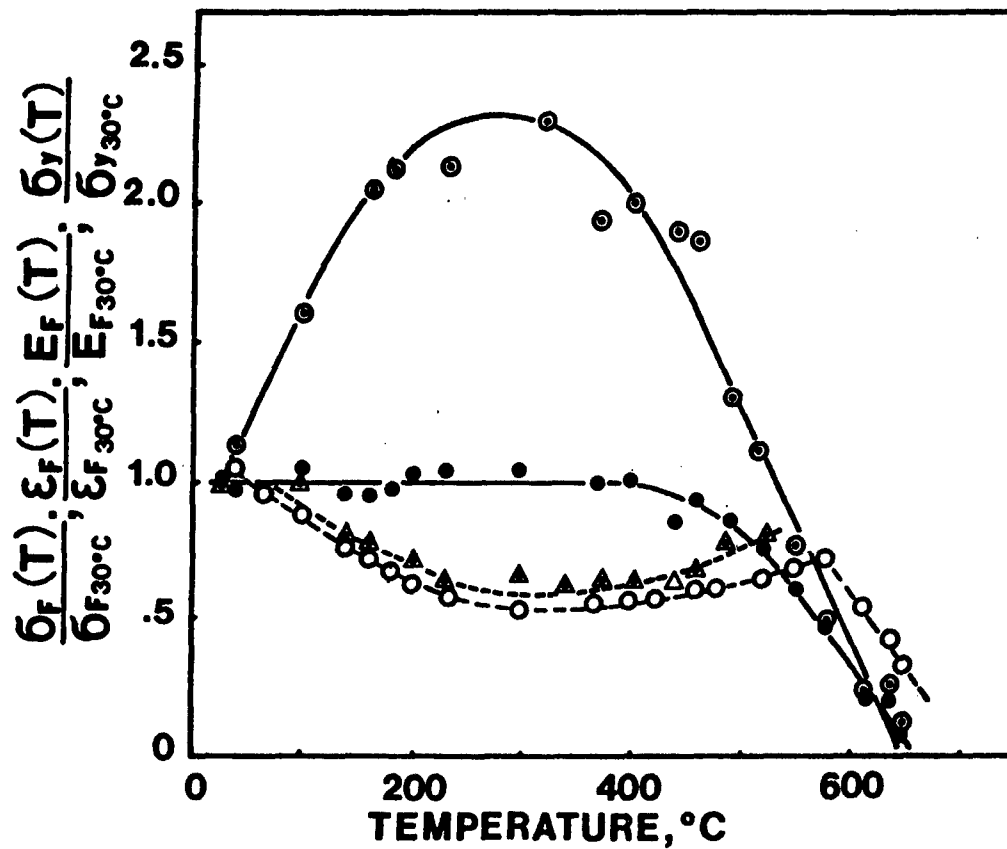


Figure V.D.2.

Effect of test temperature on the relative changes of the mean values of :
 1) ultimate strength (●●●); 2) Young's modulus (ooo); 3) yield stress (△△△);
 4) elongation of PBT film (ooo).

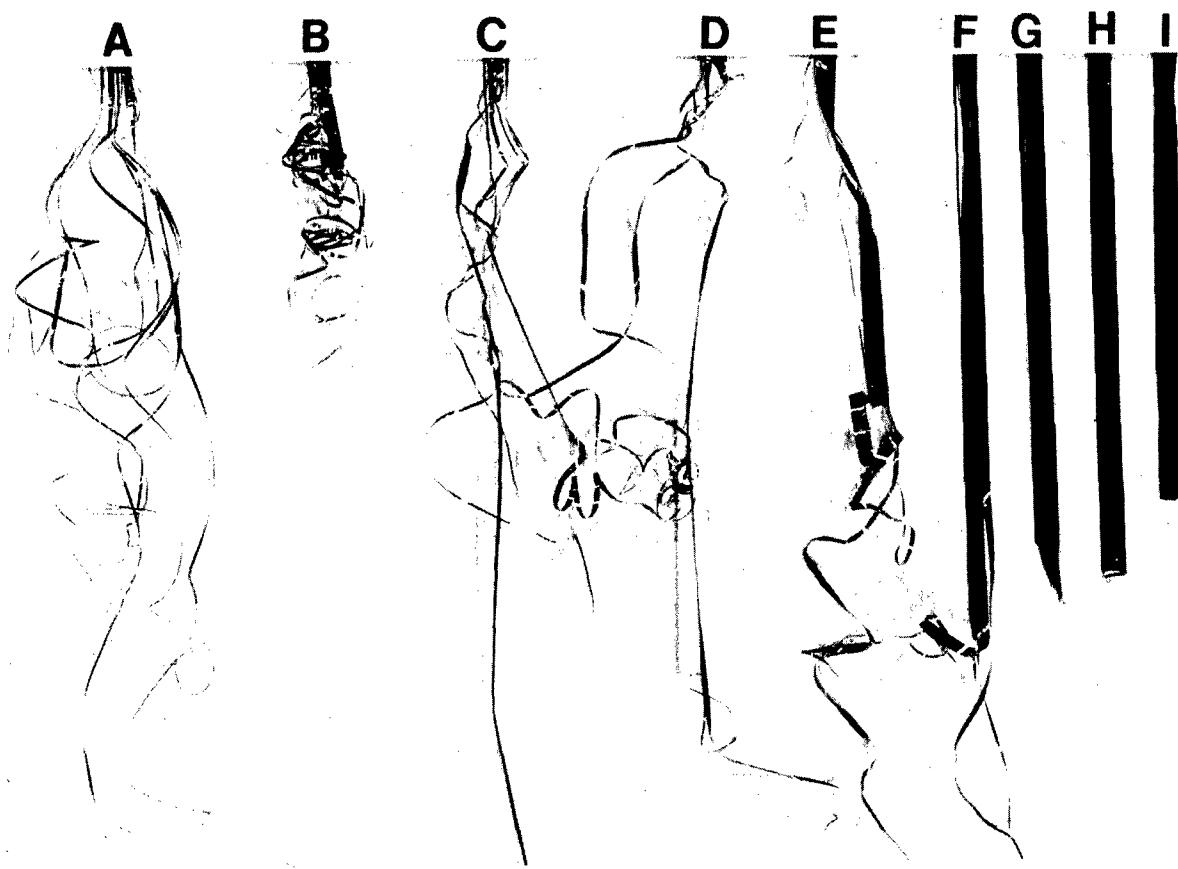


Figure V.D.3

Photograph of PBT film samples after fracture at evaluated temperatures:
A) 60°C; B) 144°C; C) 185°C; D) 370°C; E) 440°C; F) 490°C; G) 550°C; H)
613°C; I) 650°C.

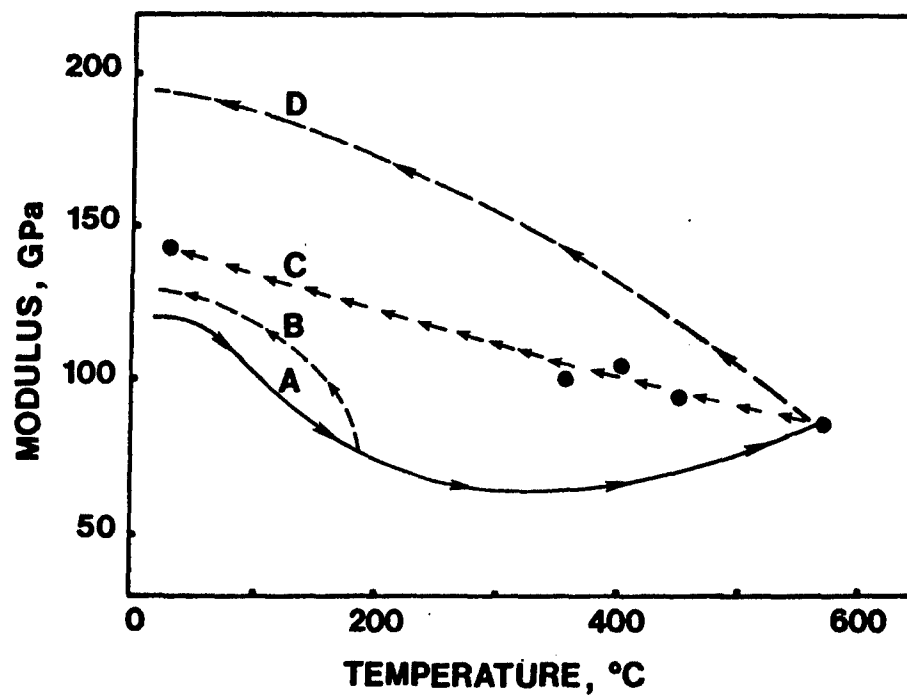


Figure V.D.4

Variation of the modulus as a function of temperature in heating-cooling experiment. Notation explained in the text.

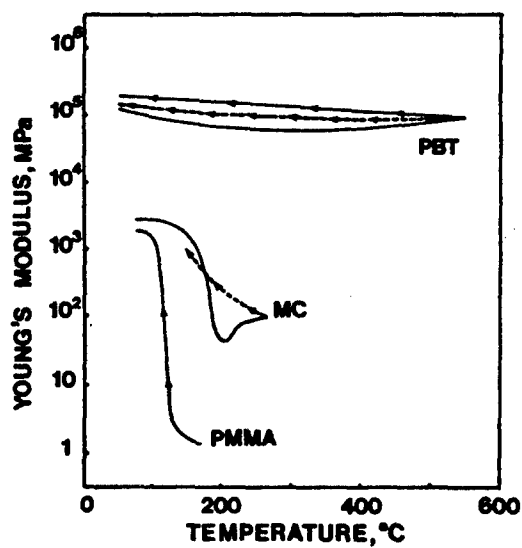


Figure V.D.5

Modulus vs. test temperature for various polymers: PBT, methylcellulose and poly(methylmethacrylate).

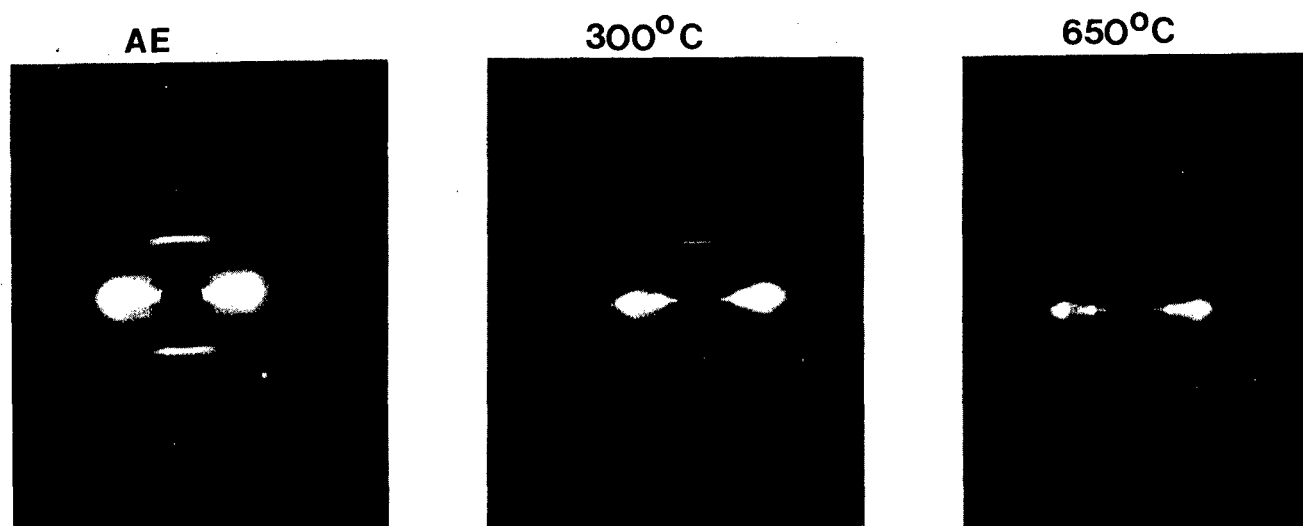


Figure V.D.6

The WAXS Flat film patterns of 1) the as-extruded sample and 2) tensioned at 300°C and 650°C samples.

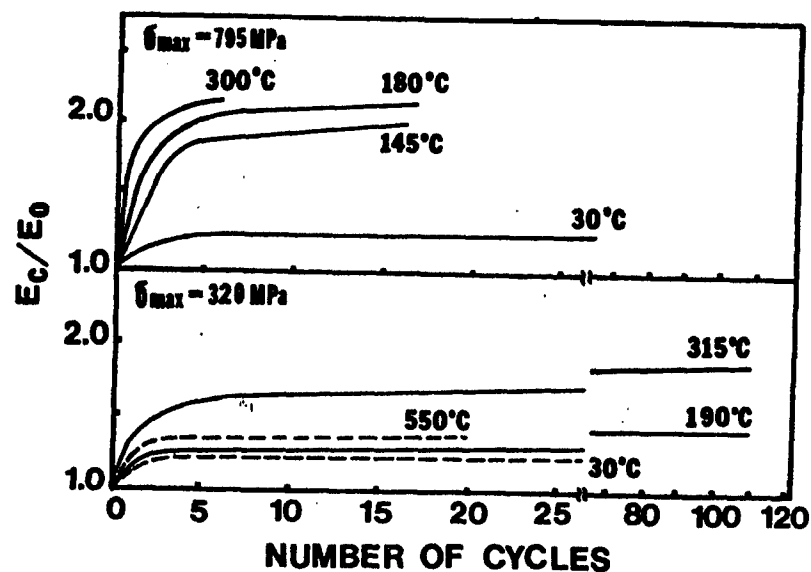


Figure V.D.7

The dependence of modulus increase measured at different temperatures on the number of cycles - top A: for a load amplitude 795 MPa; bottom B: for a load amplitude 320 MPa.

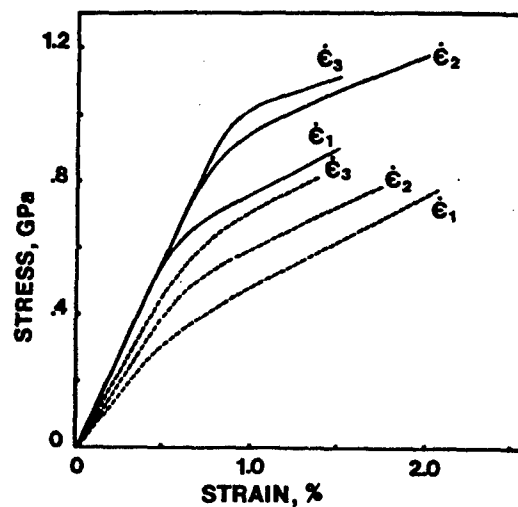


Figure V.E.1

Deformation curves obtained at 30°C (solid lines) and 160°C (dashed lines) and various strain rates: $\epsilon_2 = 0.04 \times 10^{-3} \text{ sec}^{-1}$; $\epsilon_3 = 0.42 \times 10^{-3} \text{ sec}^{-1}$; $\epsilon_1 = 4.17 \times 10^{-3} \text{ sec}^{-1}$.

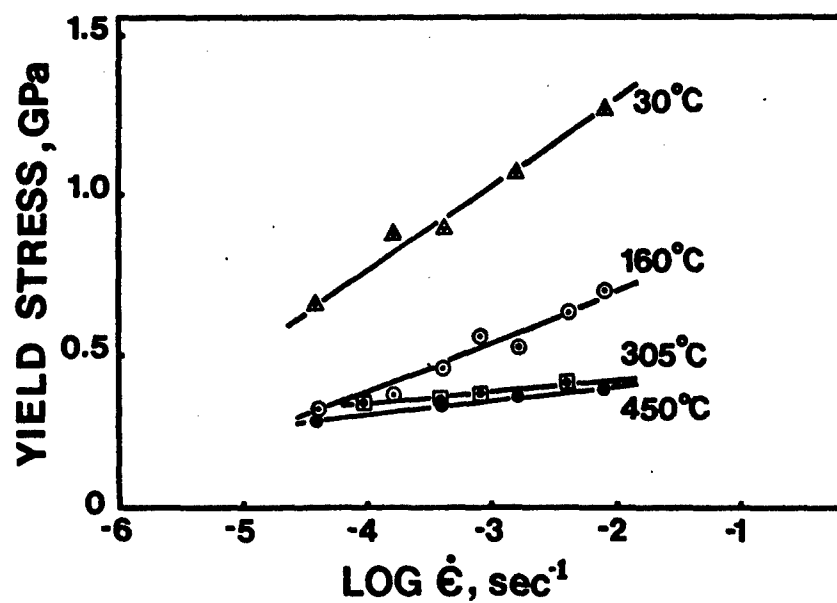


Figure V.E.2

The yield stress of PBT as a function of temperature and strain rate.

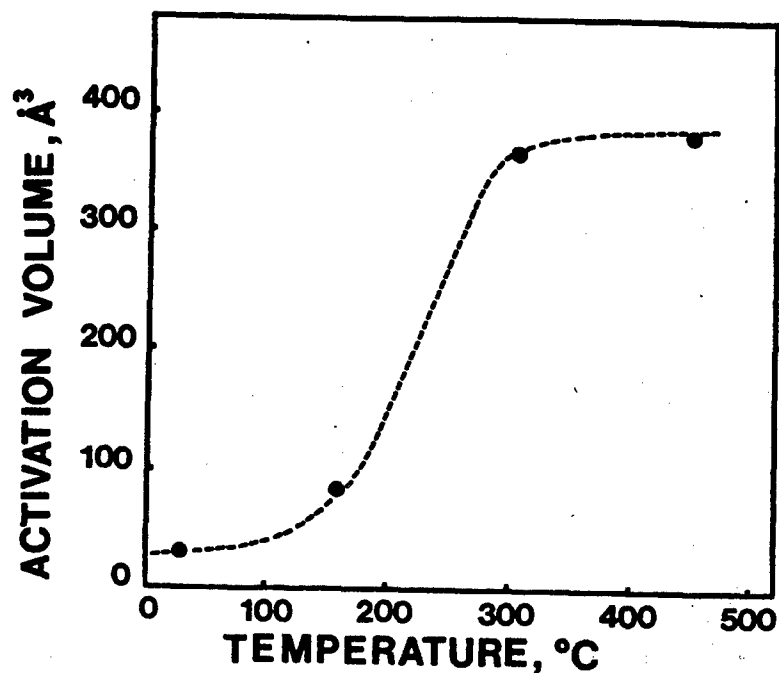


Figure V.E.3

The dependence of the activation volume on the temperature.

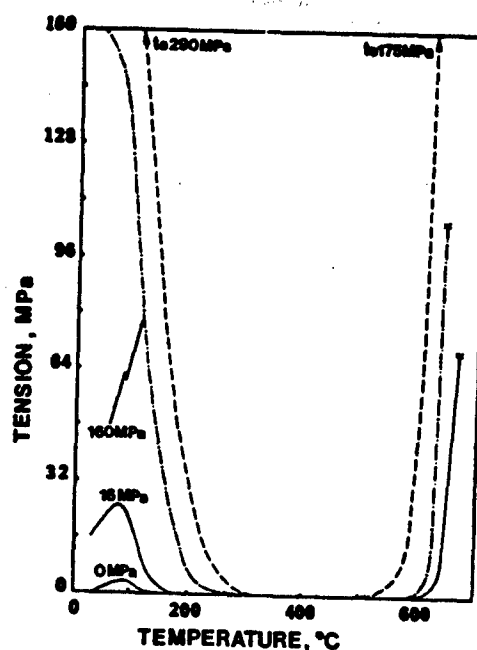


Figure V.E.4

Force-temperature dependence for PBT film: without external constraint and with an applied stress of 16 MPa, 160 MPa and 290 MPa.

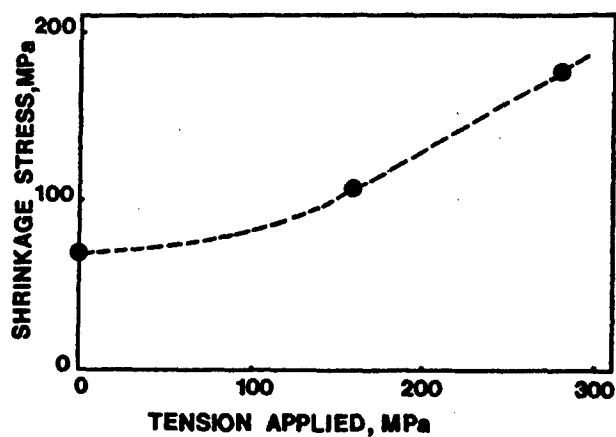


Figure V.E.5

The shrinkage force as a function of applied tension prior to annealing.

SECTION VI: FORCE-TEMPERATURE BEHAVIOR OF RIGID ROD POLYMERIC FIBERS

A. Introduction

Force versus temperature (F-T) experiments have been used extensively for the thermodynamic analysis of rubbers [1,2]. More recently, the force-temperature behavior of elastomeric materials has been used to examine structure property relationships [3,4]. In this paper, force-temperature analysis is extended to anisotropic rigid rod polymeric fibers; Kevlar®29, Kevlar®49, (duPont's heat treated version of Kevlar®29), as-spun poly (p-phenylene benzoisthiazole) and heat treated PBT.

Thermal expansion properties of materials may be readily examined from simple force-temperature experiments. Writing the total differential for force, f , in terms of length, L , and temperature, T , one can readily obtain the relation

$$\left(\frac{\partial f}{\partial T}\right)_L = - \left(\frac{\partial f}{\partial L}\right)_T \left(\frac{\partial L}{\partial T}\right)_f. \quad (1)$$

Normalizing the equation by a reference area A_0 and length L_0 , the equation becomes

$$\left(\frac{\partial \sigma}{\partial T}\right)_\epsilon = - \left(\frac{\partial \sigma}{\partial \epsilon}\right)_T \left(\frac{\partial \epsilon}{\partial T}\right)_\sigma = -E\alpha. \quad (2)$$

where σ = uniaxial stress

ϵ = uniaxial strain

E = Young's modulus

α = linear thermal expansion coefficient

The slope of the axial stress versus temperature plot is, therefore, the negative product of the axial modulus and the axial thermal expansion coefficient. The thermal expansion coefficient, α , can be obtained from the slope of the (F-T) curve if the modulus is determined independently.

Additionally, this technique provides a unique way to study material changes during the heat treatment processing of these fibers. Recently, a systematic study of the effects of heat treatment parameters (tension, temperature, residence time) on the mechanical properties of PBT has been performed [5,6]. From that work, it has been shown that both thermal input (temperature) and mechanical input (tension) are important factors for enhancement of the mechanical properties. In this paper, experiments examining the F-T behavior of PBT and Kevlar® are undertaken to examine any possible correspondence between thermal and mechanical input during heat treatment processing.

B. Experimental

A schematic of the force-temperature apparatus employed in this work is shown in Figure VI.B.1. A 30 cm yarn sample was fed through the oven; one end was clamped to a load cell while the other end was attached to a movable clamp. The sample was stretched to a fixed length by adjustment of the movable clamp and the temperature of the oven was controlled manually with a variac at a rate of approximately 5°C/min. The temperature was monitored by a platinum resistance (RDT) thermocouple situated in the middle of the oven. The resulting stress and its change with temperature was monitored on an X-Y recorder. To prevent degradation of the material at the high temperatures achieved, nitrogen was continuously flushed through the oven.

The PBT fibers investigated in this work were dry-jet wet spun at the Celanese Research Company from anisotropic polymer solutions of approximately 10 wt% PBT in polyphosphoric acid. These same fibers were heat treated at 650°C for 8 seconds and are designated PBT-HT. Kevlar®29 yarn and Kevlar®49 yarn were obtained commercially from duPont. Steel yarn was obtained from Bekeart Steelwire Corporation.

The tensile properties for these materials were determined on single filaments in accordance with ASTM standards for testing high-modulus single filament materials [7]. Reported moduli were corrected for the compliance of the testing machine and were based on the linear densities of the materials. The deniers were furnished for PBT, by the Celanese Research Co., and for Kevlar®29 and Kevlar®49 by duPont, [7,8]. The denier of the steel yarn was calculated by weighing the sample.

Wide angle X-Ray diffraction results were obtained from both diffractometric and flat film techniques. Flat film fiber patterns were obtained in a Warhus (Statton) camera employing pin-hole (0.2mm) collimation and a sample to film distance of 18 mm. Diffractomer (2θ) scans of equatorial reflections were obtained on a Siemens D-500 diffractometer utilizing line focus collimation. Incident beam diffractometer slits of 0.3° (2θ) with a final slit of $.15^\circ$ (2θ) were used for a scan rate of 1° (2θ)/min. $\text{CuK}\alpha$ tubes operated at 40KV and 30 mA were used for both the Warhus camera and Siemens diffractometer.

C. Results and Discussion

According to equation (2), materials possessing a positive thermal expansion coefficient (as most materials do), will experience a stress drop with increasing temperature when maintained at constant length. To test the validity of this equation and the accuracy of the F-T apparatus, a steel yarn was first examined. A stress drop with increasing temperature is observed for the steel yarn (Figure VI.C.1) indicating a positive thermal expansion coefficient, as expected. The F-T behavior is reversible on cooling and the thermal expansion coefficient calculated from the slope of the F-T curve is approximately $7 \times 10^{-6}/^{\circ}\text{C}$ based on a modulus of 250 g/d. Since steel is known to have a thermal expansion coefficient of $9\text{-}11 \times 10^{-6}/^{\circ}\text{C}$ [8], the calculated value for α is in reasonable agreement considering the experimental errors inherent in the apparatus such as a 30°C temperature distribution within the oven, possible load cell compliance, as well as the neglect of any thermal expansion of the clamps.

The F-T behavior of the heat treated PBT yarn is shown in Figure VI.C.2a. The stress is observed to increase with increasing temperature indicating the existence of a negative thermal expansion coefficient. Similar behavior is displayed by the Kevlar®49 yarn as shown in Figure VI.C.2b. Although the modulus of PBT and Kevlar® is known to vary with temperature [6], the thermal expansion coefficient can be approximated using the room temperature modulus values of 1600g/d for PBT-HT and 1000g/d for Kevlar 49®. In these calculations, the yarn modulus is approximated by the single filament modulus. The calculated thermal expansion coefficient for PBT-HT is approximately $-1.1 \times 10^{-6}/^{\circ}\text{C}$ and approximately $-3.2 \times 10^{-6}/^{\circ}\text{C}$ for Kevlar®49. This value of α for Kevlar®49 is in close agreement with reported values of -2 to $-4 \times 10^{-6}/^{\circ}\text{C}$ [9].

From the F-T behavior of Kevlar®49 (Figure VI.C.2b), it is observed that the stress does not increase linearly with temperature between 50°C - 100°C. On cooling followed by subsequent reheating, the stress is observed to vary linearly over this same temperature range. In order to understand this initial behavior, a sample of Kevlar®49 was heated to 200°C, cooled and allowed to relax at room temperature at atmospheric conditions for 24 hours. Upon reheating, the initial non-linear behavior returns as shown in Figure VI.C.3. A similar sample which is heated to 200°C, cooled, then placed in a desiccated environment for 24 hours, exhibited a linear increase in stress with temperature upon reheating (see Figure VI.C.3).

It, therefore, appears most likely that moisture absorption by Kevlar®49 causes this initial irreversible nonlinearity of the stress versus temperature curve. The removal of residual moisture is accomplished by the application of heat as evidenced by the linearity of the cooling curve. After removing the residual moisture, the stress level at room temperature is lower than stress level at room temperature before the application of heat (see Figure VI.C.3). This result is consistent with the possibility the Kevlar® has a negative axial swelling coefficient whereby the material gets longer when it dries.

Since the F-T profile for the PBT-HT sample is linear and completely reversible, PBT-HT yarn appears to be less moisture sensitive than Kevlar®49.

The F-T behavior of the as-spun PBT and Kevlar®29 yarns are most interesting as shown in Figure VI.C.4. For both materials, there is a dramatic stress drop with increasing temperature after the fiber has reached a critical

temperature denoted as T_T . In addition, the behavior of these fibers are seen to depend on their thermal history whereby the material upon cooling and subsequent reheating displays a linearly reversible behavior up to the maximum temperature it has been exposed to previously. At that point, the material again exhibits a drop in stress.

It is suggested that the observed stress drop with increasing temperature is associated with a change in molecular order or more simply, with the onset of effective heat treatment. If this is so, then a fiber would be expected to exhibit enhanced mechanical properties and increased molecular order if it has undergone a force-temperature history where T_T is observed.

A comparison of wide angle X-ray diffraction patterns of Kevlar®29 and Kevlar®29 forced temperature cycled (FTC)* shows sharpening of the equatorial reflections in the FTC-Kevlar®29 (Figure VI.C.5), indicative of an improvement in the extent and perfection of lateral molecular order. In addition, there is a sharpening of the meridional reflections which are now quite similar to those observed for Kevlar®49.

The WAXS diffraction patterns of as-spun PBT yarn before and after the force temperature cycling reveal no readily observable differences (see Figure VI.C.6). However, line profile analysis of the equatorial reflections shows a narrowing (measured as the full width at half maximum intensity above background (FWHM)) for the FTC-PBT (see Table VI.C.1). In addition, there is a shift in the peak position to lower scattering angles. Such narrowing of the peaks and the shifting of the peak positions indicate the existence of a higher degree of perfection of the lateral molecular order [6].

* The sample was subjected to a load of 5g/d, heated to 300°C and cooled to room temperature.

The tensile properties of Kevlar®29, FTC-Kevlar®29, as-spun PBT and FTC-PBT are shown in Table VI.C.2. For both Kevlar®29 and as-spun PBT, there is an enhancement of modulus with a reduction in strain at break for the cycled material. For PBT, the strength also increases when cycled whereas for Kevlar®29, the strength is the same within experimental error. This data agrees with known changes in mechanical properties due to heat treatment of PBT and Kevlar® [5, 10,11].

Both Kevlar®29 and as-spun PBT exhibit enhanced mechanical properties and increased molecular order after it has undergone a force-temperature history in excess of T_T . Thus, it is evident that the dramatic stress drop observed in the force temperature behavior of these materials depicts the onset of material change or of effective heat treatment.

The temperature of the onset of heat treatment, T_T , is dependent upon the applied stress as shown in Figure VI.C.7 for both as-spun PBT and Kevlar®29. With increasing applied stress, T_T decreases. By increasing the mechanical input (stress applied), less thermal input (temperature) is required to reach the activation energy required to induce material changes. The experimental data indicates that there is a linear correspondence between these two heat treatment parameters: stress and temperature. In addition, the slopes of T_T vs. applied stress for Kevlar®29 is greater than that of as-spun PBT. Thus, the onset of material changes for Kevlar®29 is much more sensitive to the application of tension than as-spun PBT, while the onset of material changes in as-spun PBT are more sensitive to temperature.

D. Summary

Force-temperature analysis provides a unique way to study the thermal expansion properties of a material. For PBT-HT and Kevlar 49®, the thermal expansion coefficients are evaluated to be approximately $-1.1 \times 10^{-6}/^{\circ}\text{C}$ and $-3.2 \times 10^{-6}/^{\circ}\text{C}$, respectively. The F-T technique provides a unique way to study the heat treatment processing of fibers. F-T results for as-spun PBT and Kevlar®29 display, in the form of a dramatic stress drop, material changes as evidenced by mechanical and structural changes which are due to a heat treatment process. A linear correspondence between the temperature at which the stress drop begins, T_T , (thermal input) and the initial stress applied (mechanical input) to induce material changes is found.

From the F-T behavior of Kevlar®29 as as-spun PBT, it is evident that these materials do not exhibit a linear thermal elastic behavior whereas Kevlar®49, PBT-HT and steel do. This complex history dependent behavior should be carefully considered in any engineering use of Kevlar®29 and as-spun PBT.

It is proposed that Kevlar®29 and as-spun PBT should exhibit considerably more creep under constant stress with the application of heat than their heat treated counterparts. It is suggested that the creep behavior of these materials is not viscous in origin since it is believed to be associated with a change in structure. The strain-temperature behavior of these rigid rod materials warrants further investigation.

References

1. P.J. Flory, "Principles of Polymer Chemistry, Cornell University Press, New York, 1953.
2. J. Aklonis, W.J. MacKnight and M. Shen, "Introduction to Polymer Viscoelasticity, Wiley-Interscience, New York, 1972.
3. D.X. Wang, R.E. Lyon and R.J. Farris, J. Macromolecular Science, submitted.
4. T. Okino, M. Maruta and K. Ito, "Thermal Stress/Strain Analyzer and Its Applications," ed. B. Miller, Thermal Analysis, John Wiley, New York, 1976.
5. S.R. Allen, R.J. Farris and E.L. Thomas, J. Materials Science, 20, 2727 (1985).
6. R.S. Allen, Ph.D. Dissertation, University of Massachusetts, 1983.
7. ASTM D3379-75e Standard Test Method for Tensile Strength and Young's Modulus of High Modulus Single Filament Materials ASTM, Philadelphia, 1975.
8. L.H. Van Vlack, "Elements of Material Science & Engineering, Addison-Wesley, 1975, Appendix C.
9. Kevlar Aramid Data Manual, duPont Textile Fibers Department, October, 1976.
10. duPont Technical Information Report, "Characteristics and Uses of Kevlar 29 Aramid," September, 1976.
11. DuPont Technical Information Report, "Characteristics and Uses of Kevlar 49 Aramid High Modulus Organic Fibers," February, 1978.

TABLE VI.C.1

WAXS DIFFRACTIONOMETRIC DATA OF AS-SPUN PBT (28555-50-2)

Sample	As-spun PBT		Cycled PBT	
	e ₁	e ₂	e ₁	e ₂
Peak Number				
Position	16.3°	25.9°	15.4°	25.6°
Peak Width	5°	4.5°	3.2°	4.1°

TABLE VI.C.2

MECHANICAL PROPERTIES

Sample	As-spun PBT	FT Cycled PBT	Kevlar®29	FT Cycled Kevlar®29
Modulus	700 gpd \pm 100 gpd	1440 gpd \pm 90 gpd	600 gpd \pm 100 gpd	1145 gpd \pm 180 gpd
Strength	8 gpd \pm 0.8 gpd	10.0 gpd \pm 1.25 gpd	26 gpd \pm 5 gpd	23 gpd \pm 3 gpd
Strain	2.1% \pm 0.2%	0.7% \pm 0.1%	3.9% \pm 0.4%	2.5% \pm 0.8%

- A - OVEN
- B - LOAD CELL
- C - ADJUSTABLE CLAMP
- D - X-Y RECORDER
- E - TEMPERATURE READOUT-THERMOCOUPLE
- F - N₂ SOURCE
- G - VARIAC

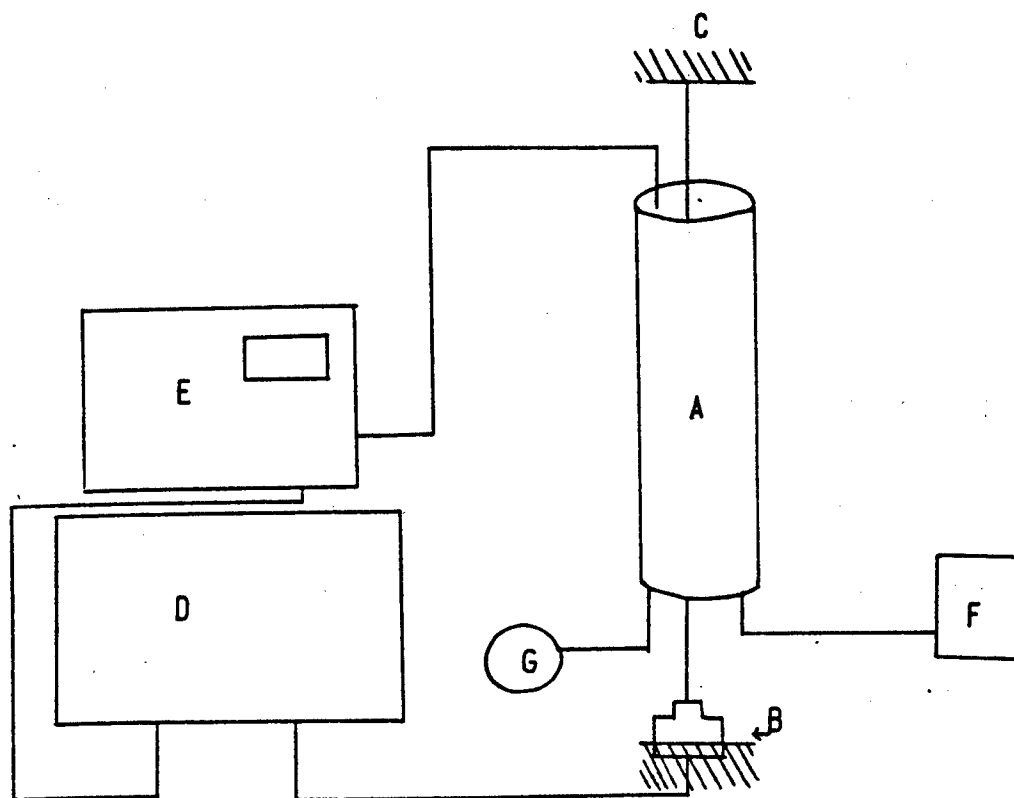


Figure VI.B.1

Schematic of force-temperature apparatus.

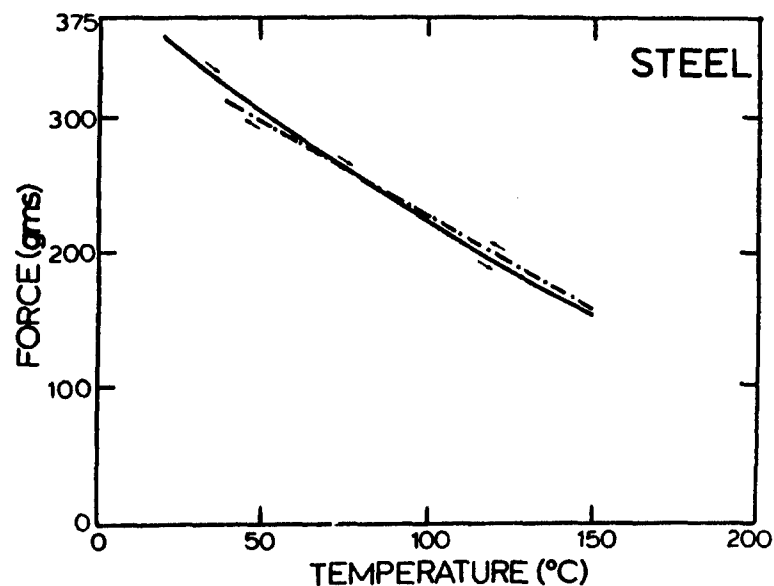


Figure VI.C.1

Force versus temperature profile for steel yarn (solid line = heating; dashed line = cooling).

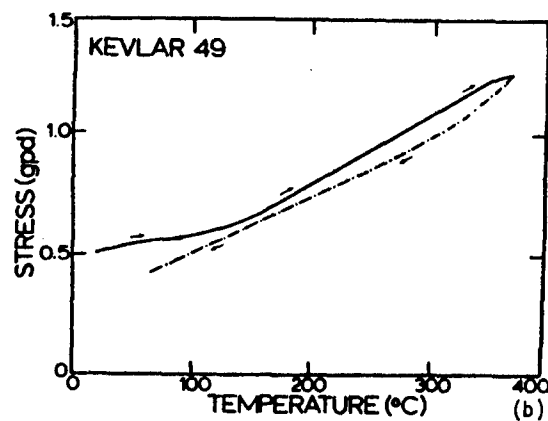
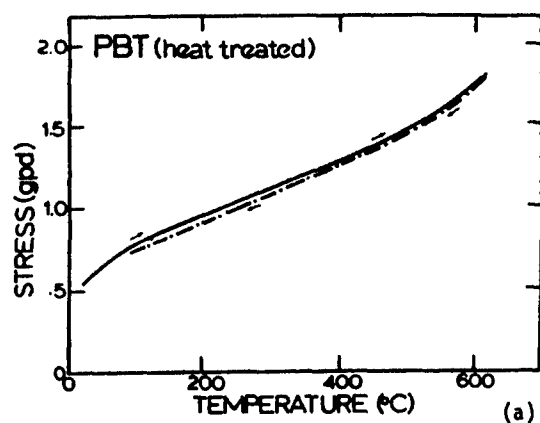


Figure VI.C.2

a) Stress versus temperature profile for PBT heat treated yarn at 650°C for 8 seconds (solid line = heating; dashed line = cooling). b) Stress versus temperature profile for Kevlar[®] 49 yarn (solid line = heating; dashed line = cooling).

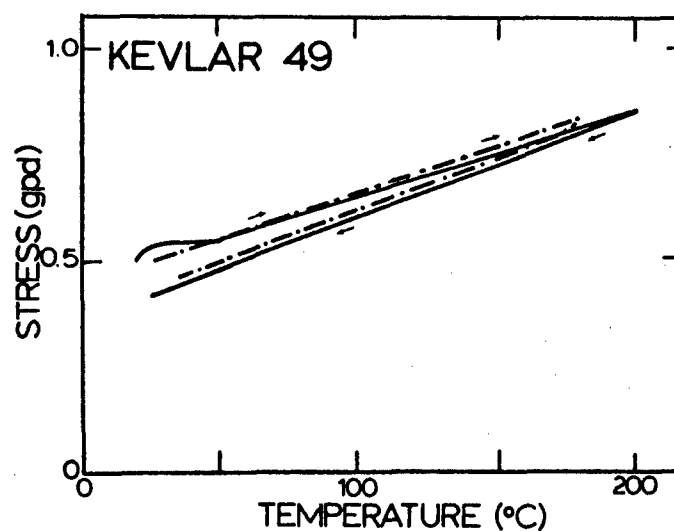


Figure VI.C.3

Stress versus temperature profile of Kevlar®49 yarn 24 hours after the first heating cycle (solid line = undessicated; dashed line = dessicated).

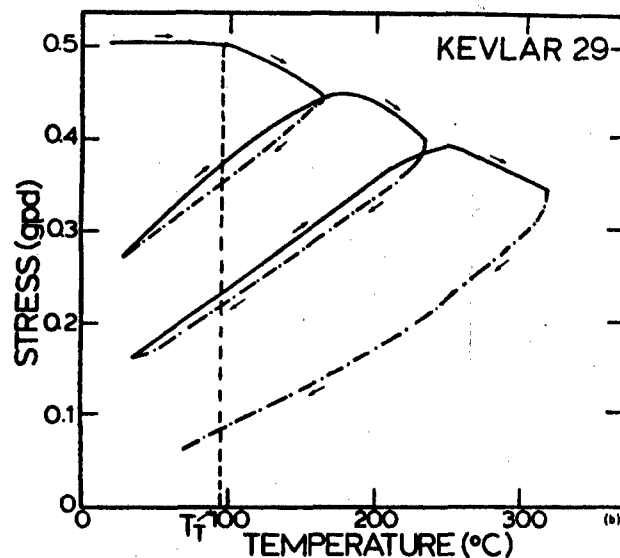
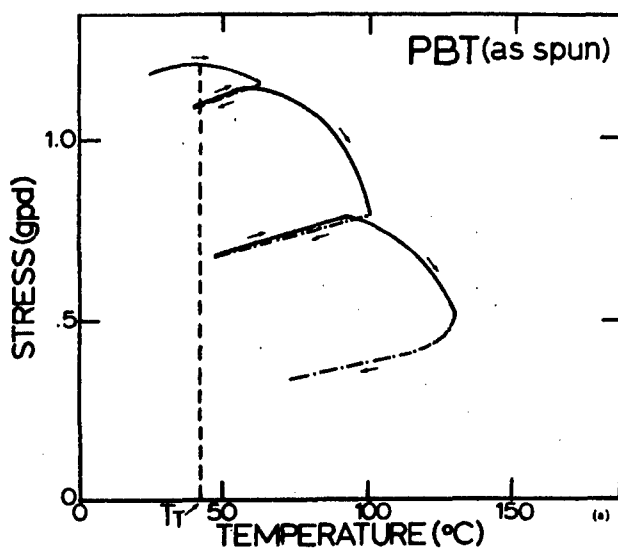


Figure VI.C.4

a) Stress versus temperature profile of as-spun PBT yarn (solid line = heating; dashed line = cooling). b) Stress versus temperature profile of Kevlar® yarn (solid line = heating; dashed line = cooling).

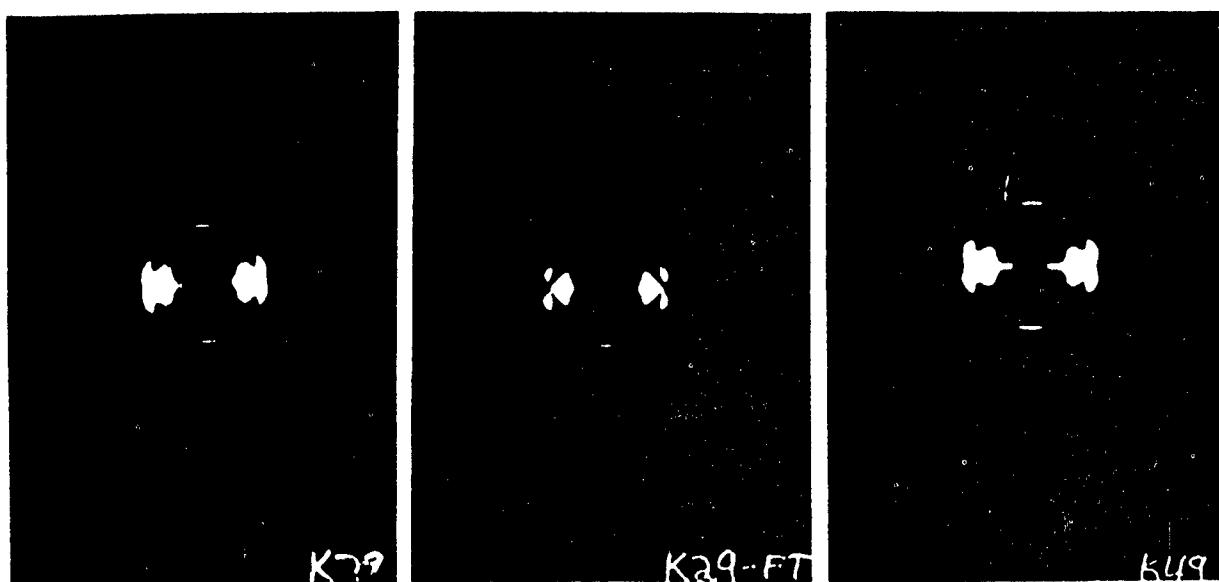


Figure VI.C.5

Wide angle X-ray diffraction patterns of a) Kevlar®29, b) FTC-Kevlar®29, c) Kevlar®49.

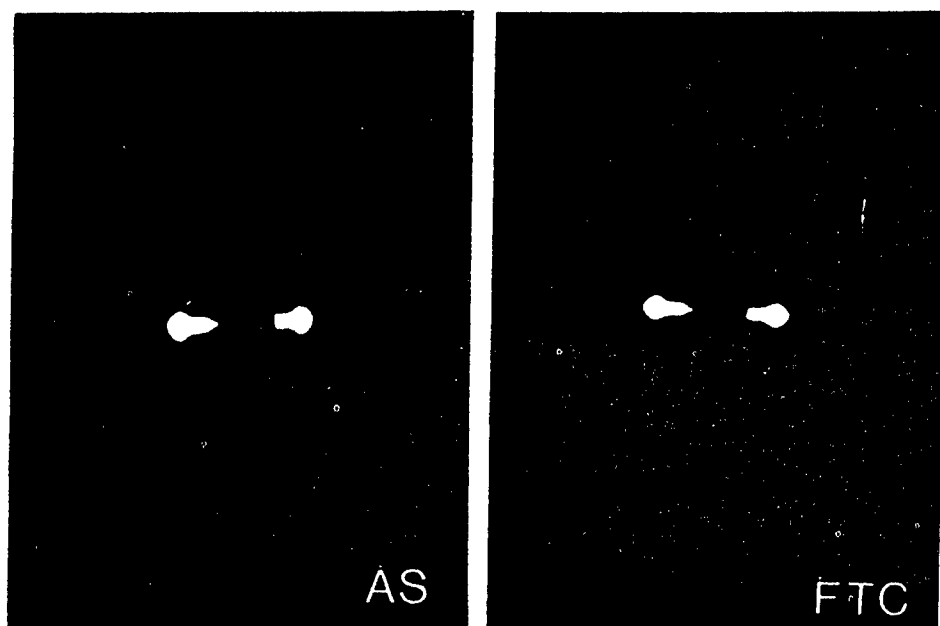


Figure VI.C.6

Wide angle x-ray diffraction patterns of PBT a) as-spun, b) FTC-PBT.

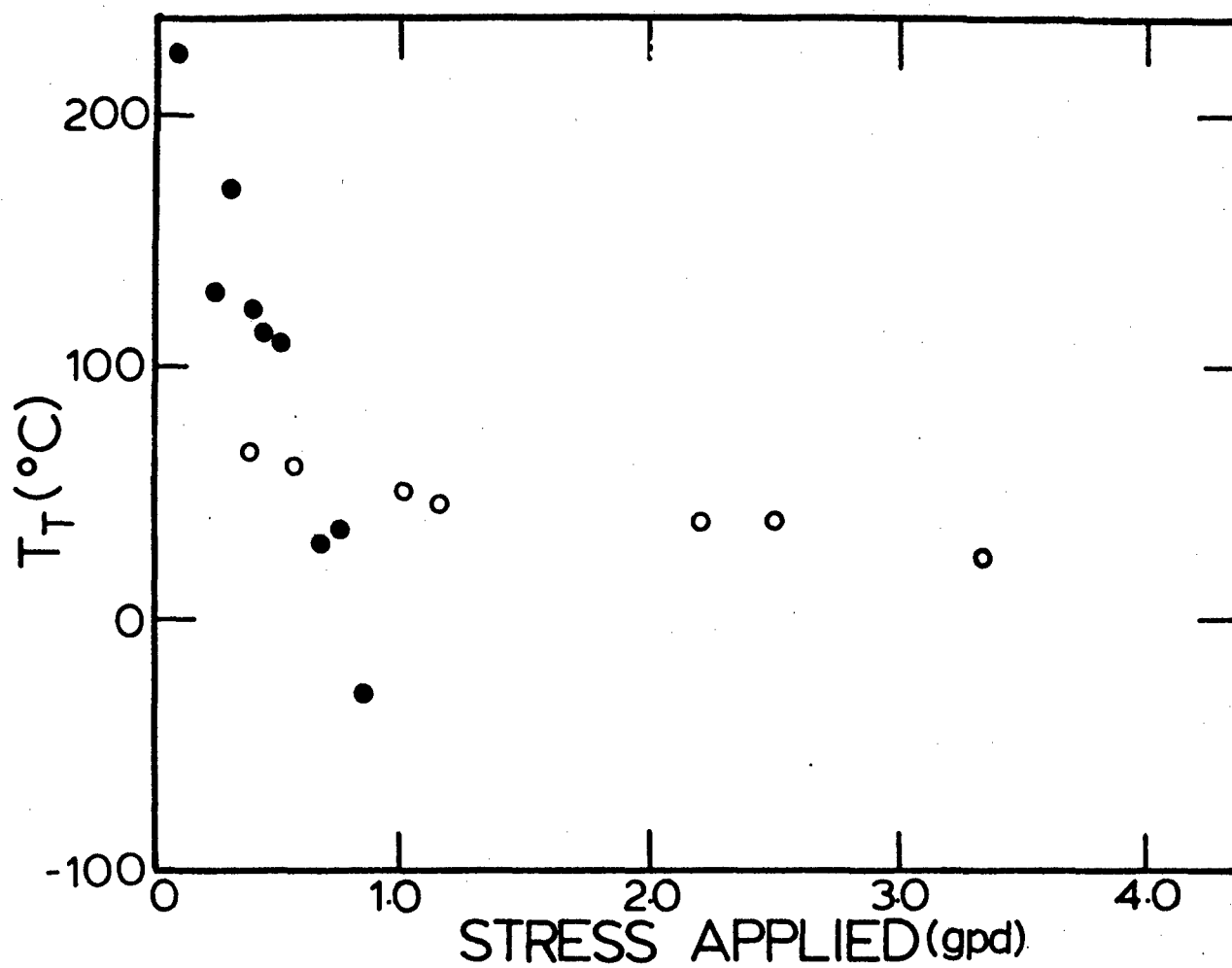


Figure VI.C.7

Plot of T_T , temperature of onset of stress drop, versus applied stress for
 ○ = PBT (as-spun), ● = Kevlar®29.